AN ABSTRACT OF THE THESIS OF

Chenchen Wu for the degree of Master of Science in Electrical and Computer Engineering presented on September 5, 2017

Title: Dynamic Frequency and Amplitude Estimation for Three-Phase Power Systems.

Abstract approved: _____

Mario E. Magaña

Several frequency and amplitude estimation algorithms are presented for balanced and unbalanced three-phase power grid systems. All the estimators are dynamic in nature and are implemented in the complex domain by transforming the three-phase power signals using Clarke's transform. Specifically, we first construct a non-linear dynamic model of the complex representation of the three-phase voltage (fundamental frequency components and harmonics) and then we use the unscented Kalman filter to estimate both the magnitude and the fundamental frequency and its harmonics. The performance evaluation of the algorithm shows the accurate tracking accuracy and convergence time when the frequency and amplitude of the grid voltage waveform change continuously or abruptly. Comprehensive simulations are implemented for both balanced and unbalanced conditions based on the real-world power grid system data. Specifically, 4 types of input amplitudes and 2 types of frequency changes are applied to test estimation algorithm performance.

Dynamic Frequency and Amplitude Estimation for Three-Phase Power Systems

by
Chenchen Wu

A THESIS

submitted to

Oregon State University

in partial fulfillment of
the requirements for the
degree of

Master of Science

Presented September 5, 2017
Commencement June 2018

Master of Science thesis of Chenchen Wu presented on September 5, 2017

APPROVED:

Major Professor, representing Electrical and Computer Engineering

Director of the School of Electrical Engineering and Computer Science

Dean of the Graduate School

I understand that my thesis will become part of the permanent collection of Oregon State University libraries. My signature below authorizes release of my thesis to any reader upon request.

Chenchen Wu, Author

ACKNOWLEDGEMENTS

The author expresses sincere appreciation…..

TABLE OF CONTENTS

Page

1 Introduction 1

2 Model of the Three-Phase Power System 4

2.1 Unscented Transformation 5

2.2 Unscented Transformation 7

3 Unscented Kalman Filter 11

3.1 Unscented Transformation 11

3.2 The UKF Algorithm 12

4 Frequency Estimation of Balanced Power System 14

4.1 Frequency Estimate Calculation 17

4.2 Linear Frequency Change 18

4.3 Step Frequency Change 21

5 Frequency and Magnitude of Unbalanced Power System 24

5.1 Frequency and Magnitude Estimate Calculation 25

5.2 Experiment 1 27

5.2.1 Linear Frequency Change Results 28

5.2.2 Linear Frequency Change Results 34

5.3 Experiment 2 40

5.3.1 Linear Frequency Change Results 41

5.3.2 Linear Frequency Change Results 47

5.4 Experiment 3 53

5.4.1 Linear Frequency Change Results 54

TABLE OF CONTENTS (Continued)

Page

5.4.2 Linear Frequency Change Results 60

5.5 Experiment 4 65

5.5.1 Linear Frequency Change Results 67

5.5.2 Linear Frequency Change Results 73

6 Conclustions.....79

Bibliography 81

1 Introduction

With the development of power electronic technology, many nonlinear loads are brought in power networks and result in a corresponding rise in harmonic levels. However, the frequency of a power system is a significant power quality parameter and is only allowed to shift around its nominal value within a small predefined range [1]. The amplitude of voltage is another important power quality parameter that could be distorted by harmonic and inter-harmonic components [2]. Recently, the frequency and amplitude variations of a power system are envisaged because the power networks are undergoing the dynamic abundant imbalanced changes between the generation and the load. Unexpected frequency, magnitude, and phase variations, such as grid faults, are harmful to the system and may further cause other problems. In order to maintain the stability of the power grid and the electrical devices in normal operation, accurate frequency and amplitude tacking and estimation is necessary. Besides, accurate and real-time frequency estimation in a power system is a prerequisite for the future smart grid, where the generation, loading, and topology will be dynamically updated [3].

Throughout the last few decades, various algorithms have been proposed for frequency and amplitude estimation of a power system. Traditionally, the definition of frequency is described by the time period between two zero crossing as well as the number of cycles in the brief period of time [4], [5]. However, this method is apparently sensitive when the signal undergoes transient or abnormal changes, or the distorted signal under harmonics and noise pollution [6]. In order to suppress this disadvantage, a number of alternative techniques have been proposed during recent years. Based on the analysis of the voltage frequency spectrum, some methods are suggested to solve the problem, such as discrete Fourier transform (DFT). The author in [7] proposed a hybrid method for power system frequency estimation. This method is applied using a second-order Taylor series expansion and a DFT algorithm, however, it is assumed that the power system operates in a noise-free environment. Moreover, to compensate for the spectral leakage, which is caused by incoherent sampling and finite frequency resolution problems of the discrete Fourier transform, the advanced windowed functions and interpolation schemes are utilized here [8].

Phase-locked loop (PLL) techniques and adaptive notch filters (ANFs) are the other effective frequency and amplitude estimation methods. The key idea of the PLL is to actively generate a

signal whose phase angle adaptively tracks variations of a given signal via a control loop [9]. In the same spirit, adaptive notch filtering (ANF) passively derives its phase angle output from a given signal [10]. However, it has the drawback of an estimation error in steady state and has a slow dynamic response in the filtering process. Many other PLL-based techniques are developed and presented in the literature such as the enhanced PLL [11], [12], the quadrature PLL [13], and the state-variable feedback PLL [14], [15]. All the authors in the aforementioned PLLs need to compromise between the desirable transient response and the acceptable steady-state estimation error according to desired purposes of their experiments.

The least squares (LS) and other LS-based algorithms are widely used signal processing methods to estimate frequency, magnitude, and phase as well, such as least mean squares-based adaptive filtering (LMS), weighted least square (WLS), Complex-valued least square (CLS), and self-tuning least square (STLS). Pradhan et al presented a LMS technique to compute the frequency of three-phase voltages in complex domain [16]. They used an adaptive step size approach that showed good performance when smooth changes in frequency occurred, however, the algorithm had difficulties tracking a frequency step change. In [6], the authors built three estimators for the frequency estimation under both noise and harmonic contamination, based on time-series voltage sample relationship, to find the optimal phase interval. All the approaches provided accurate response under balanced operating system, but one of the estimators did not produce comparable frequency estimation results under the unbalanced three-phase voltage with noise. The weakness of least squares and LS-based algorithms is the tradeoff between accuracy and response speed when the signal is under heavy noise and higher order harmonics pollution [17], [18].

Another widely accepted real-time dynamic estimation algorithm is the Kalman filter (KF) and its variants. The linear Kalman filter and non-linear extended Kalman filter (EKF) approaches are widely use to estimate accurate frequency, amplitude and phase of the fundamental and harmonic components of a noisy signal. The authors in [19] use a linear Kalman filter (KF) to detect the fast modal changes in power system. The approach in [19] estimates the frequency through the differentiation of the phase angle. A point in this thesis worth noting is that there is not a phase angle abrupt change in this case. Since the prerequisite of the EKF is to linearize the non-linear system, one must be careful to choose the initial conditions to avoid the divergence phenomena of the linearized filter. Wiltshire et al [20] combined a robust

extended complex Kalman filter and a sliding-surface-enhanced fuzzy adaptive controller (RECKF-FAC) to estimate frequency and amplitude of the distorted signals in power system. The authors studied the feasibility of their approach in three different cases, including a single sinusoid, harmonic signals and an actual signal from a stainless-steel factory. Even though the approach shows good performance on steady-state tracking, the drawback is that the approach cannot converge fast enough after an abrupt frequency change. Another common shortcoming of the extended Kalman filter (EKF) is the complicated computation of Jacobian matrices. It increases the processing requirements and execution time which affects the real-time response [21].

In this thesis, we use an alternative real-time algorithm called Unscented Kalman filter (UKF) to estimate the frequency and magnitude of balanced and unbalanced power systems. This technique originally appeared in 1997 to overcome the disadvantages of the extended Kalman filter (EKF) [21]. Instead of linearizing the non-linear system for the EKF, the Unscented Kalman filter creates a statistical distribution of the state, which is propagated based on the Unscented Transformation (UT). Therefore, this method could perform better in terms of tracking accuracy because it produces a more accurate posterior covariance matrix [22]. The thesis presents the frequency and magnitude estimation in the complex domain. In order to characterize the power system from three-phase measurements, the complex-valued Clarke's transform is exploited here. It casts the available three-phase information into the complex domain. In this thesis, we tests two types of frequency changes, namely, linear change and step change for the frequency estimation and also test four types of amplitude changes for the magnitude estimation. The magnitude estimation is conducted under both the linear and step frequency changes. The computer simulation is implemented using realistic initial conditions of the UKF to assess performance of the proposed algorithm.

2 Model of the Three-Phase Power System

In a power grid voltage system, the three phase voltages can be described by

$$V_a(t) = \sum_{i=1}^{N} V_{a_i} \cos(i\omega_1 t + \phi_i) + W_a$$

$$V_b(t) = \sum_{i=1}^{N} V_{b_i} \cos[i\left(\omega_1 t - \frac{2\pi}{3}\right) + \phi_i] + W_b$$

$$V_c(t) = \sum_{i=1}^{N} V_{c_i} \cos[i\left(\omega_1 t + \frac{2\pi}{3}\right) + \phi_i] + W_c$$

$$i = 1, 2, 3, \cdots$$

where V_{a_i}, V_{b_i} and V_{c_i} are the peak voltage of the amplitudes ith harmonic; ϕ_i is the fixed initial phase angle; W_a, W_b and W_c are noise terms associated with the measurements.

In order to represent the three phase voltages in complex form, the Clarke's transform is used here. At the kth sampling instant, we get

$$\begin{bmatrix} V_0(k) \\ V_\alpha(k) \\ V_\beta(k) \end{bmatrix} = \sqrt{\frac{2}{3}} \times \begin{bmatrix} \frac{\sqrt{2}}{2} & \frac{\sqrt{2}}{2} & \frac{\sqrt{2}}{2} \\ 1 & -\frac{1}{2} & -\frac{1}{2} \\ 0 & \frac{\sqrt{3}}{2} & -\frac{\sqrt{3}}{2} \end{bmatrix} = \begin{bmatrix} V_a(k) \\ V_b(k) \\ V_c(k) \end{bmatrix}$$

After applying the Clarke's transform, the three phases voltages are cast into V_0 and the quadrature-axis components V_α and V_β. Normally, only the V_α and V_β parts are utilized to construct the complex voltage model $V(k)$ at the kth sampling instant, namely,

$$V(k) = V_\alpha(k) + j\, V_\beta(k)$$

In general, the complex voltage $V(k)$ can be written as

$$V(k) = \sum_{i=1}^{N} A_i e^{j(\omega_i kT + \phi_i)} + B_i e^{-j(\omega_i kT + \phi_i)}$$

2.1 Model of balanced power system

In a balanced power grid voltage system, due to the fact that V_{a_i}, V_{b_i} and V_{c_i} are identical, the three phase voltages can be written as

$$V_a(t) = \sum_{i=1}^{N} V_i \cos(i\omega_1 t + \phi_i) + W_a$$

$$V_b(t) = \sum_{i=1}^{N} V_i \cos[i\left(\omega_1 t - \frac{2\pi}{3}\right) + \phi_i] + W_b$$

$$V_c(t) = \sum_{i=1}^{N} V_i \cos[i\left(\omega_1 t + \frac{2\pi}{3}\right) + \phi_i] + W_c$$

$$i = 1, 2, 4, 5, \cdots$$

where: V_{a_i}, V_{b_i} and V_{c_i} are the peak voltage amplitudes of the ith harmonic; ϕ_i is the fixed initial phase angle; W_a, W_b and W_c are noise terms associated with the measurements.

When the amplitudes of the three-phase are identical, $V(k) = 0$.

The complex voltage can be simplified to

$$V(k) = \sum_{i=1}^{N} A_i e^{j(\omega_i kT + \phi_i)}$$

$$i = 1, 2, 4, 5, \cdots$$

Under balanced conditions, the 3rd harmonic is eliminated when applying the Clarke's transform, so we just list the fundamental frequency, 2nd, 4th and 5th harmonics.

In a balanced system, after lengthy calculations, we get

$$V_\alpha(k) = \sqrt{\frac{3}{2}}[V_1 \cos(\omega_1 kT + \phi_1) + V_2 \cos(\omega_2 kT + \phi_2) + V_4 \cos(\omega_4 kT + \phi_4) + V_5 \cos(\omega_5 kT + \phi_5)]$$

$$V_\beta(k) = \sqrt{\frac{3}{2}}[V_1 \sin(\omega_1 kT + \phi_1) - V_2 \sin(\omega_2 kT + \phi_2) + V_4 \sin(\omega_4 kT + \phi_4) - V_5 \sin(\omega_5 kT + \phi_5)]$$

As a result, the complex representation of system voltage $V(k)$ is given as

$$V(k) = \sqrt{\frac{3}{2}}\left[V_1\, e^{j(\omega_1 kT+\phi_1)} + V_2\, e^{-j(\omega_2 kT+\phi_2)} + V_4\, e^{j(\omega_4 kT+\phi_4)} + V_1\, e^{-j(\omega_5 kT+\phi_5)}\right] + W(k)$$

where $W(k) = W_\alpha(k) + j\,W_\beta(k)$ is zero-mean complex Gaussian noise. In order to transfer the grid voltage signal to state space model, the initial step is to define the discrete-time presentation of the system voltage $V(k)$. The phase angle of the discretized version of $V(k)$ can be written in time-varying form as

$$\int_0^{kT} \omega_i(\tau)\, d\tau + \phi_i = \theta_i(kT) \quad i = 1, 2, 4, 5, \cdots,$$

where T is sampling period and $\omega_i(\tau)$ is the time-varying radian/s frequency.

Therefore, the discretized complex representation of the grid voltage is obtained as

$$V(k) = \sqrt{\frac{3}{2}}\left[V_1\, e^{j\theta_1(kT)} + V_2\, e^{-j\theta_2(kT)} + V_4\, e^{j\theta_4(kT)} + V_1\, e^{-j\theta_5(kT)}\right] + W(k)$$

and at the next sampling period, $V(k+1)$ is given by

$$V(k+1) = \sqrt{\frac{3}{2}}\left[V_1\, e^{j\theta_1[(k+1)T]} + V_2\, e^{-j\theta_2[(k+1)T]} + V_4\, e^{j\theta_4[(k+1)T]} + V_1\, e^{-j\theta_5[(k+1)T]}\right] + W(k+1)$$

However, at the $(k+1)$th sampling instant,

$$\begin{aligned}\theta_i[(k+1)T] &= \int_0^{(k+1)T} \omega_i(\tau)d\tau + \phi_i \\ &= \int_0^{kT} w_i(\tau)\, d\tau + \int_{kT}^{(k+1)T} \omega_i(\tau)d\tau + \phi_i \\ &= \theta_i(kT) + \Delta\theta_i(T) \qquad i = 1, 2, 4, 5, \cdots,\end{aligned}$$

where $\Delta\theta_i(T) = \int_{kT}^{(k+1)T} \omega_i(\tau)d\tau$

Thus, the discretized complex representation of the grid voltage is given by

$$V(k+1) = \sqrt{\frac{3}{2}}\left[V_1\, e^{j[\theta_1(kT)+\Delta\theta_1(T)]} + V_2\, e^{-j[\theta_2(kT)+\Delta\theta_2(T)]} + V_4\, e^{j[\theta_4(kT)+\Delta\theta_4(T)]} + V_1\, e^{-j[\theta_5(kT)+\Delta\theta_5(T)]}\right] + W(k+1)$$

where $\Delta\theta_1(T) = \frac{1}{2}\Delta\theta_2(T) = \frac{1}{4}\Delta\theta_4(T) = \frac{1}{5}\Delta\theta_5(T)$

The nonlinear model of three-phase voltage could be written in a complex state space model with 8 state variables: $x_{1k}, x_{2k}, x_{3k}, x_{4k}, x_{5k}, x_{6k}, x_{7k}, x_{8k}$, i.e.

$$\mathbf{x}_k = \begin{bmatrix} x_{1k} \\ x_{2k} \\ x_{3k} \\ x_{4k} \\ x_{5k} \\ x_{6k} \\ x_{7k} \\ x_{8k} \end{bmatrix} = \begin{bmatrix} e^{\Delta\theta_1(T)} \\ \sqrt{\frac{3}{2}} V_1 e^{j\theta_1(kT)} \\ e^{-\Delta\theta_2(T)} \\ \sqrt{\frac{3}{2}} V_2 e^{-j\theta_2(kT)} \\ e^{\Delta\theta_4(T)} \\ \sqrt{\frac{3}{2}} V_4 e^{j\theta_4(kT)} \\ e^{-\Delta\theta_5(T)} \\ \sqrt{\frac{3}{2}} V_5 e^{-j\theta_5(kT)} \end{bmatrix}$$

Moreover, the measurements and observations of this model can be defined as

$$\mathbf{x}_{k+1} = \mathbf{f}(x_k) + \boldsymbol{\eta}_k$$

$$y_k = h(\mathbf{x}_k) + W_k$$

where $\mathbf{f}(\mathbf{x}_k) = \begin{bmatrix} x_{1k} \\ x_{1k} \cdot x_{2k} \\ x_{3k} \\ x_{3k} \cdot x_{4k} \\ x_{5k} \\ x_{5k} \cdot x_{6k} \\ x_{7k} \\ x_{7k} \cdot x_{8k} \end{bmatrix}$, $h(\mathbf{x}_k) = [0 \quad 1 \quad 0 \quad 1 \quad 0 \quad 1 \quad 0 \quad 1] \begin{bmatrix} x_{1k} \\ x_{2k} \\ x_{3k} \\ x_{4k} \\ x_{5k} \\ x_{6k} \\ x_{7k} \\ x_{8k} \end{bmatrix}$,

$\boldsymbol{\eta}_k$ is the process noise vector and W_k is the measurement noise.

In a balanced power system, this state space model will be adopted to estimate the frequency and amplitude of the time-varying sinusoid signals with fundamental frequency, 2nd, 4th and 5th harmonics in a white Gaussian noise environment.

2.2 Model under unbalanced conditions

For an unbalanced power system, due to voltage sags, V_{a_i}, V_{b_i} and V_{c_i} are not identical. Then the complex voltage $V(k)$ can be written as

$$V(k) = \sum_{i=1}^{N} A_i e^{j(\omega_i kT + \phi_i)} + B_i e^{-j(\omega_i kT + \phi_i)}$$

Again, after lengthy calculations, the values of A_i and B_i for the fundamental frequency, the 2nd and the 3rd harmonic are given by

$$i = 1 \qquad A_1 = \frac{\sqrt{6}(V_{a_1} + V_{b_1} + V_{c_1})}{6} \quad B_1 = \frac{\sqrt{6}\,(2V_{a_1} - V_{b_1} - V_{c_1})}{12} - j\frac{\sqrt{2}\,(V_{b_1} - V_{c_1})}{4}$$

$$i = 2 \qquad A_2 = \frac{\sqrt{6}\,(2V_{a_2} - V_{b_2} - V_{c_2})}{12} - j\frac{\sqrt{2}\,(V_{b_2} - V_{c_2})}{4} \quad B_2 = \frac{\sqrt{6}(V_{a_2} + V_{b_2} + V_{c_2})}{6}$$

$$i = 3 \qquad A_3 = \frac{\sqrt{6}\,(2V_{a_3} - V_{b_3} - V_{c_3})}{12} + j\frac{\sqrt{2}\,(V_{b_3} - V_{c_3})}{4}$$

$$i = 3 \qquad B_3 = \frac{\sqrt{6}\,(2V_{a_3} - V_{b_3} - V_{c_3})}{12} + j\frac{\sqrt{2}\,(V_{b_3} - V_{c_3})}{4}$$

We can generalize this calculation as follows:

$i = 3l + 1$

$$A_{3l+1} = \frac{\sqrt{6}(V_{a_{3l+1}} + V_{b_{3l+1}} + V_{c_{3l+1}})}{6} \quad B_{3l+1} = \frac{\sqrt{6}\,(2V_{a_{3l+1}} - V_{b_{3l+1}} - V_{c_{3l+1}})}{12} - j\frac{\sqrt{2}\,(V_{b_{3l+1}} - V_{c_{3l+1}})}{4};$$

$i = 3l + 2$

$$A_{3l+2} = \frac{\sqrt{6}(V_{a_{3l+2}} + V_{b_{3l+2}} + V_{c_{3l+2}})}{6} \quad B_{3l+2} = \frac{\sqrt{6}\,(2V_{a_{3l+2}} - V_{b_{3l+2}} - V_{c_{3l+2}})}{12} - j\frac{\sqrt{2}\,(V_{b_{3l+2}} - V_{c_{3l+2}})}{4};$$

$i = 3l$

$$A_{3l} = \frac{\sqrt{6}(V_{a_{3l}} + V_{b_{3l}} + V_{c_{3l}})}{6} + j\frac{\sqrt{2}\,(V_{b_{3l}} - V_{c_{3l}})}{4} \quad B_{3l} = \frac{\sqrt{6}\,(2V_{a_{3l}} - V_{b_{3l}} - V_{c_{3l}})}{12} + j\frac{\sqrt{2}\,(V_{b_{3l}} - V_{c_{3l}})}{4};$$

where $l = 0, 1, 2, 3, \cdots$

As a result, the system voltage $V(k)$ with harmonics can be expressed as

$$V(k) = A_1 e^{j(\omega_1 kT + \phi_1)} + B_1 e^{-j(\omega_1 kT + \phi_1)} + A_2 e^{j(\omega_2 kT + \phi_2)} + B_2 e^{-j(\omega_2 kT + \phi_2)} + A_3 e^{j(\omega_3 kT + \phi_3)} + B_3 e^{-j(\omega_3 kY + \phi_3)} + W(k)$$

where $W(k) = W_\alpha(k) + j\,W_\beta(k)$ is zero-mean complex Gaussian noise. In the same way, to represent the grid voltage signal in state space form, we define the discrete-time presentation of the system voltage $V(k)$ again. The phase angle of $V(k)$ in discretized time-varying form has the exact same form as illustrated in balanced system.

Therefore, the discretized complex representation of the grid voltage under unbalanced system conditions at the kth sampling instant is given by

$$V(k) = A_1 e^{j\theta_1(kT)} + B_1 e^{-j\theta_1(kT)} + A_2 e^{j\theta_2(kT)} + B_2 e^{-j\theta_2(kT)} + A_3 e^{j\theta_3(kT)} + B_3 e^{-j\theta_3(kT)} + W(k)$$

and at the next sampling period, $V(k+1)$ is given by

$$V(k+1) = A_1 e^{j\theta_1[(k+1)T]} + B_1 e^{-j\theta_1[(k+1)T]} + A_2 e^{j\theta_2[(k+1)T]} + B_2 e^{-j\theta_2[(k+1)T]} + A_3 e^{j\theta_3[(k+1)T]} + B_3 e^{-j\theta_3[(k+1)T]} + W(k+1)$$

However, as in the balanced system case, at the $(k+1)$th sampling instant, we get

$$\theta_i[(k+1)T] = \theta_i(kT) + \Delta\theta_i(T) \qquad i = 1, 2, 3, \cdots$$

where $\Delta\theta_i(T) = \int_{kT}^{(k+1)T} \omega_i(\tau) d\tau$

Thus, the discretized complex representation of the grid voltage is rewritten as

$$V(k+1) = A_1 e^{j[\theta_1(kT) + \Delta\theta_1(T)]} + B_1 e^{-j[\theta_1(kT) + \Delta\theta_1(T)]} + A_2 e^{j[\theta_2(kT) + \Delta\theta_2(T)]} + B_2 e^{-j[\theta_2(kT) + \Delta\theta_2(T)]} + A_3 e^{j[\theta_3(kT) + \Delta\theta_3(T)]} + B_3 e^{-j[\theta_3(kT) + \Delta\theta_3(T)]} + W(k+1),$$

where $\Delta\theta_1(T) = \frac{1}{2}\Delta\theta_2(T) = \frac{1}{3}\Delta\theta_3(T)$

The nonlinear model of the three-phase voltage under unbalanced system will be written as 12 complex state variables: $x_{1k}, x_{2k}, x_{3k}, x_{4k}, x_{5k}, x_{6k}, x_{7k}, x_{8k}, x_{9k}, x_{10k}, x_{11k}, x_{12k}$

$$\mathbf{x}_k = \begin{bmatrix} x_{1k} \\ x_{2k} \\ x_{3k} \\ x_{4k} \\ x_{5k} \\ x_{6k} \\ x_{7k} \\ x_{8k} \\ x_{9k} \\ x_{10k} \\ x_{11k} \\ x_{12k} \end{bmatrix} = \begin{bmatrix} e^{\Delta\theta_1(T)} \\ A_1 e^{j\theta_1(kT)} \\ e^{-\Delta\theta_1(T)} \\ B_1 e^{-j\theta_1(kT)} \\ e^{\Delta\theta_2(T)} \\ A_2 e^{j\theta_2(kT)} \\ e^{-\Delta\theta_2(T)} \\ B_2 e^{-j\theta_2(kT)} \\ e^{\Delta\theta_3(T)} \\ A_3 e^{j\theta_3(kT)} \\ e^{-\Delta\theta_3(T)} \\ B_3 e^{-j\theta_3(kT)} \end{bmatrix}$$

Moreover, the measurements and observations are defined again as

$$x_{k+1} = \mathbf{f}(\mathbf{x}_k) + \boldsymbol{\eta}_k$$

$$y_k = h(\mathbf{x}_k) + W_k$$

where $\mathbf{f}(\mathbf{x}_k) = \begin{bmatrix} x_{1k} \\ x_{1k} \cdot x_{2k} \\ x_{3k} \\ x_{3k} \cdot x_{4k} \\ x_{5k} \\ x_{5k} \cdot x_{6k} \\ x_{7k} \\ x_{7k} \cdot x_{8k} \\ x_{9k} \\ x_{9k} \cdot x_{10k} \\ x_{11k} \\ x_{11k} \cdot x_{12k} \end{bmatrix}$,

$$h(\mathbf{x}_k) = \begin{bmatrix} 0 & 1 & 0 & 1 & 0 & 1 & 0 & 1 & 0 & 1 & 0 & 1 \end{bmatrix} \begin{bmatrix} x_{1k} \\ x_{2k} \\ x_{3k} \\ x_{4k} \\ x_{5k} \\ x_{6k} \\ x_{7k} \\ x_{8k} \\ x_{9k} \\ x_{10k} \\ x_{11k} \\ x_{12k} \end{bmatrix},$$

$\boldsymbol{\eta}_k$ is the process noise vector and W_k is the measurement noise.

This nonlinear state space model will be used to estimate the frequency and magnitude of the time-varying sinusoid signals with the fundamental frequency, the 2nd and the 3rd harmonics in a white Gaussian noise environment under unbalanced power grid system.

3 Unscented Kalman Filter

3.1 Unscented Transformation

The Unscented Transformation (UT) is a transformation based on the insight that it is easier to approximate a Gaussian distribution than a highly nonlinear function [22]. It is assumed that the original signal vector has mean $\bar{\mathbf{x}}$ and covariance $P_{\mathbf{xx}}$. The UT is a mechanism used to find a new set with mean $\bar{\boldsymbol{\gamma}}$ and covariance $P_{\boldsymbol{\gamma\gamma}}$ that is propagated with so called sigma points through a nonlinear transformation. The following formulas are used to calculate the sigma points based on the original signal vector mean $\bar{\mathbf{x}}$ and covariance $P_{\mathbf{xx}}$

$$\boldsymbol{\chi}_0 = \bar{\mathbf{x}}$$

$$\boldsymbol{\chi}_i = \bar{\mathbf{x}} + (\sqrt{(n + \lambda)P_{\mathbf{xx}}})_i$$

$$\boldsymbol{\chi}_{i+n} = \bar{\mathbf{x}} - (\sqrt{(n + \lambda)P_{\mathbf{xx}}})_i \quad i = 1, 2, \dots, n$$

where $(\sqrt{(n + \lambda)P_{\mathbf{xx}}})_i$ is the ith column of matrix $\sqrt{(n + \lambda)P_{\mathbf{xx}}}$ and $\lambda = \alpha^2(n + \kappa) - n$. The parameter α, which is used to describe the spread of the sigma points around mean $\bar{x}$, is suggested to be between 10^{-4} and 1. The value of κ is often set to 0 or $3 - n$.

After the sigma points are calculated, the nonlinear function is utilized to propagate them

$$\boldsymbol{\gamma}_i = \mathbf{f}(\boldsymbol{\chi}_i) \qquad i = 0,1, 2, \dots, 2n$$

The new signal vector with mean $\bar{\boldsymbol{\gamma}}$ and covariance $P_{\boldsymbol{\gamma\gamma}}$ are calculated as follows:

$$\bar{\boldsymbol{\gamma}} = \sum_{i=0}^{2n} w_i^m \boldsymbol{\gamma}_i$$

$$P_{\boldsymbol{\gamma\gamma}} = \sum_{i=0}^{2n} w_i^c [(\boldsymbol{\gamma}_i - \bar{\boldsymbol{\gamma}})(\boldsymbol{\gamma}_i - \bar{\boldsymbol{\gamma}})^T]$$

where the weights w_i^m and w_i^c are defined as

$$w_0^m = \frac{\lambda}{n + \lambda}$$

$$w_0^c = \frac{\lambda}{n + \lambda} + (1 - \alpha^2 + \beta)$$

$$w_i^m = w_i^c = \frac{1}{2(n + \lambda)}$$

where β is utilized to incorporate prior knowledge of the distribution of sigma points x; and usually it is set to 2 for Gaussian distribution.

3.2 The UKF Algorithm

The UKF algorithm is designed to obtain estimates of a nonlinear system with state space model

$$\mathbf{x}_{k+1} = \mathbf{f}(\mathbf{x}_k) + \mathbf{q}_k$$

$$\mathbf{y}_k = h(\mathbf{x}_k) + \mathbf{r}_k$$

where **x** is discrete observation state vector; **y** is the discrete measurement vector; **q** is the process Gaussian noise vector with zero mean and covariance matrix Q; **r** is the measurement Gaussian noise vector with zero mean and covariance matrix R [23].

The sigma points are generated based on the mean of the initial condition $\overline{\mathbf{x}}_{k-1}$, i.e.

$$\mathbf{x}_{0,k-1} = \overline{\mathbf{x}}_{k-1}$$

$$\mathbf{x}_{i,k-1} = \overline{\mathbf{x}}_{k-1} + (\sqrt{(n + \lambda)P_{\mathbf{xx}}})_i \quad i = 1, 2, \dots, n$$

$$\mathbf{x}_{i+n,k-1} = \overline{\mathbf{x}}_{k-1} - (\sqrt{(n + \lambda)P_{\mathbf{xx}}})_i \quad i = 1, 2, \dots, n$$

The sigma points are then propagated through

$$\mathbf{x}_{i,k/\,k-1} = \mathbf{f}(\mathbf{x}_{i,k-1}), \quad i = 0,1, 2, \dots, 2\,n$$

The predicted state mean $\overline{\mathbf{x}}_{k/\,k-1}$ and predicted covariance $P_{k/\,k-1}$ update are given by

$$\overline{\mathbf{x}}_{k/\,k-1} = \sum_{i=0}^{2n} w_i^m \, \mathbf{x}_{i,k/\,k-1}$$

$$P_{k/\,k-1} = \sum_{i=0}^{2n} w_i^c [(\mathbf{x}_{i,k/\,k-1} - \overline{\mathbf{x}}_{k/\,k-1})(\mathbf{x}_{i,k/\,k-1} - \overline{\mathbf{x}}_{k/\,k-1})^T]$$

The sigma points related to the predicted state vector mean and covariance matrix are generated by

$$\mathbf{x}_{0,k/\,k-1} = \overline{\mathbf{x}}_{k/\,k-1}$$

$$\mathbf{x}_{i,k/\,k-1} = \overline{\mathbf{x}}_{k/\,k-1} + (\sqrt{(n+\lambda)P_{k/\,k-1}})_i, \quad i = 1, 2, \dots, n$$

$$\mathbf{x}_{i,k/\,k-1} = \overline{\mathbf{x}}_{k/\,k-1} - \left(\sqrt{(n+\lambda)P_{k/\,k-1}}\right)_i, \quad i = 1, 2, \dots, n$$

Therefore, the sigma points of the measurements are obtained through the measurement-update function

$$\mathbf{y}_{i,k/\,k-1} = h(\mathbf{x}_{i,k/\,k-1}), \quad i = 01, 2, \dots, 2n$$

The measurement state mean $\overline{\mathbf{y}}_{k/\,k-1}$ is calculated with the following formula:

$$\overline{\mathbf{y}}_{k/\,k-1} = \sum_{i=0}^{2n} w_i^m \mathbf{y}_{i,k/\,k-1}.$$

Meanwhile, the measurement covariance matrix $P_{\mathbf{yy}}$ and cross-covariance of the state and measurement $P_{\mathbf{xy}}$ are represented as follows:

$$P_{\mathbf{yy}} = \sum_{i=0}^{2n} w_i^c \left[\left(\mathbf{y}_{i,k/\,k-1} - \overline{\mathbf{y}}_{k/k-1}\right)\left(\mathbf{y}_{i,k/\,k-1} - \overline{\mathbf{y}}_{k/k-1}\right)^T\right] + R$$

$$P_{\mathbf{xy}} = \sum_{i=0}^{2n} w_i^c [(\mathbf{x}_{i,k/\,k-1} - \overline{\mathbf{x}}_{k/\,k-1})(\mathbf{y}_{i,k/\,k-1} - \overline{\mathbf{y}}_{k/\,k-1})^T]$$

As a result, the Kalman gain, the state mean and covariance at iteration k can be obtained as follows:

$$K_k = P_{\mathbf{xy}} {P_{\mathbf{yy}}}^{-1}$$

$$\overline{\mathbf{x}}_k = \overline{\mathbf{x}}_{k/\,k-1} + K_k(\mathbf{y}_{k/\,k-1} - \overline{\mathbf{y}}_{k/\,k-1})$$

$$P_k = P_{k/\,k-1} - K_k P_{\mathbf{yy}} {K_k}^T$$

4 Frequency Estimation of Balanced Power System

In order to evaluate the performance of the Unscented Kalman Filter to estimate frequency and amplitude of the power system on a real-time basis, we select the parameters of the system to implement the MATLAB simulation based on realistic data. Estimation is implemented for linear and step frequency changes. We test the algorithm and compared the results within different input signals based on the same initial conditions.

The linear variation of voltage fundamental frequency from 55Hz to 62Hz starts at $t = 0.2s$ and ends at $t = 0.8s$, is shown in Figure1.

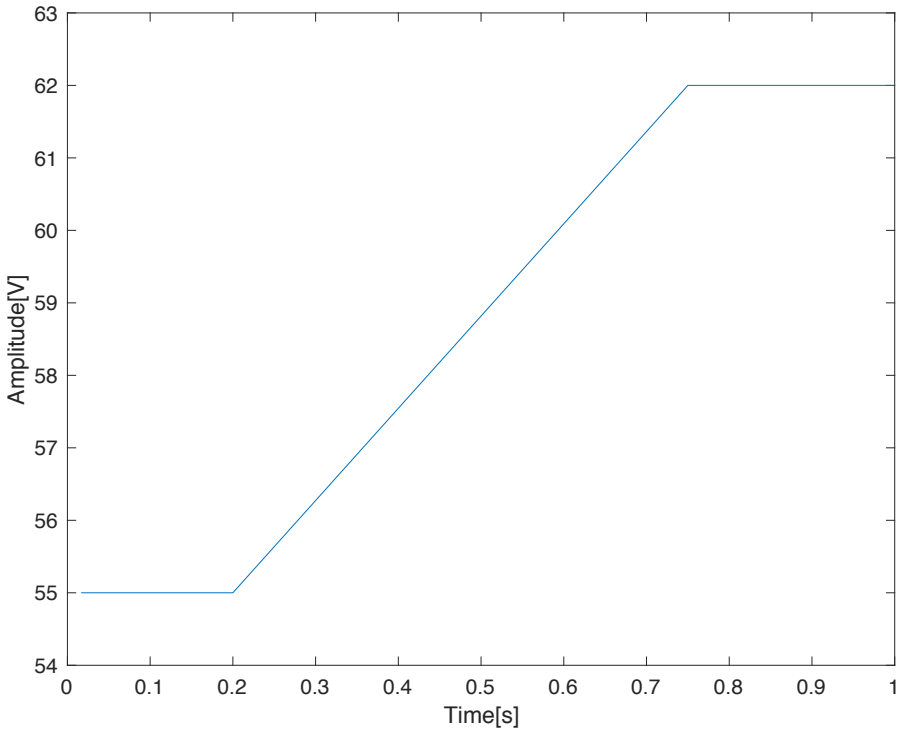

Figure 1 Linear fundamental frequency change

The fundamental frequency of the second input signal undergoes step change from 55Hz to 62Hz at $t = 0.4s$, is shown in Figure 2.

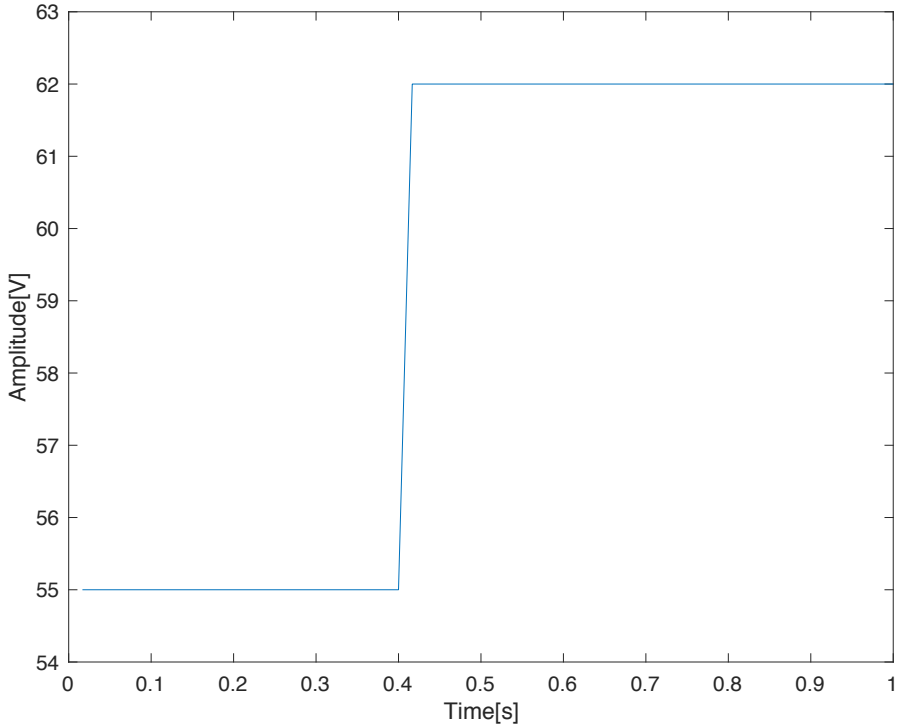

Figure 2 Step change of the fundamental frequency

In the experiment, we use the sampling frequency $f_s = 500\text{Hz}$. The amplitudes of fundamental frequency, 2nd harmonic, 4th harmonic and 5th harmonic are set to $120\text{V}, 12\text{V}, 6\text{V}$ and 3.6V, respectively. The initial phase shift of each harmonic is randomly chosen from 0° to 180° without overlapping. The sinusoidal waveforms of the combined signal, fundamental frequency and harmonics are shown in Figure 3.

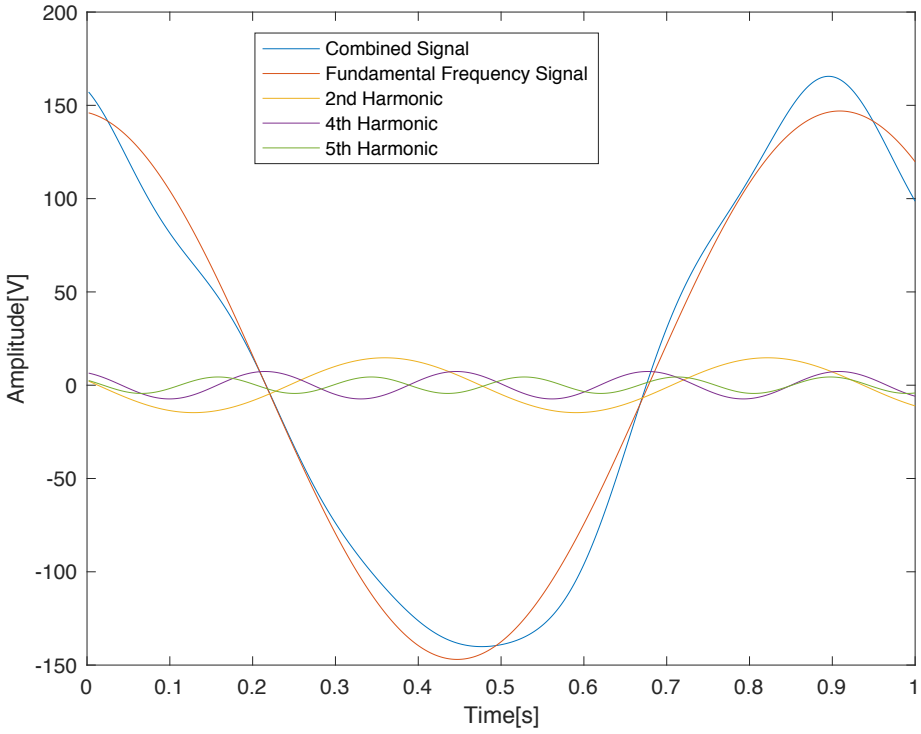

Figure 3 Combined signal, fundamental frequency signal and harmonics

The measurement and process noise variances are selected based on realistic data. According to [24], the average value of the observation noise power is in the order of 10^{-2} for 110 volt power signals and we select the value of 4.21×10^{-2} for the variance of the observation noise. As far as the process is concerned, we use a variance of 1×10^{-4}.

Moreover, when we choose the initial conditions for the Unscented Kalman filter (UKF), the parameter α is used to describe the deviation between the sigma points and mean $\bar{f}$, and is selected to be 10^{-2} here. The value of κ is set to 0. Thus, for $n = 8$ (the dimension of our model for the balanced case), $\lambda = \alpha^2(n + \kappa) - n = -7.992$. Another important parameter β is utilized to incorporate prior knowledge of the distribution of sigma points. In [25], it is established that high β means smoother tracking and longer convergence time; on the other hand, small β value could achieve higher sensitivity to frequency changes. In our experiment, since we assume that the distribution of the sigma points is Gaussian, β is set to 2. Now we have the weights w_i^m and w_i^c for the sigma points in Table 1.

	w_i^m	w_i^c
1	-9999	-9996
2	625	625
3	625	625
4	625	625
5	625	625
6	625	625
7	625	625
8	625	625
9	625	625
10	625	625
11	625	625
12	625	625
13	625	625
14	625	625
15	625	625
16	625	625
17	625	625

Table 1 Initial values of weights w_i^m and w_i^c for the balanced power system case

4.1 Frequency Estimate Calculation

After the Unscented Kalman filter is updated, we get the estimated state

$$\mathbf{x}_{k+1} = \begin{bmatrix} x_{1\,k+1} \\ x_{2\,k+1} \\ x_{3\,k+1} \\ x_{4\,k+1} \\ x_{5\,k+1} \\ x_{6\,k+1} \\ x_{7\,k+1} \\ x_{8\,k+1} \end{bmatrix}.$$

In order to get an estimate close to the true value, we first estimate the fundamental, the second, the fourth and the fifth harmonic from state variables $x_{1\,k+1}, x_{3\,k+1}, x_{5\,k+1}, and\ x_{7\,k+1}$, namely,

$$f_1 = \frac{1}{2\pi T_s} sin^{-1}\left(Im(x_{1\,k+1})\right)$$

$$f_2 = \frac{1}{2\pi T_s} sin^{-1}\left(Im(x_{3\,k+1})\right)$$

$$f_4 = \frac{1}{2\pi T_s} sin^{-1}\left(Im(x_{5\,k+1})\right)$$

$$f_5 = \frac{1}{2\pi T_s} sin^{-1}\left(Im(x_{7\,k+1})\right)$$

and then obtain the estimate of the fundamental frequency by averaging the estimates, i.e.

$$f_{est} = (f_1 + f_2/2 + f_4/4 + f_5/5)/4$$

4.2 Linear Frequency Change

In the experiment, the fundamental frequency of system voltage experience linear variation from 55Hz to 62Hz. In Figure 4 the estimated state tracks the actual frequency change accurately and the errors are displayed in Figure 7. We can see that the maximum error is at sample 302, and the proportion of error and current frequency is $0.3886/59.7133 = 0.0065$. Furthermore, the RMSE over 500 independent runs for a linear variation in frequency is 0.1285.

$$RMSE = \sqrt{\frac{1}{500} \times \sum_{500}^{1} (f_{est} - f_{real})^2} = 0.1285$$

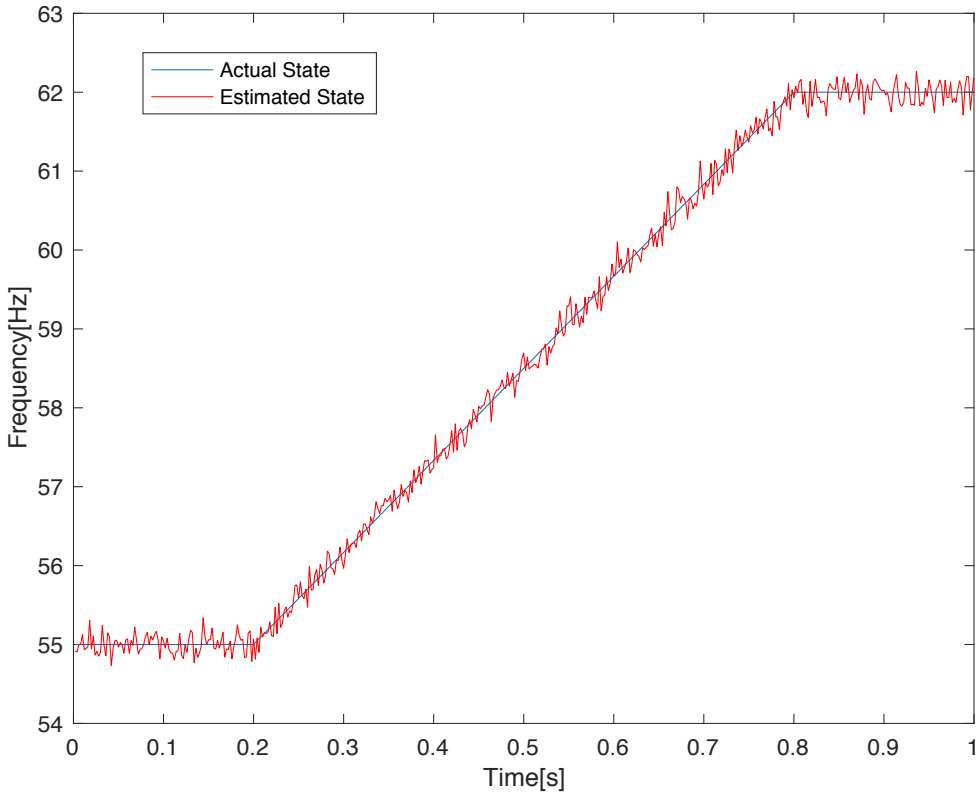

Figure 4 Linear frequency change

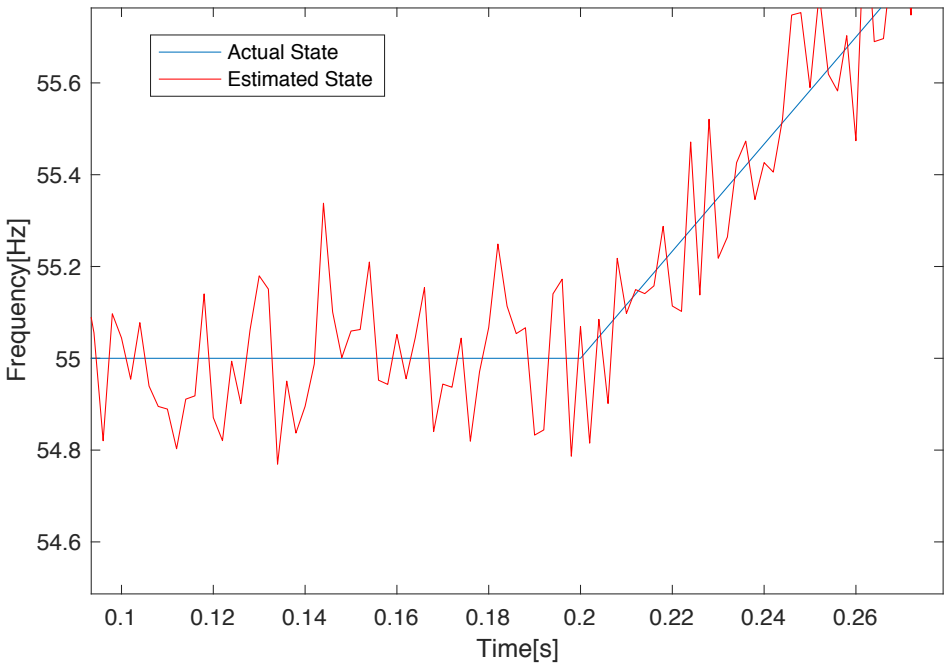

Figure 5 Linear frequency tracking around $t = 0.2s$

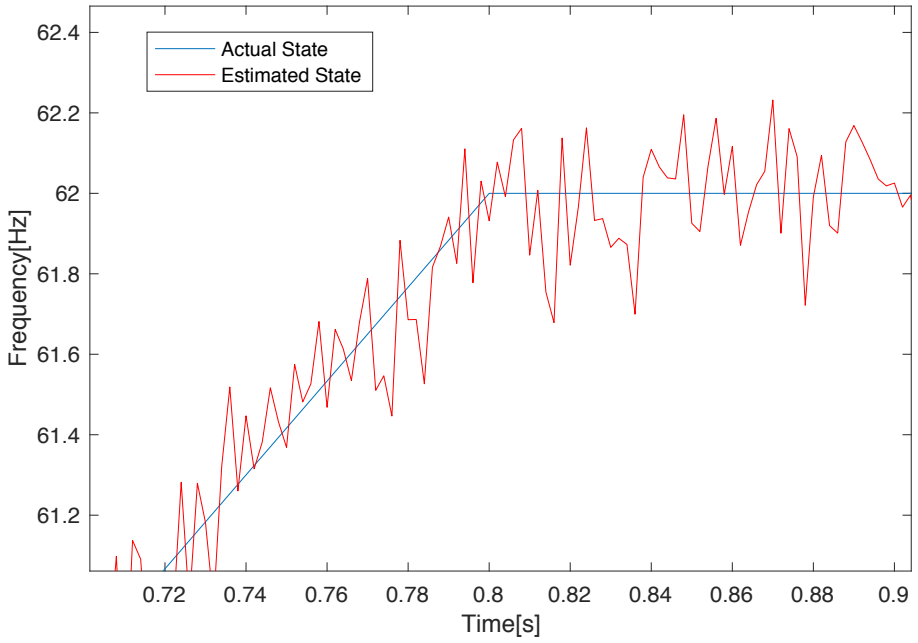

Figure 6 Linear frequency tracking around $t = 0.8s$

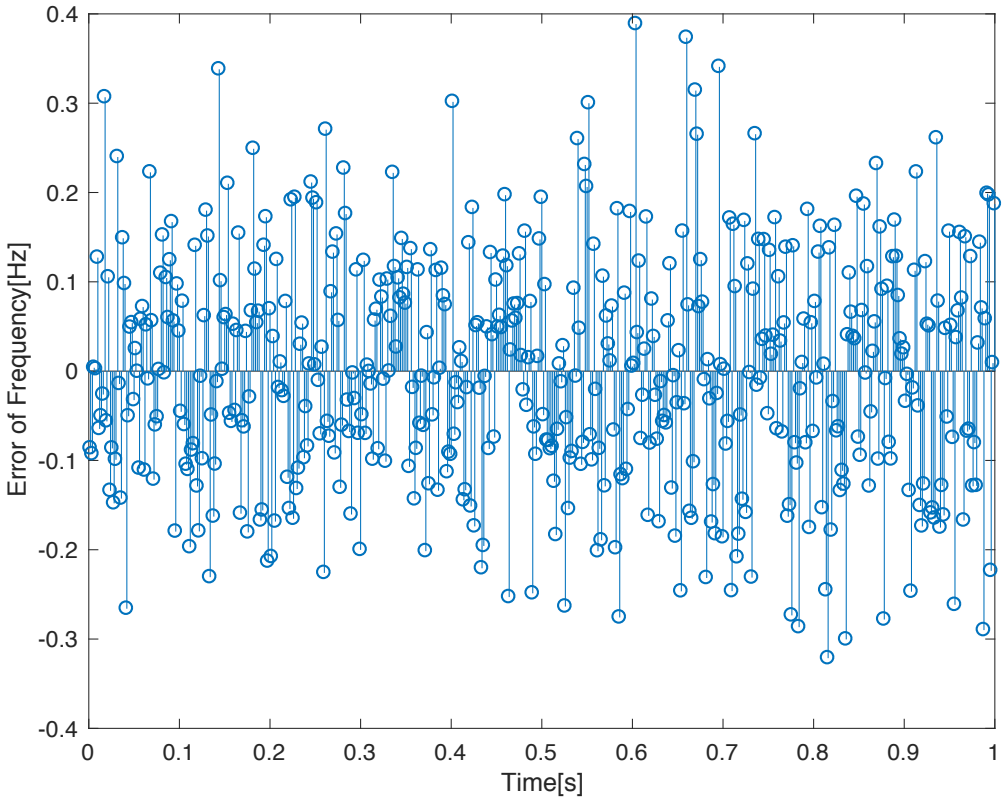

Figure 7 Errors between actual and estimated frequency for linear change

4.3 Step Frequency Change

In this case, the fundamental frequency of the input signal undergoes step change from 55Hz to 62Hz. Figure 8 shows the tracking accuracy between estimated and actual frequency. We can see in this figure that convergence to the actual value is quick. Figure 9 shows tracking performance near the transition. Figure 11 presents the errors of every run and the maximum percentage error is $0.3442/55 = 6.3\times10^{-3}$ at sample point 4. The RMSE in this experiment is 0.1240, which is similar to the linear change of the fundamental frequency.

$$RMSE = \sqrt{\frac{1}{500}\times\sum_{500}^{1}(f_{est}-f_{real})^2} = 0.1240$$

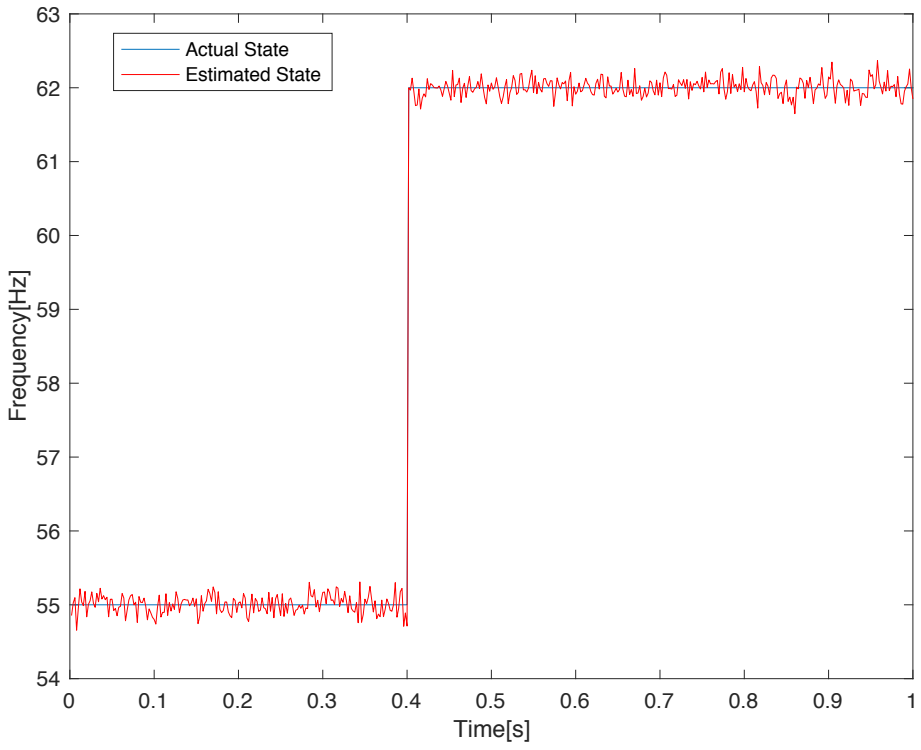

Figure 8 Step change of the fundamental frequency from 55Hz to 62Hz

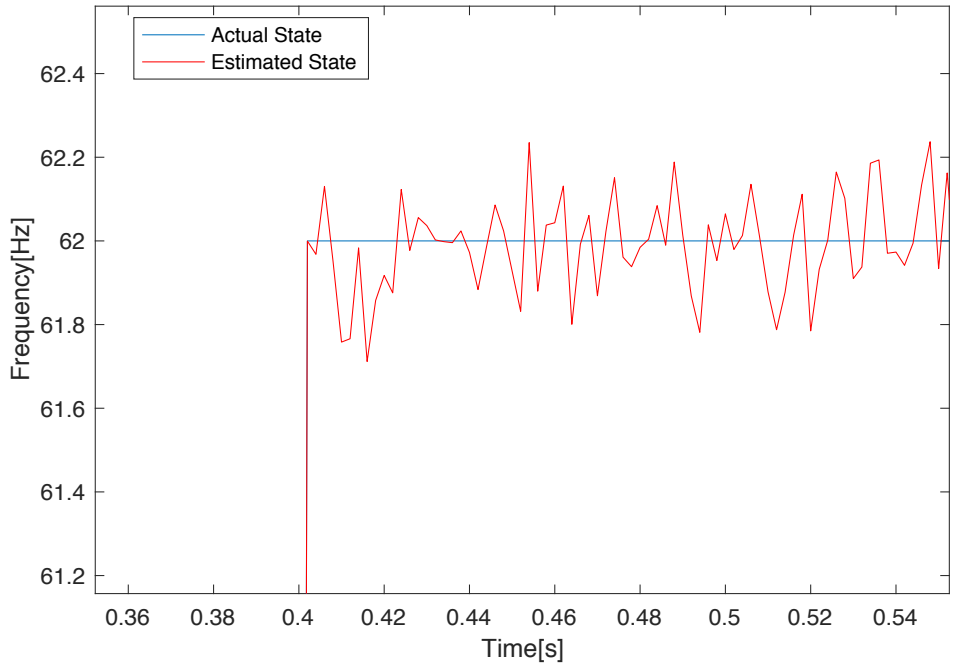

Figure 9 Upper part of step change

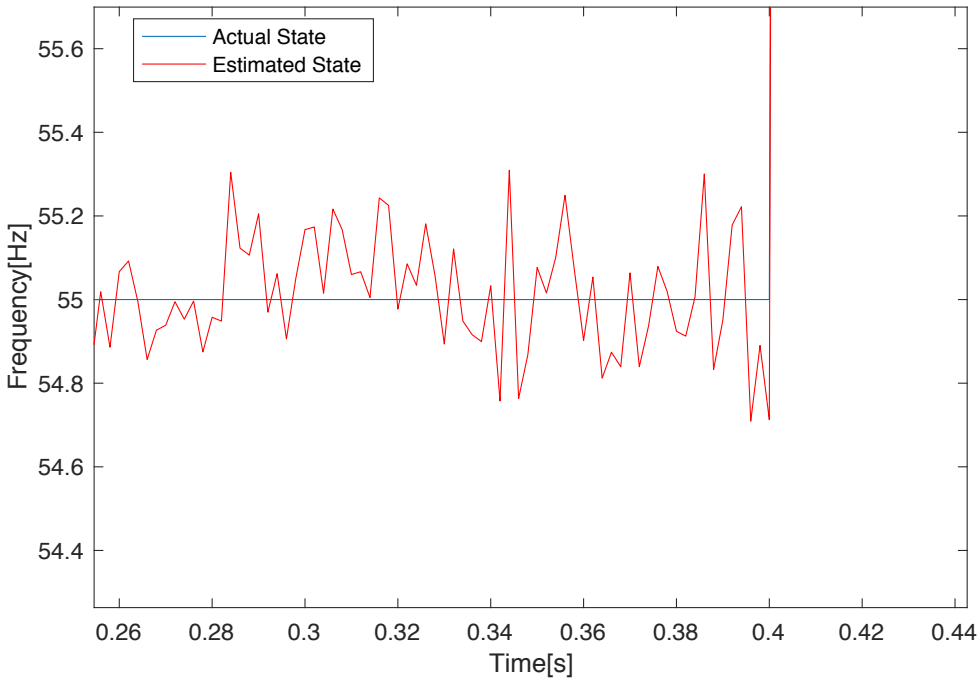

Figure 10 Lower part of step change

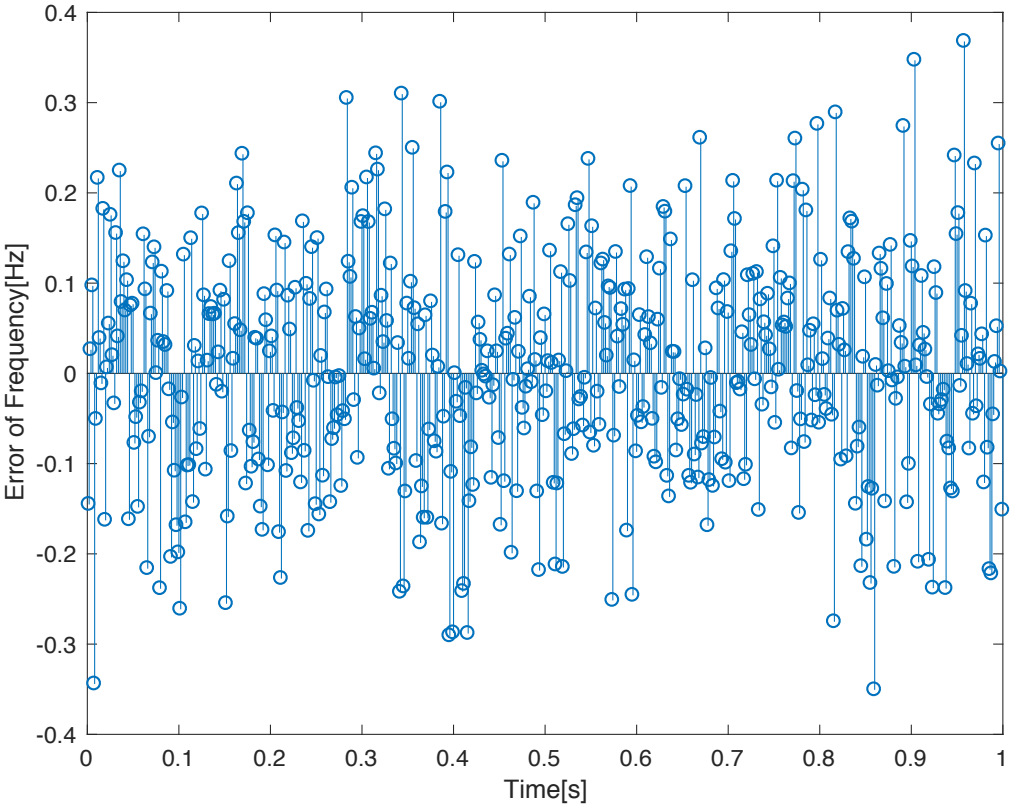

Figure 11 Errors between actual and estimated frequency for step change

5 Frequency and Magnitude Estimation of Unbalanced Power System

Just as in the balanced system case, we use the realistic data to verify the performance of the UKF algorithm in the unbalanced system. The step and linear frequency changes are applied as the input signals to our model to evaluate the performance of the UKF algorithm on frequency estimation. We observe and compare the simulation results between the balanced system and the unbalanced system. Furthermore, we evaluate the tracking accuracy of the UKF algorithm based on the same initial conditions. We use the root mean square error (RMSE) as the index of tracking accuracy again.

$$RMSE = \sqrt{\frac{1}{n} \times \sum_{n}^{1} (f_{est} - f_{actual})^2}$$

Again, we use measurement and process noise levels that are realistic. As in the balanced case, we select an observation noise variance of 4.21×10^{-2} and a process noise variance of 1×10^{-4} to assess estimation algorithm performance.

Further, in unbalanced power system, we utilize the same initial conditions in the Unscented Kalman filter (UKF) algorithm. The parameter α is set to 10^{-2} and the value of κ is set to 0 as well. Hence, for $n = 12$ (the dimension of our model for the unbalanced case), we have $\lambda = \alpha^2(n + \kappa) - n = -11.9988$. The scaling parameter β is set to 2 for the Gaussian distribution of sigma points. The weights w_i^m and w_i^c for the sigma points have the exact same values in Table 2.

	w_i^m	w_i^c
1	-9999	-9996
2	416.6667	416.6667
3	416.6667	416.6667
4	416.6667	416.6667
5	416.6667	416.6667
	w_i^m	w_i^c
6	416.6667	416.6667

7	416.6667	416.6667
8	416.6667	416.6667
9	416.6667	416.6667
10	416.6667	416.6667
11	416.6667	416.6667
12	416.6667	416.6667
13	416.6667	416.6667
14	416.6667	416.6667
15	416.6667	416.6667
16	416.6667	416.6667
17	416.6667	416.6667
18	416.6667	416.6667
19	416.6667	416.6667
20	416.6667	416.6667
21	416.6667	416.6667
22	416.6667	416.6667
23	416.6667	416.6667
24	416.6667	416.6667
25	416.6667	416.6667

Table 1 Initial values of weights w_i^m and w_i^c for the unbalanced power system case

5.1 Frequency and Magnitude Estimate Calculation

Similar to the balanced case, we use the updated UKF state at the $(k+1)$ time step, i.e.

$$\mathbf{x}_{k+1} = \begin{bmatrix} x_{1\,k+1} \\ x_{2\,k+1} \\ x_{3\,k+1} \\ x_{4\,k+1} \\ x_{5\,k+1} \\ x_{6\,k+1} \\ x_{7\,k+1} \\ x_{8\,k+1} \\ x_{9\,k+1} \\ x_{10\,k+1} \\ x_{11\,k+1} \\ x_{12\,k+1} \end{bmatrix}$$

and then use the state variables $x_{1\,k+1}, x_{5\,k+1}$, and $x_{9\,k+1}$ to first calculate estimates of the fundamental frequency, the second and the third harmonic, namely,

$$f_1 = \frac{1}{2\pi T_s} sin^{-1}\left(Im(x_{1\,k+1})\right)$$

$$f_2 = \frac{1}{2\pi T_s} sin^{-1}\left(Im(x_{5\,k+1})\right)$$

$$f_3 = \frac{1}{2\pi T_s} sin^{-1}\left(Im(x_{9\,k+1})\right)$$

and then calculate the final estimate by averaging out the three estimates, i.e.

$$f_{est} = (f_1 + f_2/2 + f_3/3)/3$$

For the magnitude estimation, after we have the updated state variables, each estimated magnitude is obtained by taking the absolute value of the complex state, that is,

$$A_1 = |x_{2\,k+1}| \quad B_1 = |x_{4\,k+1}|$$

$$A_2 = |x_{6\,k+1}| \quad B_2 = |x_{8\,k+1}|$$

$$A_3 = |x_{10\,k+1}| \quad B_3 = |x_{12\,k+1}|$$

5.2 Experiment 1

In this experiment, we use the sampling frequency $f_s = 500\text{Hz}$. To implement the unbalanced system, the amplitudes of fundamental frequency phase A, B and C are set to

$$V_{a1} = 110 \times (1 + 0.05\sin(2\pi t))$$

$$V_{b1} = 110 \times \left(1 + 0.1\sin\left(2\pi t - \frac{2\pi}{3}\right)\right)$$

$$V_{c1} = 110 \times \left(1 + 0.15\sin\left(2\pi t + \frac{2\pi}{3}\right)\right),$$

respectively. Then the 2nd harmonic and 3rd harmonic are defined to be 10%, and 5% of the fundamental frequency amplitude. The initial phase shift of each harmonic is randomly chosen from 0° to 180° without overlapping. The amplitude waveforms of the fundamental frequency and harmonics are shown in Figure 12.

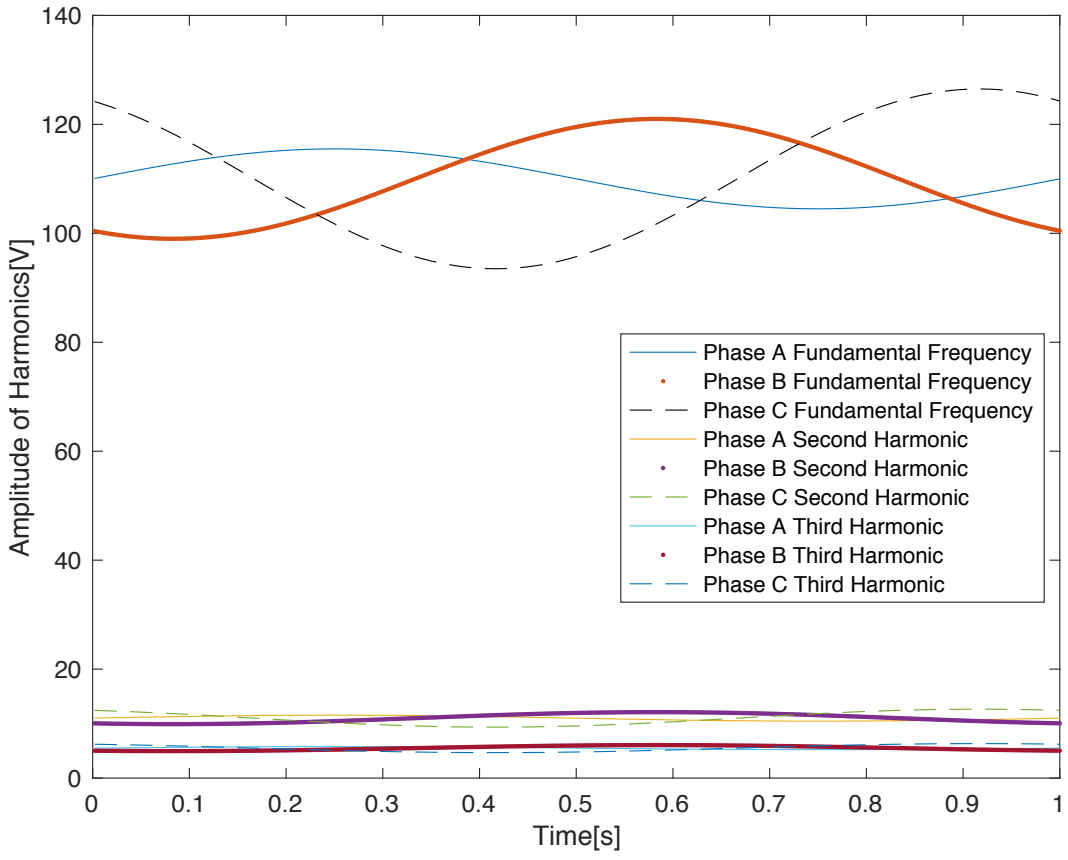

Figure 12 The amplitude of the fundamental frequency and harmonics

5.2.1 Linear frequency change results

In the experiment, the fundamental frequency of the system voltage experiences a linear variation from 55Hz to 62Hz. In Figure 13 the estimated frequency tracks the actual frequency change accurately and the errors are displayed in Figure 16. We can see that the maximum error is at sample 312, and the proportion of error and current frequency is $0.6657/59.9467 = 0.0111$. Furthermore, the RMSE over 500 independent runs for a linear variation in frequency is 0.1890.

$$RMSE = \sqrt{\frac{1}{500} \times \sum_{500}^{1} (f_{est} - f_{actual})^2} = 0.1890$$

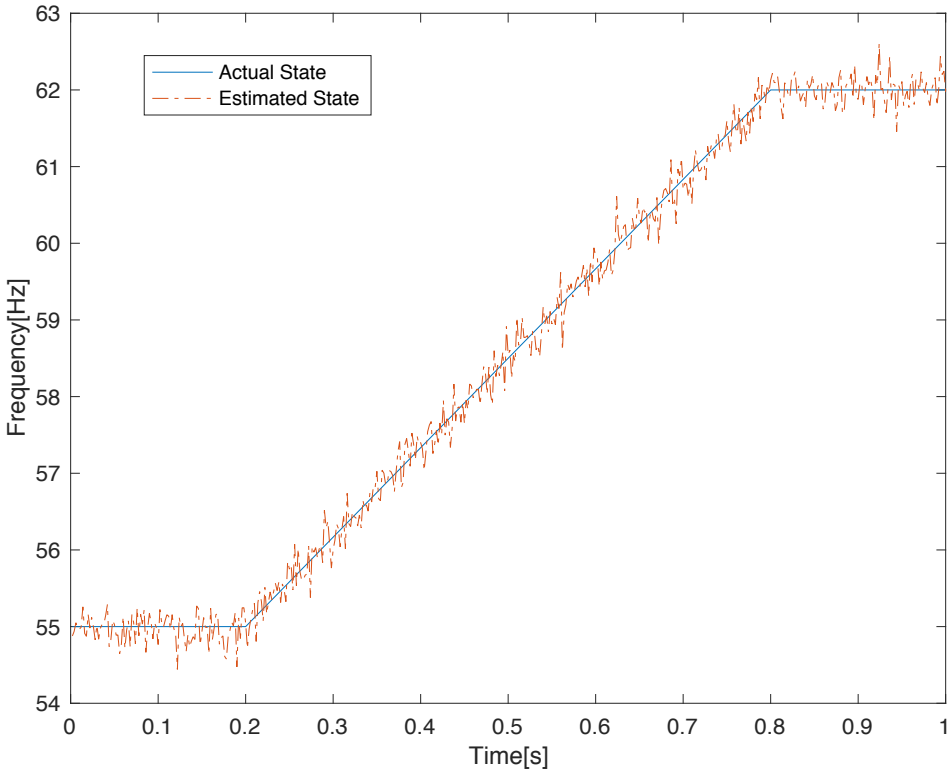

Figure 13 Linear frequency change

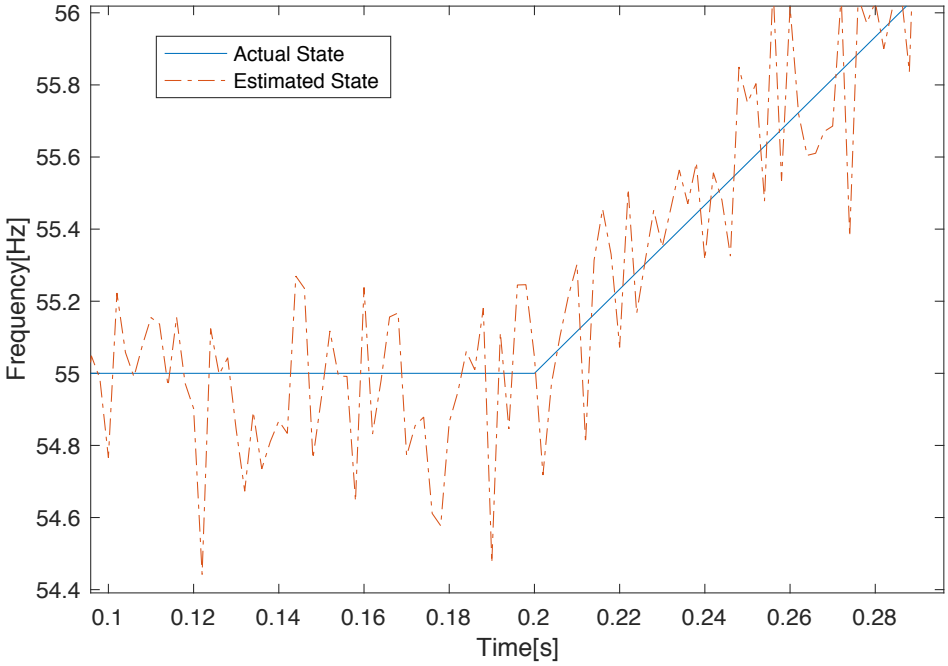

Figure 14 Linear frequency tracking around t = 0.2s

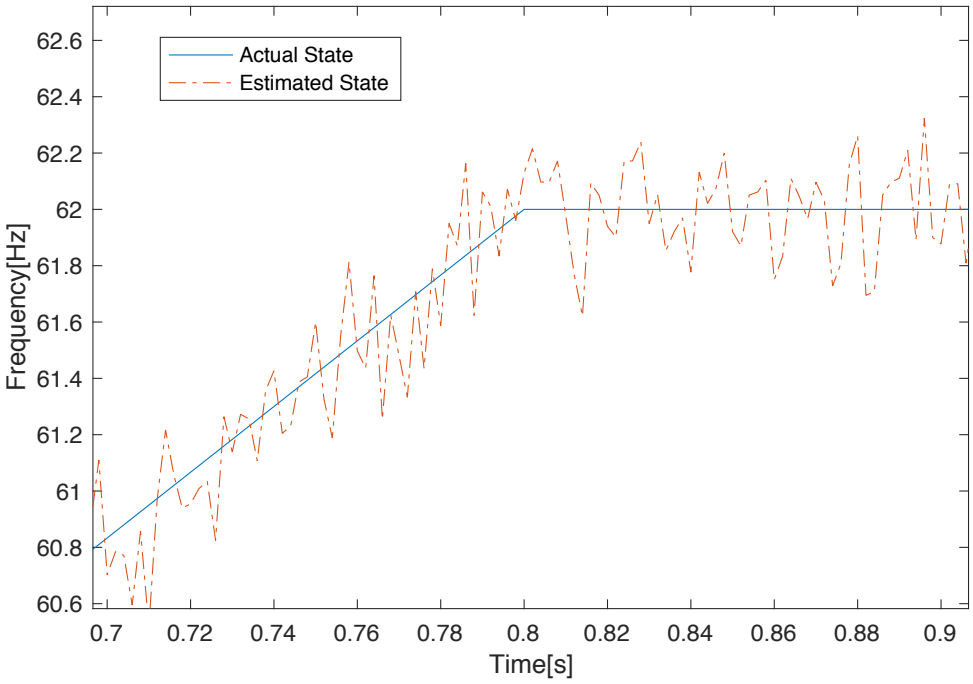

Figure 15 Linear frequency tracking around t = 0.8s

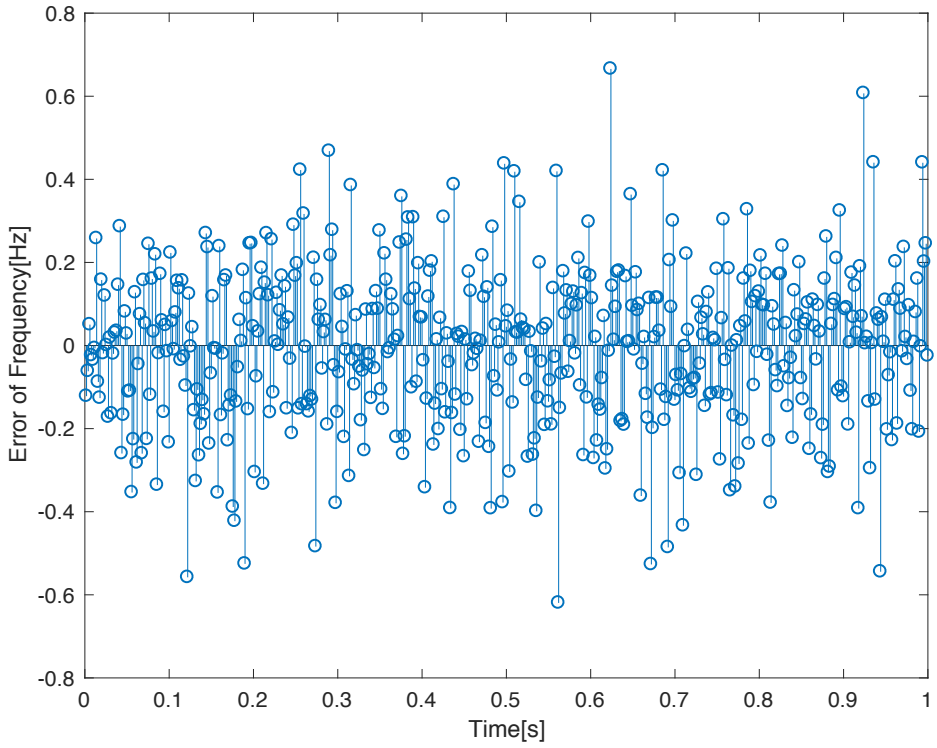

Figure 16 Errors between actual and estimated frequency for linear change

Moreover, in order to estimate amplitude, we first need to collect the coefficient magnitudes A_1, B_1, A_2, B_2, A_3 and B_3. Those coefficients are shown in figures 17 and 18. The blue line is the actual magnitude and the dotted line is the estimated value.

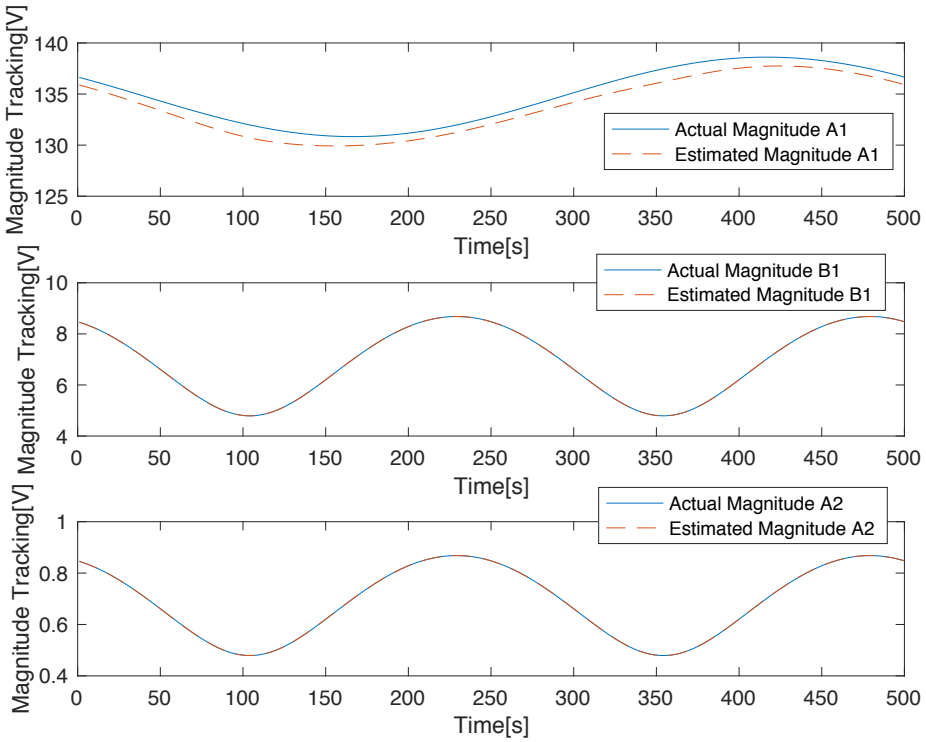

Figure 17 Errors between actual and estimated magnitude of A_1, B_1, A_2

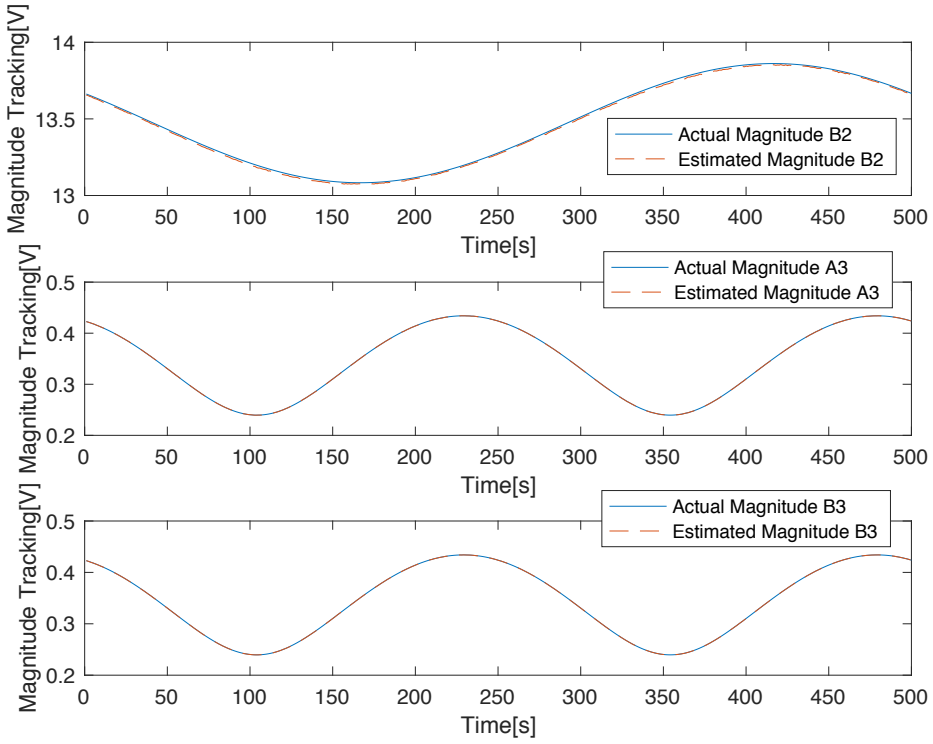

Figure 18 Errors between actual and estimated magnitude of B_2, A_3, B_3.

Another significant parameter is the true error between actual and estimated amplitude. In figure 19, the errors of all coefficients are plotted over time.

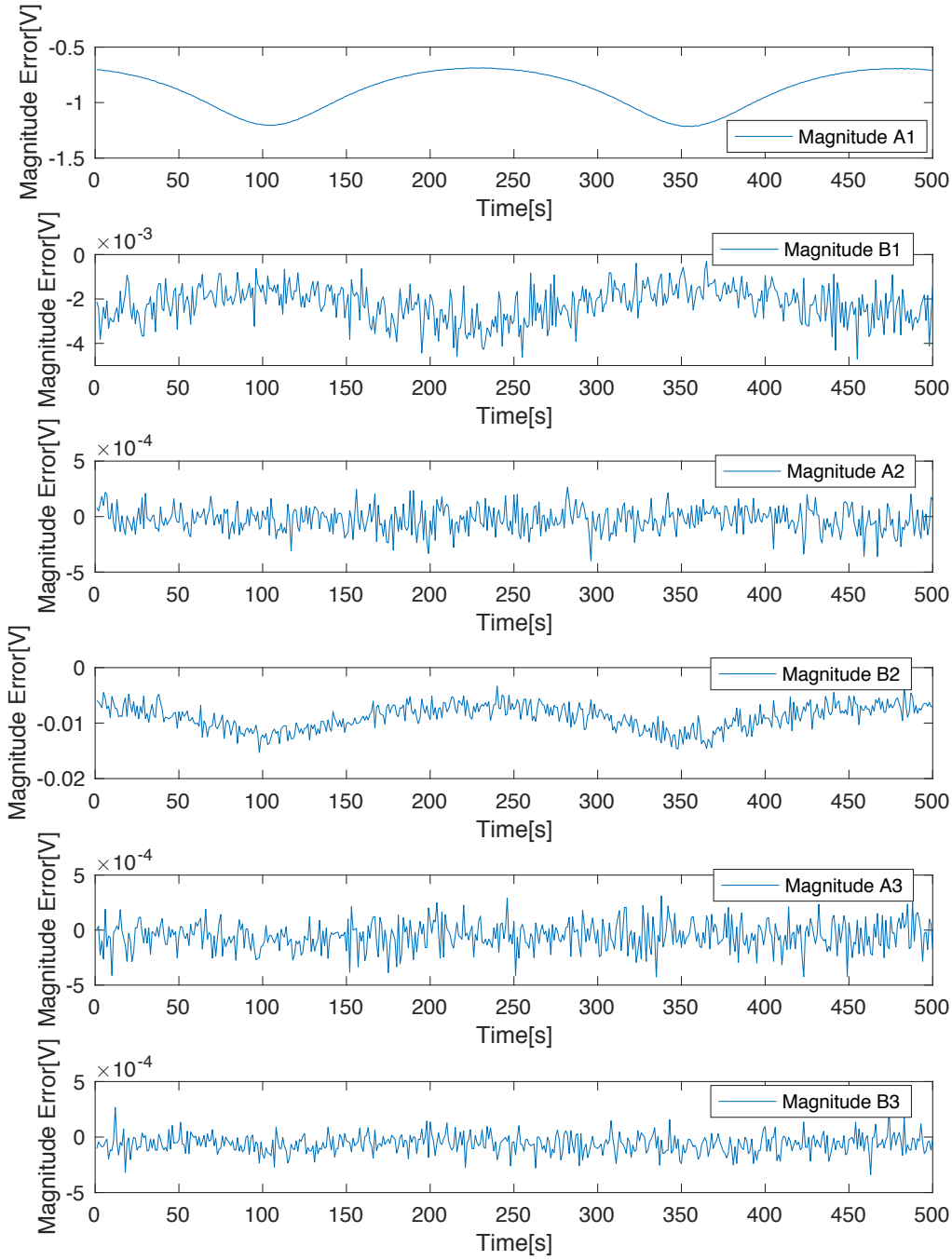

Figure 19 Error gaps of the coefficient magnitude

Even though we have plotted the errors of all coefficients, we cannot judge them directly since they have different bases. In figure 20, we plot of all coefficients based on their bases. We could compare them under each amplitude change.

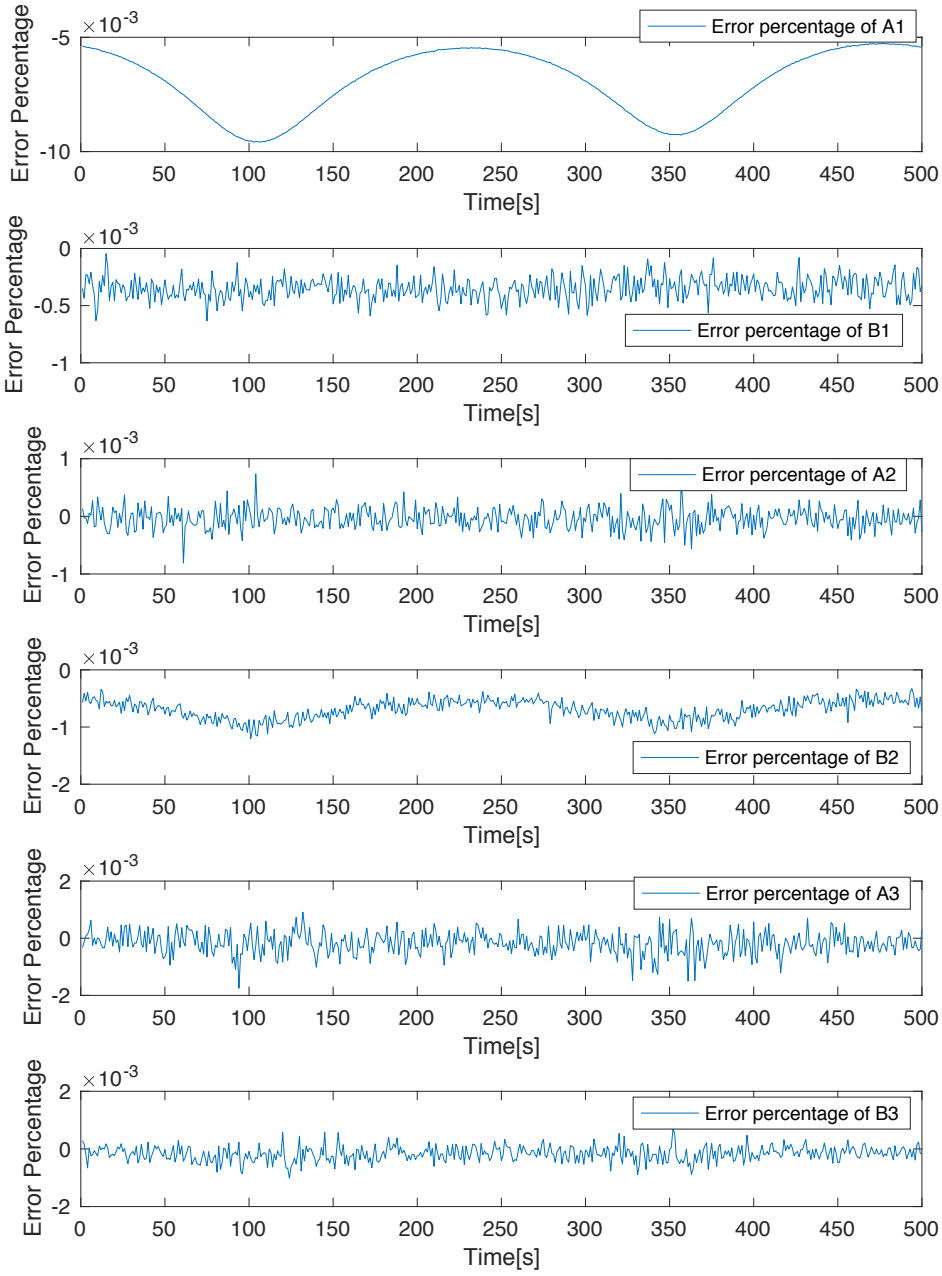

Figure 20 Magnitude error as a percentage

5.2.2 Step change results

In this case, the fundamental frequency of the input signal undergoes step change from 55Hz to 62Hz. Figure 21 shows the tracking accuracy between estimated and actual frequency. We can see that the convergence time is almost negligible in Figure 22. Figure 24 presents the errors of every run and the maximum percentage error is $0.5563/55 = 0.0101$ at sample point 119. After averaging the errors, we obtain the RMSE in this experiment of 0.1833 that is similar to the linear change of fundamental frequency.

$$RMSE = \sqrt{\frac{1}{500} \times \sum_{500}^{1} (f_{est} - f_{actual})^2} = 0.1833$$

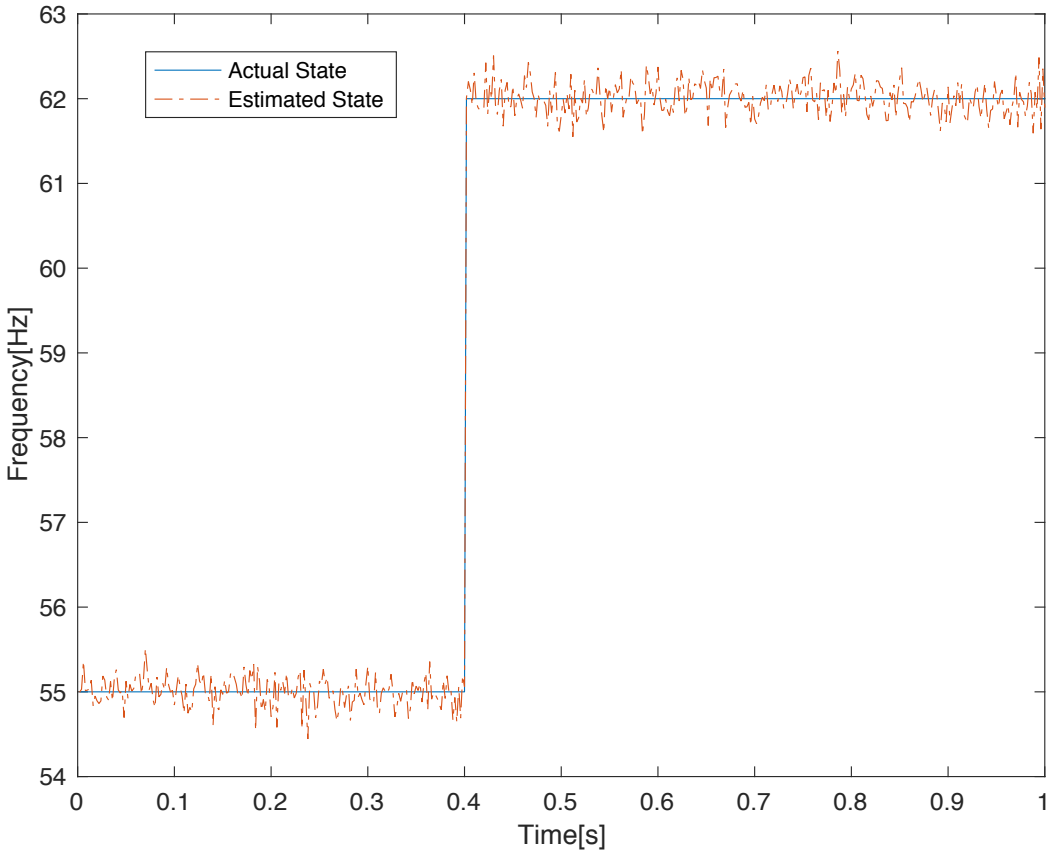

Figure 21 Step change of the fundamental frequency from 55Hz to 62Hz

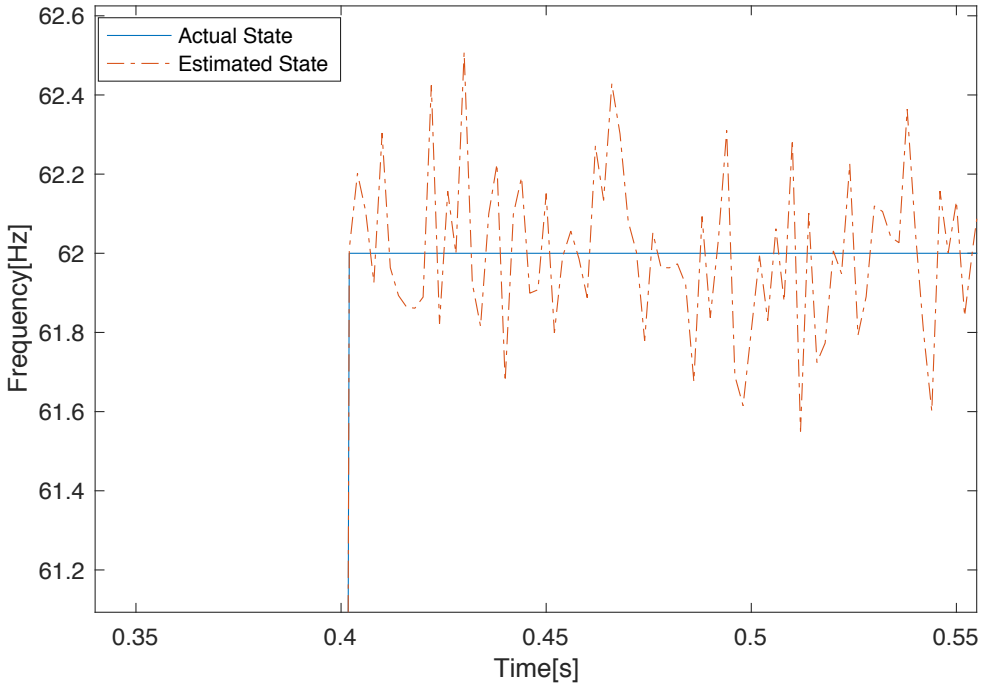

Figure 22 Upper part of step change

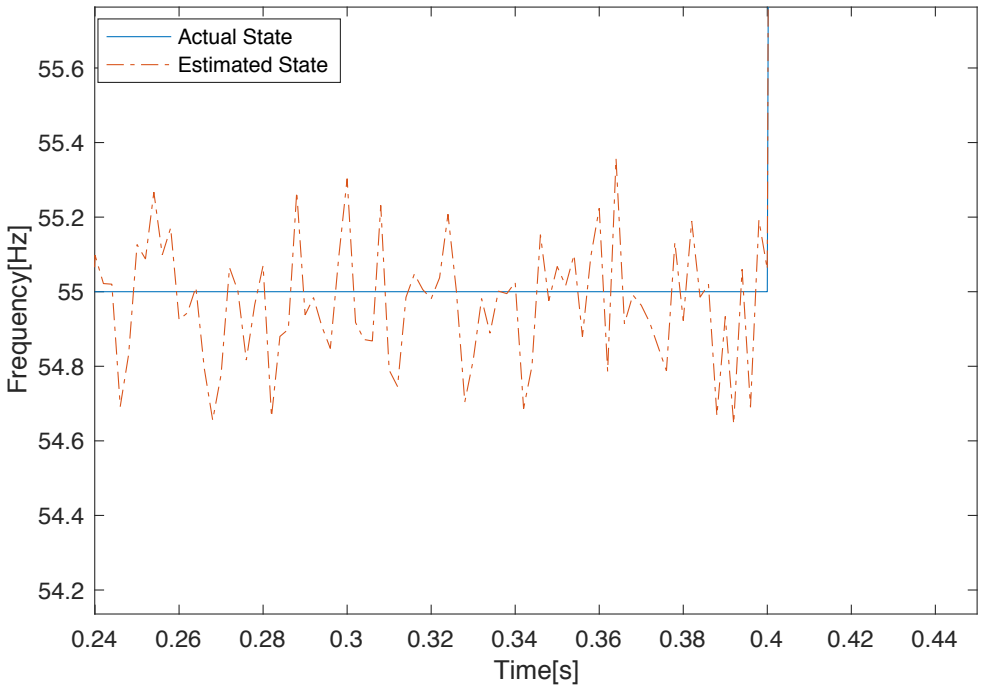

Figure 23 Lower part of step change

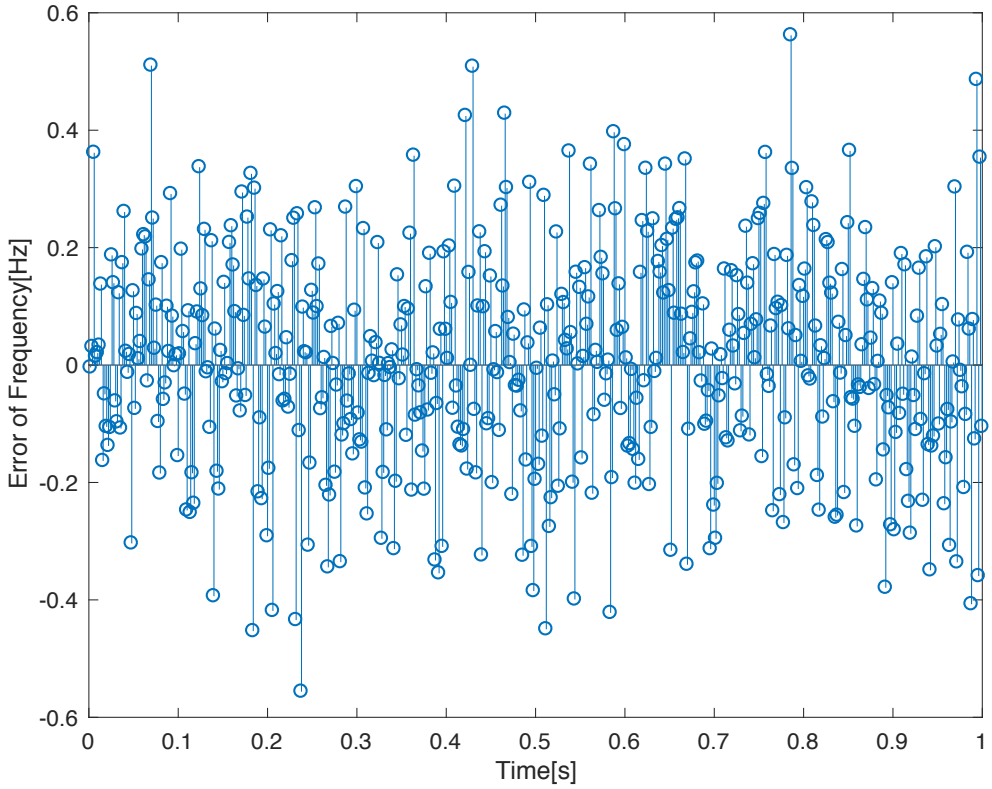

Figure 24 Errors between actual and estimated frequency for linear change

On the other hand, we can get the coefficient magnitudes $A_1, B_1, A_2, B_2,\ A_3$ and B_3. In figure 25 and 26, they are the estimated value compared with the actual value. Moreover, the tracking accuracy of the magnitude is expressed as a percentage in figure 27.

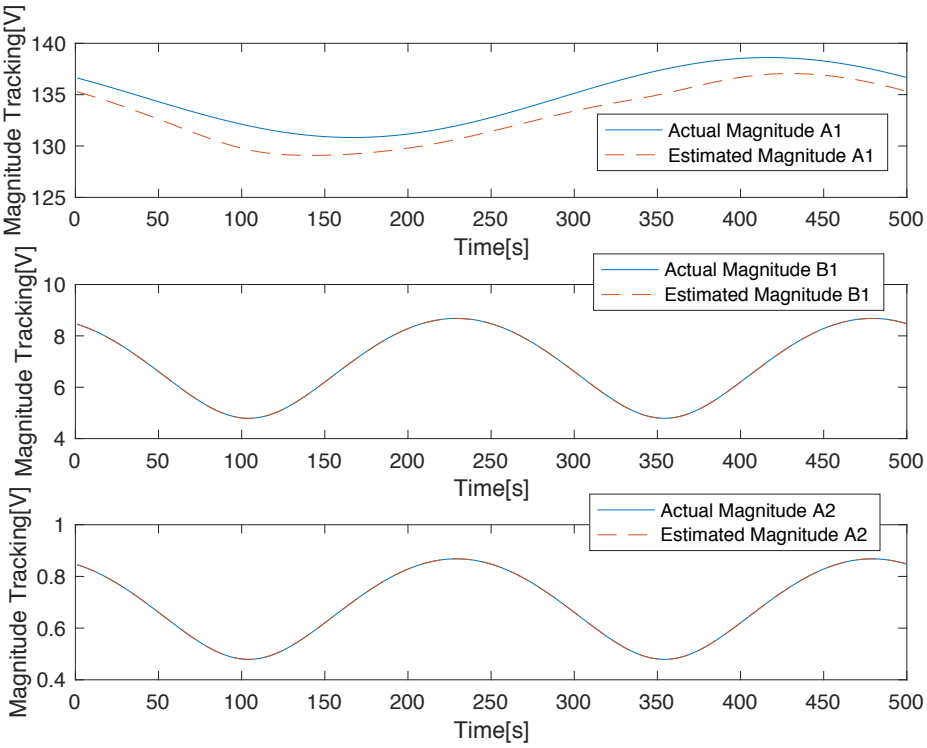

Figure 25 Errors between actual and estimated magnitude of A_1, B_1, A_2

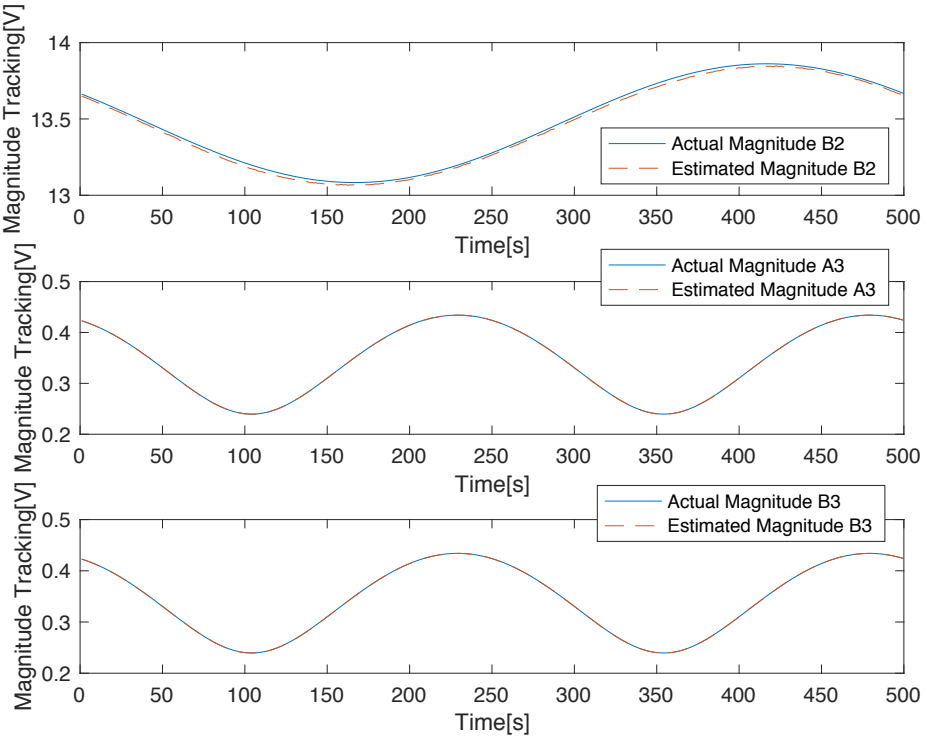

Figure 26 Errors between actual and estimated magnitude of B_2, A_3, B_3.

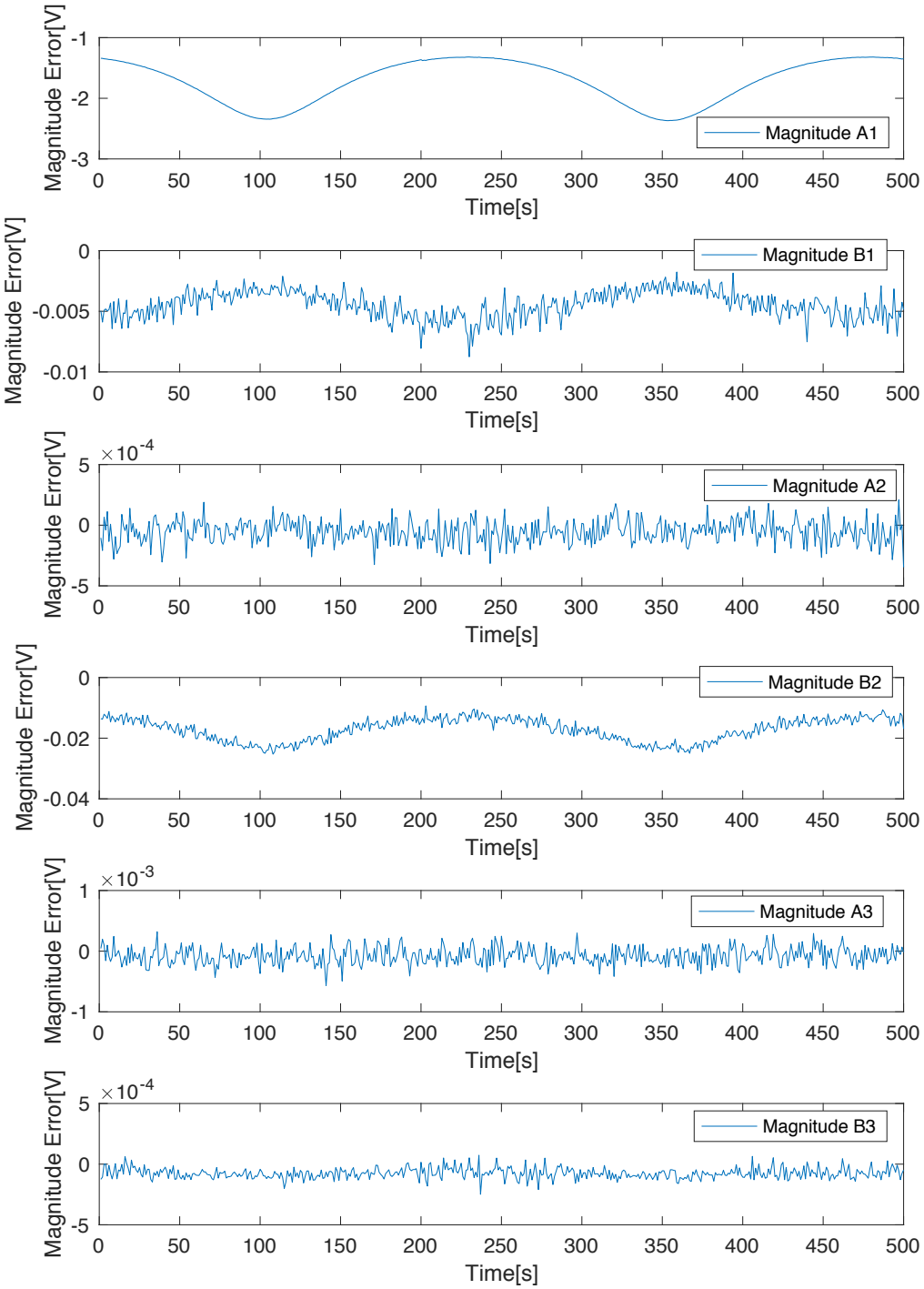

Figure 27 Error gaps of the coefficient magnitude

In the above three figures, all the parameters and comparisons are absolute values. In order to get a direct view of the magnitude errors, the percentage errors are shown in figure 28.

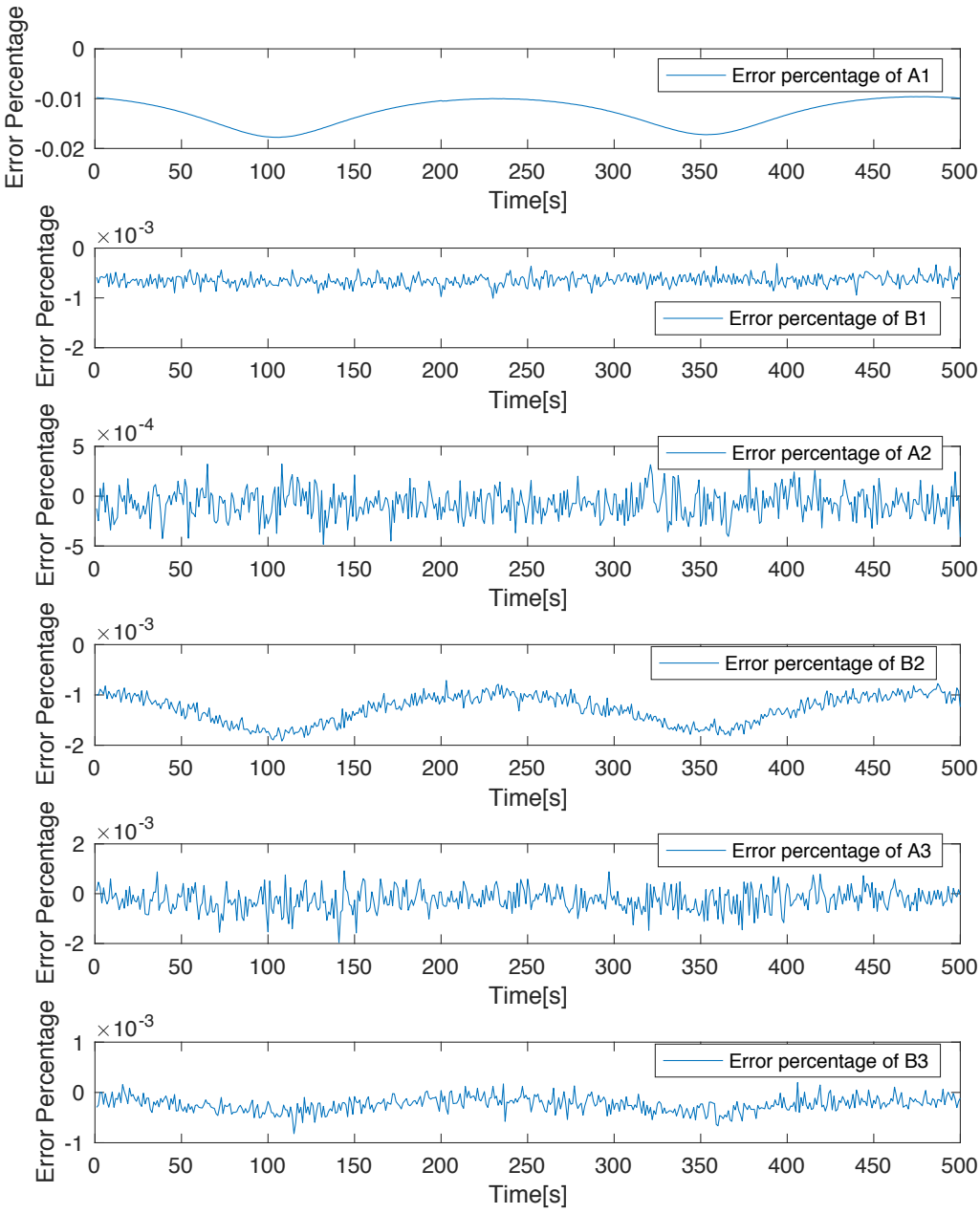

Figure 28 Magnitude error as a percentage

5.3 Experiment 2

In this experiment, we set the amplitudes of the fundamental frequency phase A, phase B and phase C respectively to

$$V_{a1} = 110 \times (1.05 + 0.05\sin(2\pi t)),$$

$$V_{b1} = 110 \times \left(1.1 + 0.1\sin\left(2\pi t - \frac{2\pi}{3}\right)\right),$$

$$V_{c1} = \begin{cases} 55 \times \left(1.15 + 0.15\sin\left(2\pi t + \frac{2\pi}{3}\right)\right) & 100 \times T_s < t < 200 \times T_s \\ 110 \times \left(1.15 + 0.15\sin\left(2\pi t + \frac{2\pi}{3}\right)\right) & \text{OW} \end{cases}$$

where $T_s = \frac{1}{500} s$

Meanwhile, the 2nd harmonic and 3rd harmonic are defined to be 10%, and 5% of the fundamental frequency amplitude. The amplitude waveforms of the fundamental frequency and harmonics are shown in Figure 29.

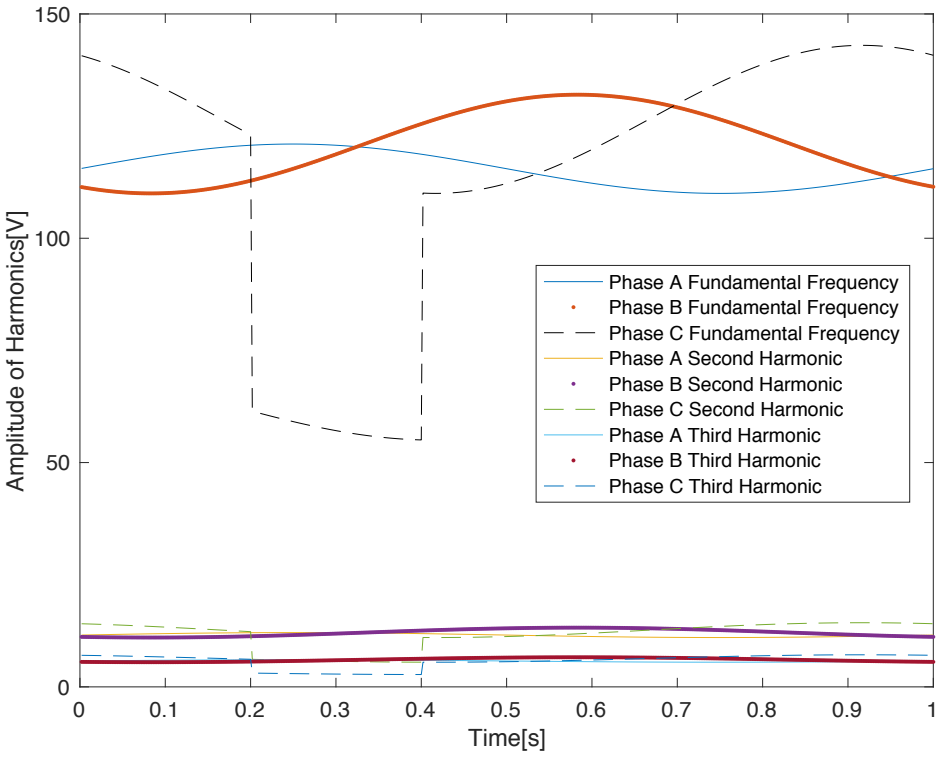

Figure 29 Amplitude of the fundamental frequency and harmonics

5. 3. 1 Linear frequency change results

In the experiment, we have the same input in Figure 1. The estimated state tracks the actual frequency change accurately and the errors are displayed in Figure 30. We can see that the maximum error is at sample 63, and the proportion of error and current frequency is $0.5918/55 = 0.0108$. Furthermore, the RMSE over 500 independent runs for a linear variation in frequency is 0.1727.

$$RMSE = \sqrt{\frac{1}{500} \times \sum_{500}^{1} (f_{est} - f_{actual})^2} = 0.1727$$

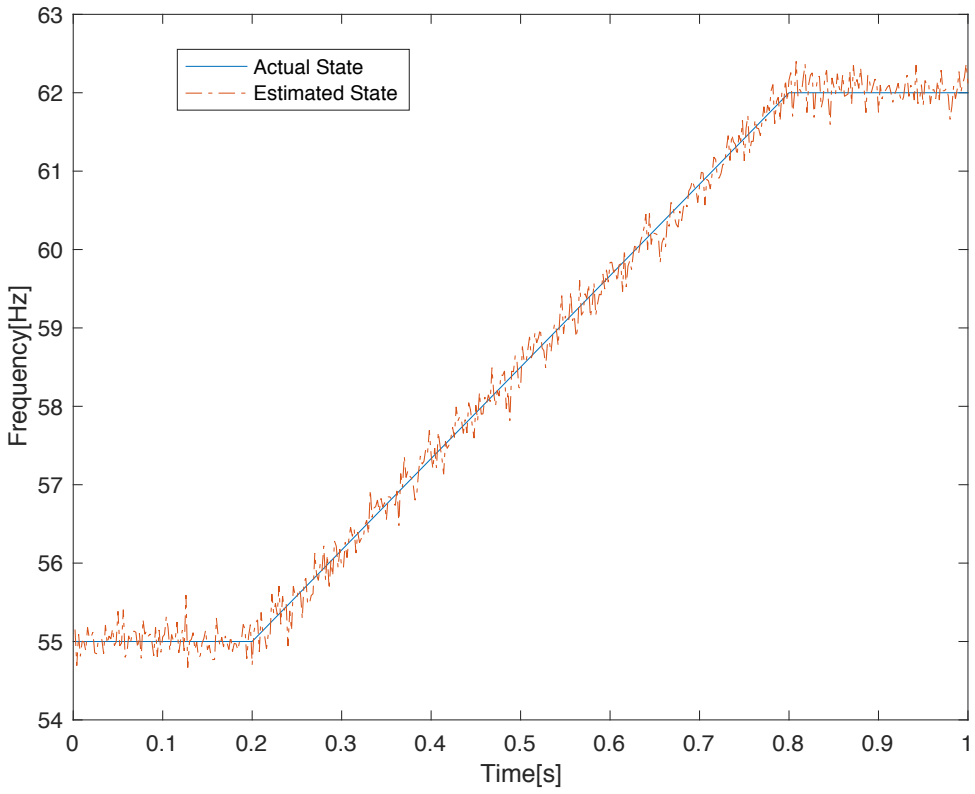

Figure 30 Linear frequency change

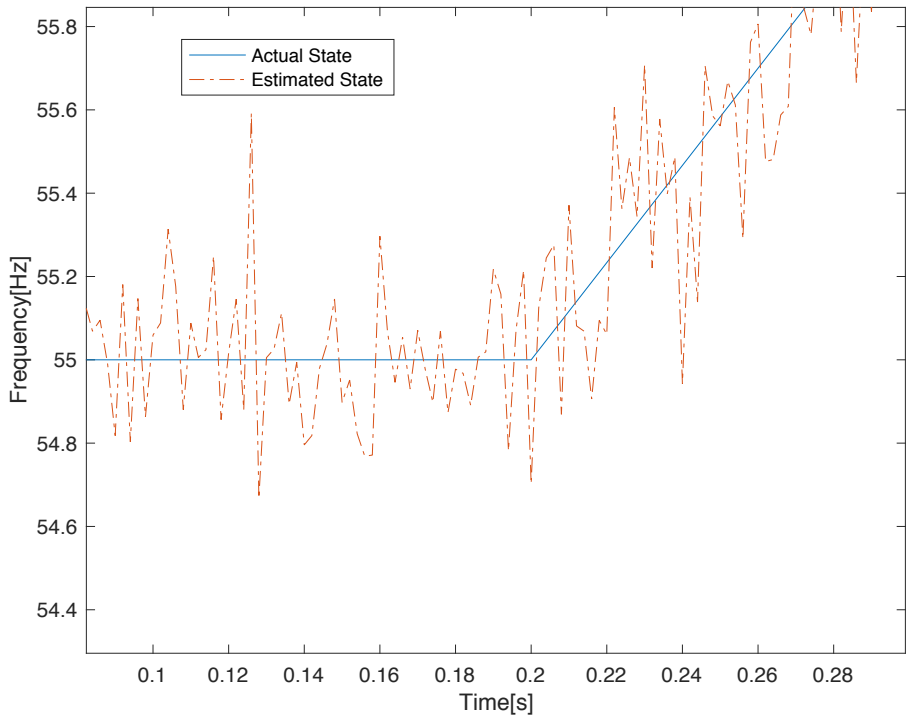

Figure 31 Linear frequency tacking around t = 0.2s

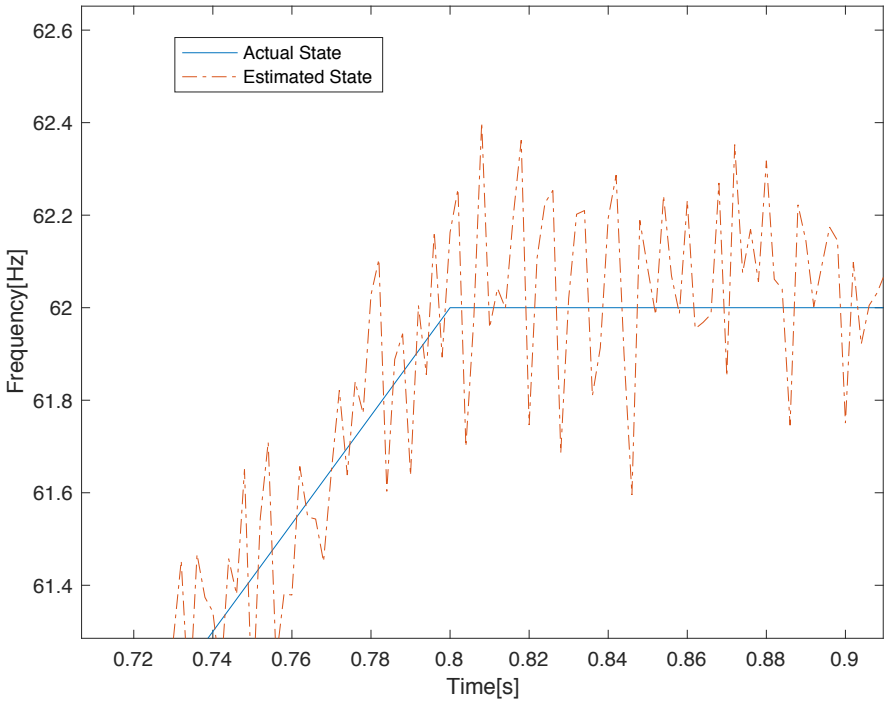

Figure 32 Linear frequency tracking around t = 0.8s

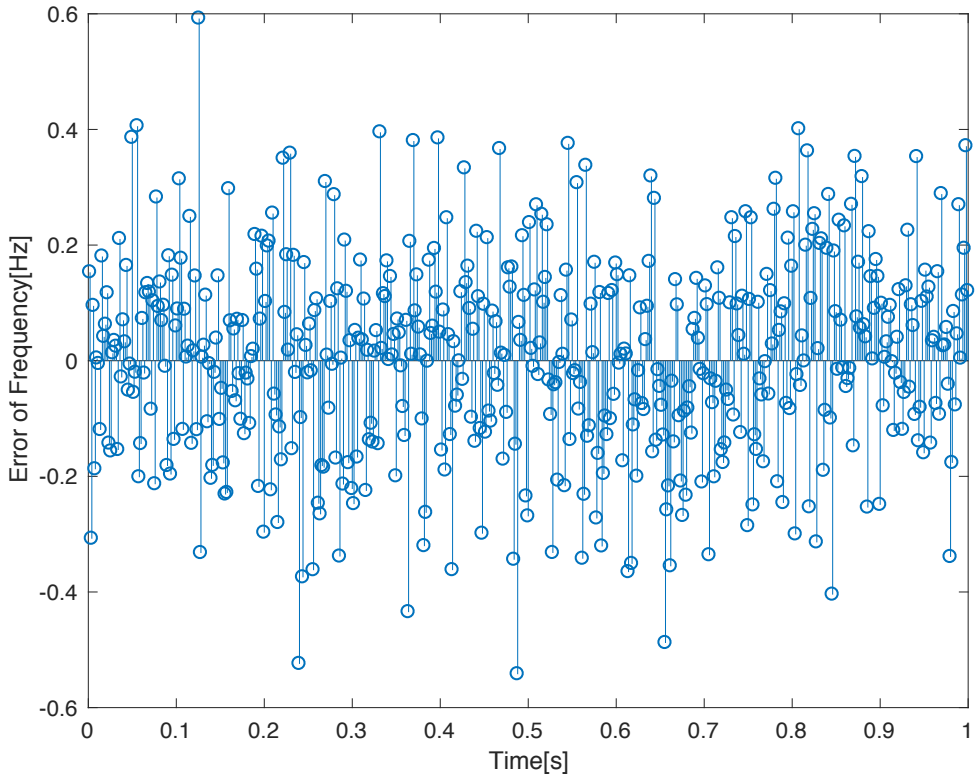

Figure 33 Errors between actual and estimated frequency for linear change

For the estimation of the amplitudes, based on the linear frequency input and sharply amplitude change, the tracking results of magnitude are showed in figure 34 and 35.

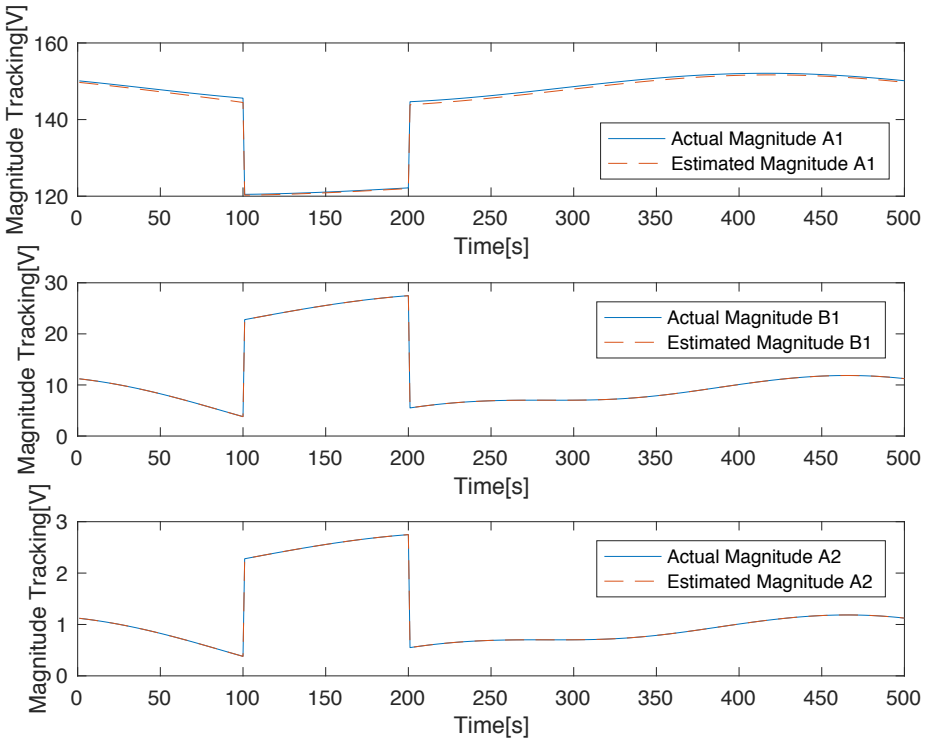

Figure 34 Errors between actual and estimated magnitude of A_1, B_1, A_2

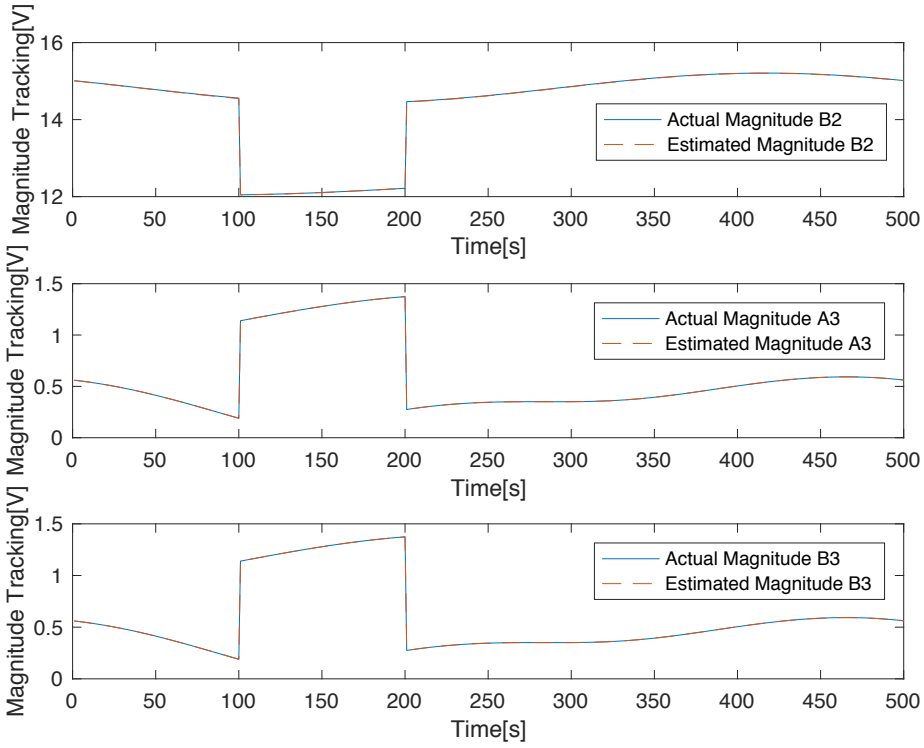

Figure 35 Errors between actual and estimated magnitude of B_2, A_3, B_3.

Furthermore, the true errors between actual and estimated amplitude at each time sampling instant are plotted in figure 36.

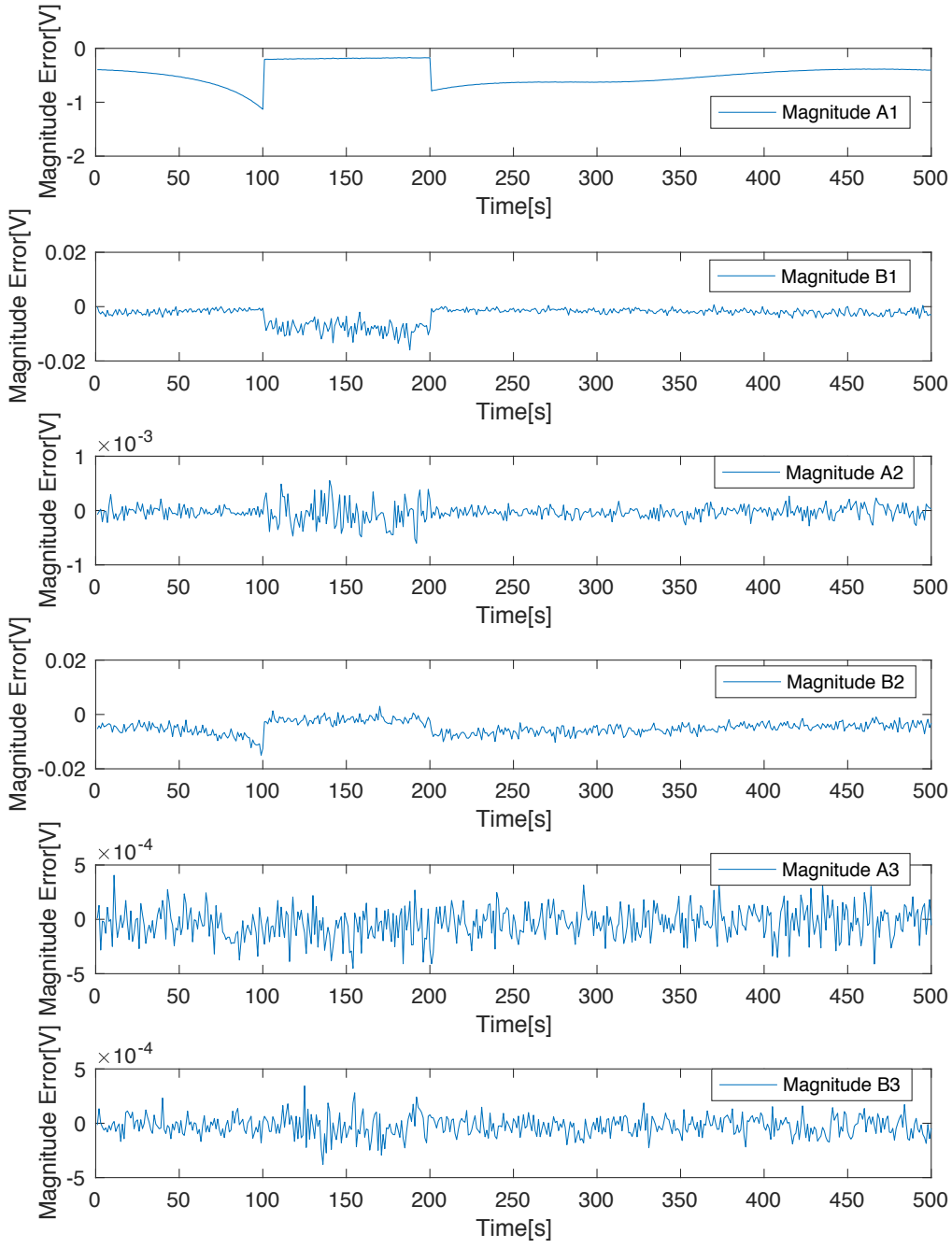

Figure 36 Error gaps of the coefficient magnitude

The direct views of the performances of the amplitude estimation are listed in figure 37. We could easily observe the error magnitude of coefficient.

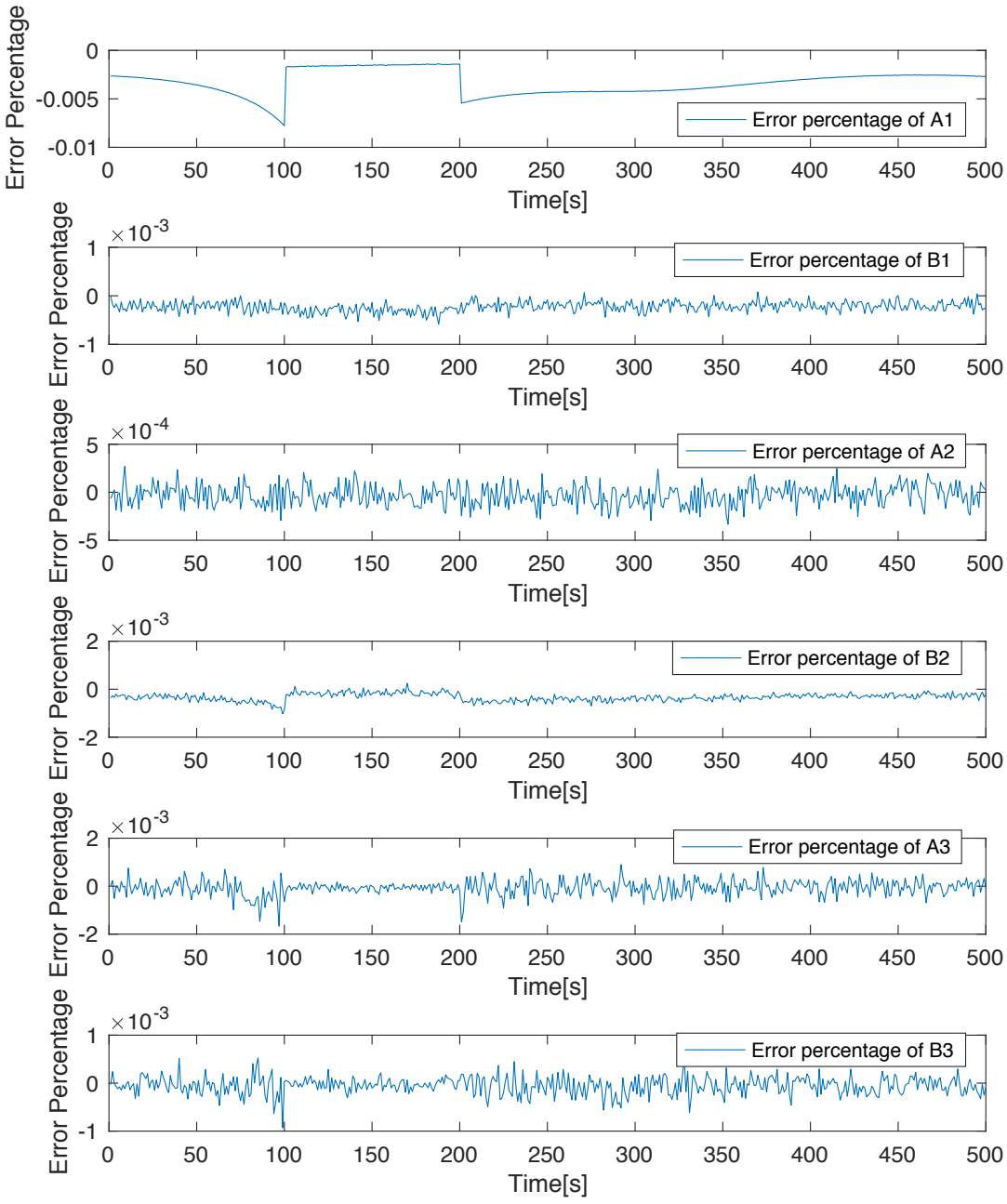

Figure 37 Magnitude error as a percentage

5.3.2 Step frequency change results

In this case, under the same initial conditions, we estimate the frequency and amplitude of the fundamental frequency, the 2nd harmonic and the 3rd harmonic. The estimated and actual frequency are shown in figure 38. We can se in figure 39 that the convergence time is negligible. Figure 41 presents the errors of every run and the maximum percentage error is $0.5886/62 = 0.0095$ at sample point 330. Integrating the errors, we have the RMSE in this experiment is 0.1772.

$$RMSE = \sqrt{\frac{1}{500} \times \sum_{500}^{1} (f_{est} - f_{actual})^2} = 0.1772$$

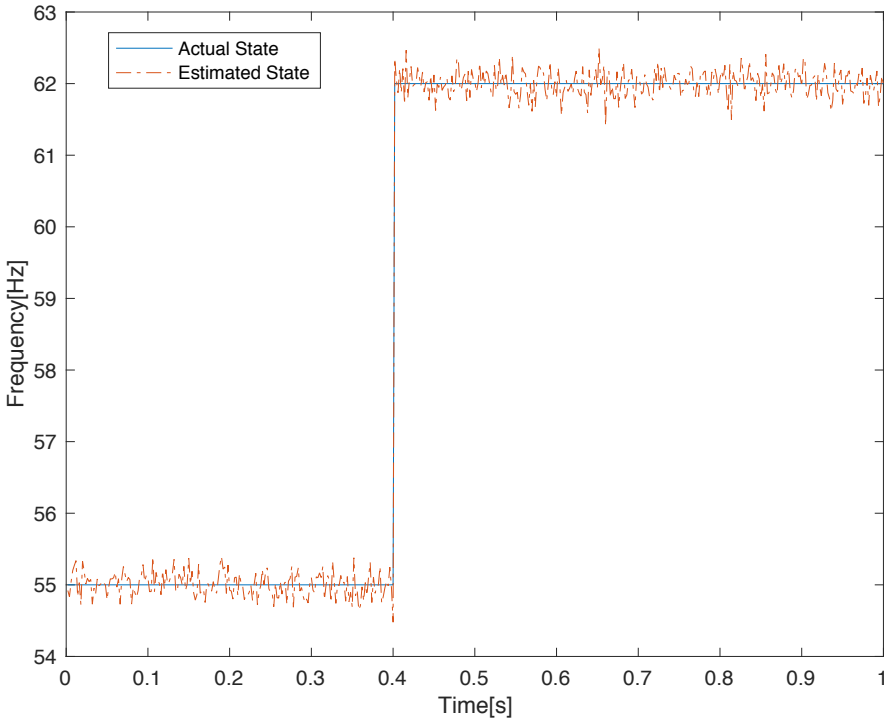

Figure 38 Step change of the fundamental frequency from 55Hz to 62Hz

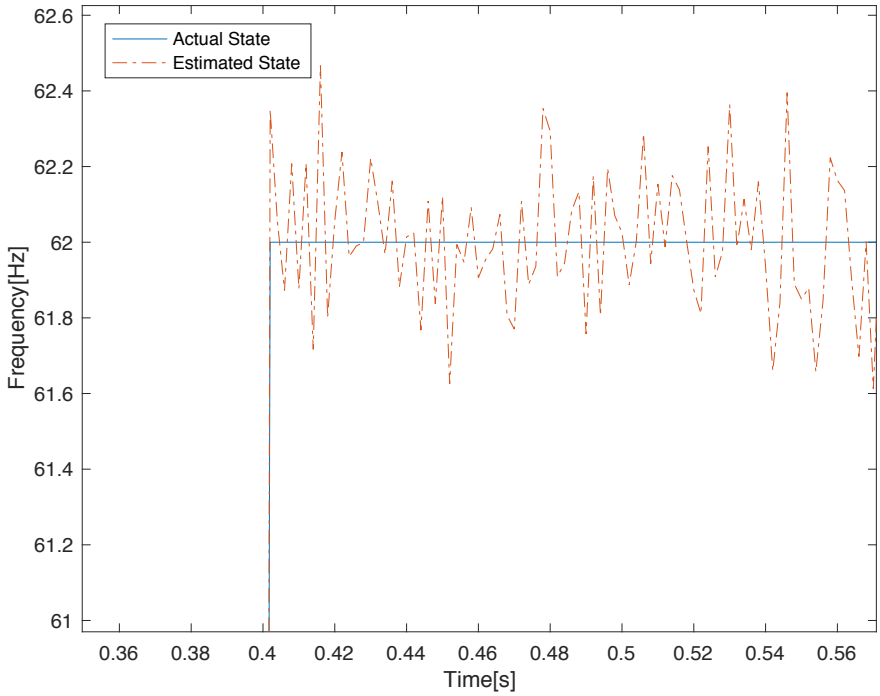

Figure 39 Upper part of step change

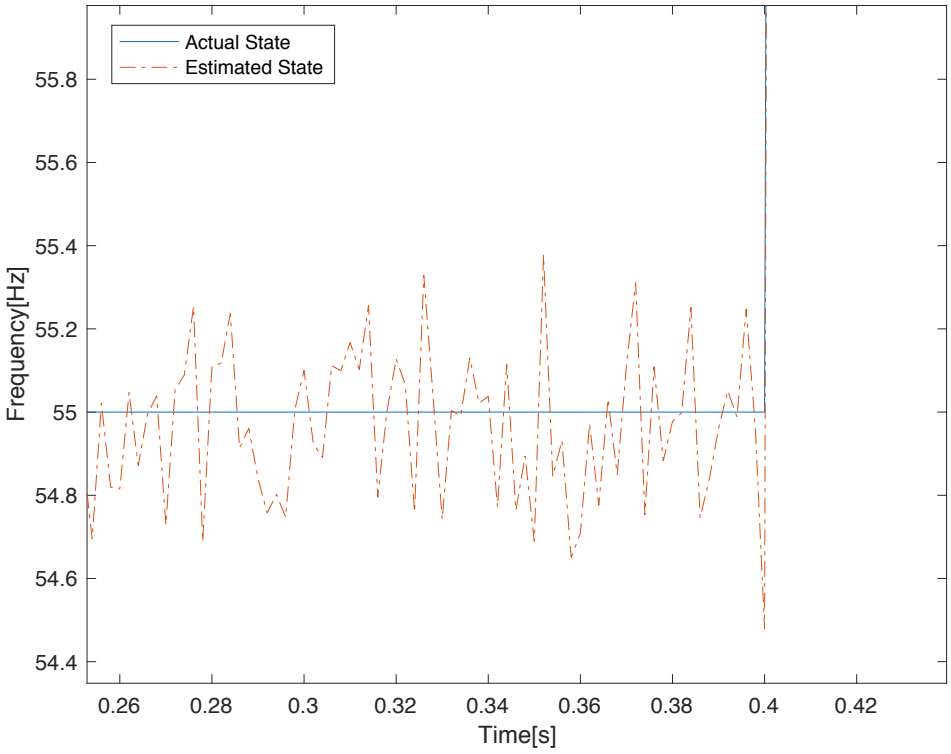

Figure 40 Lower part of step change

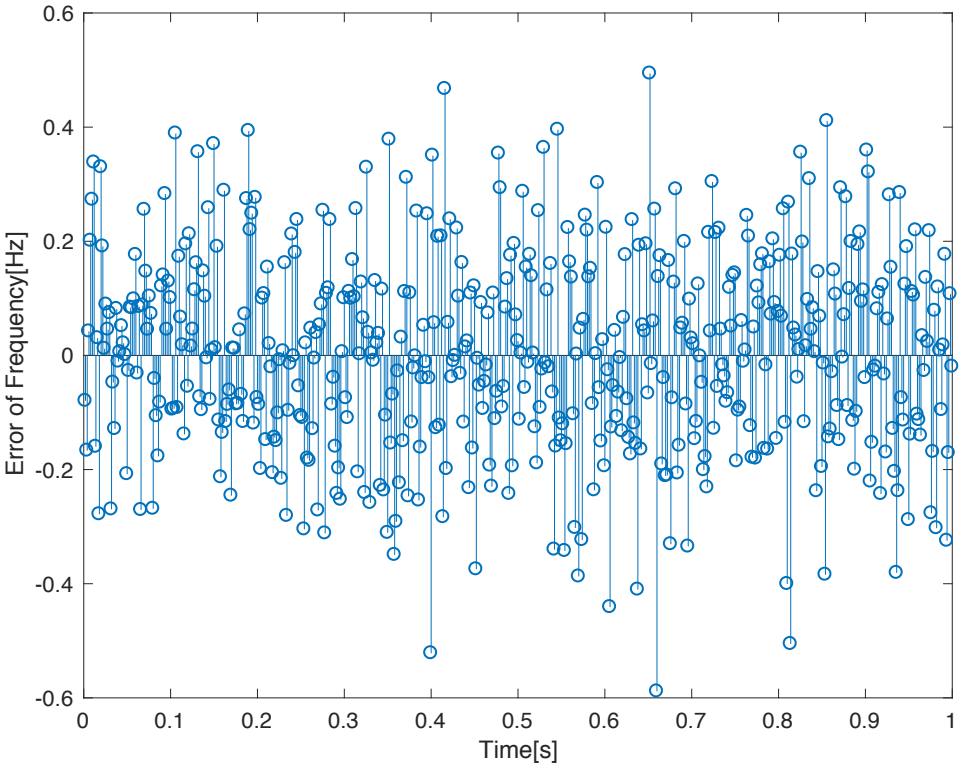

Figure 41 Errors between actual and estimated frequency for step change

To observe the accuracy of estimation, in figure 42 and 43, the actual and estimated values are generated together.

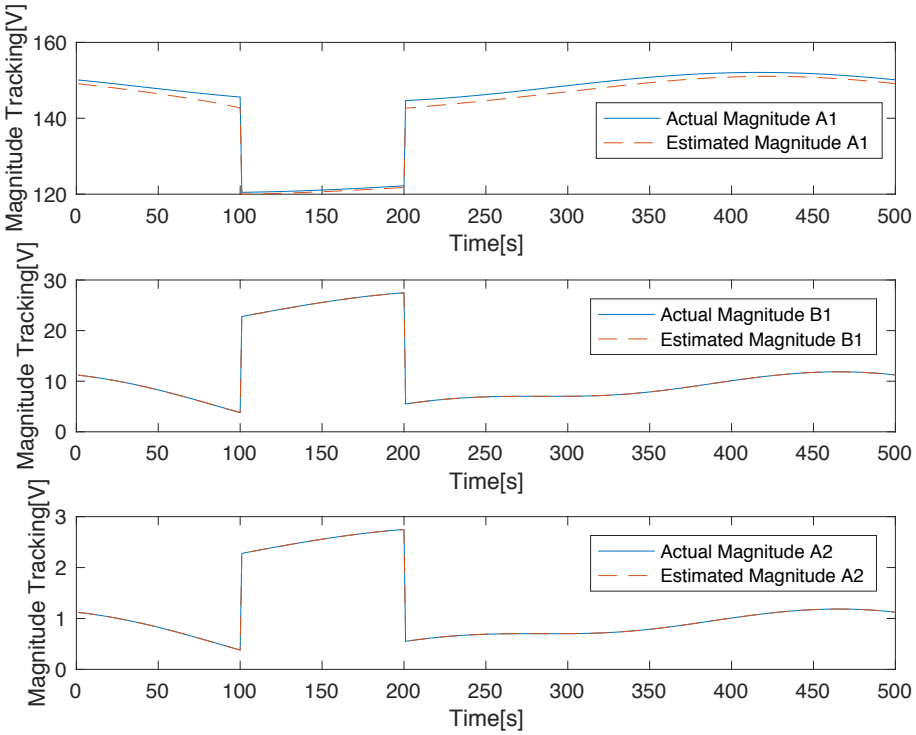

Figure 42 Errors between actual and estimated magnitude of A_1, B_1, A_2

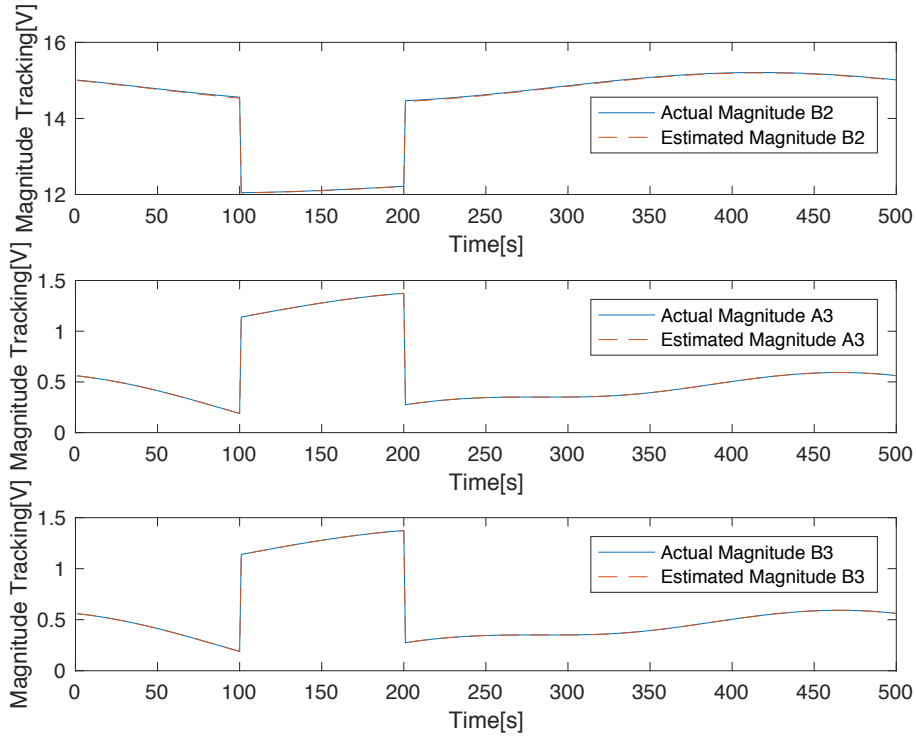

Figure 43 Errors between actual and estimated magnitude of B_2, A_3, B_3.

Moreover, the error gaps on each sampling instant are plotted in figure 44.

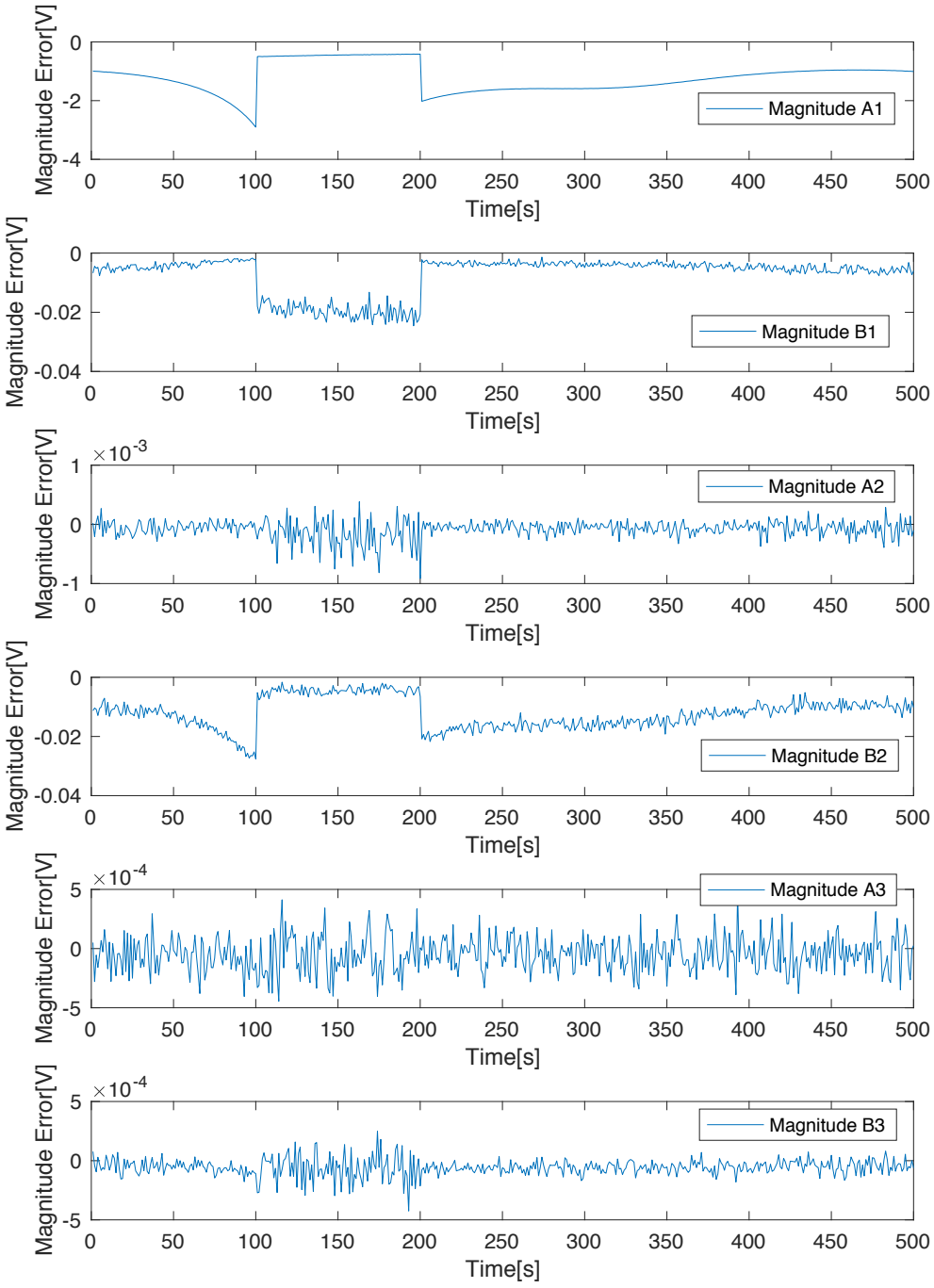

Figure 44 Error gaps of the coefficient magnitude

Compared with the error gaps, the direct view of the magnitude errors in percentage is plotted in figure 45. We can compare the amplitude errors among A_1, B_1, A_2, B_2, A_3 and B_3.

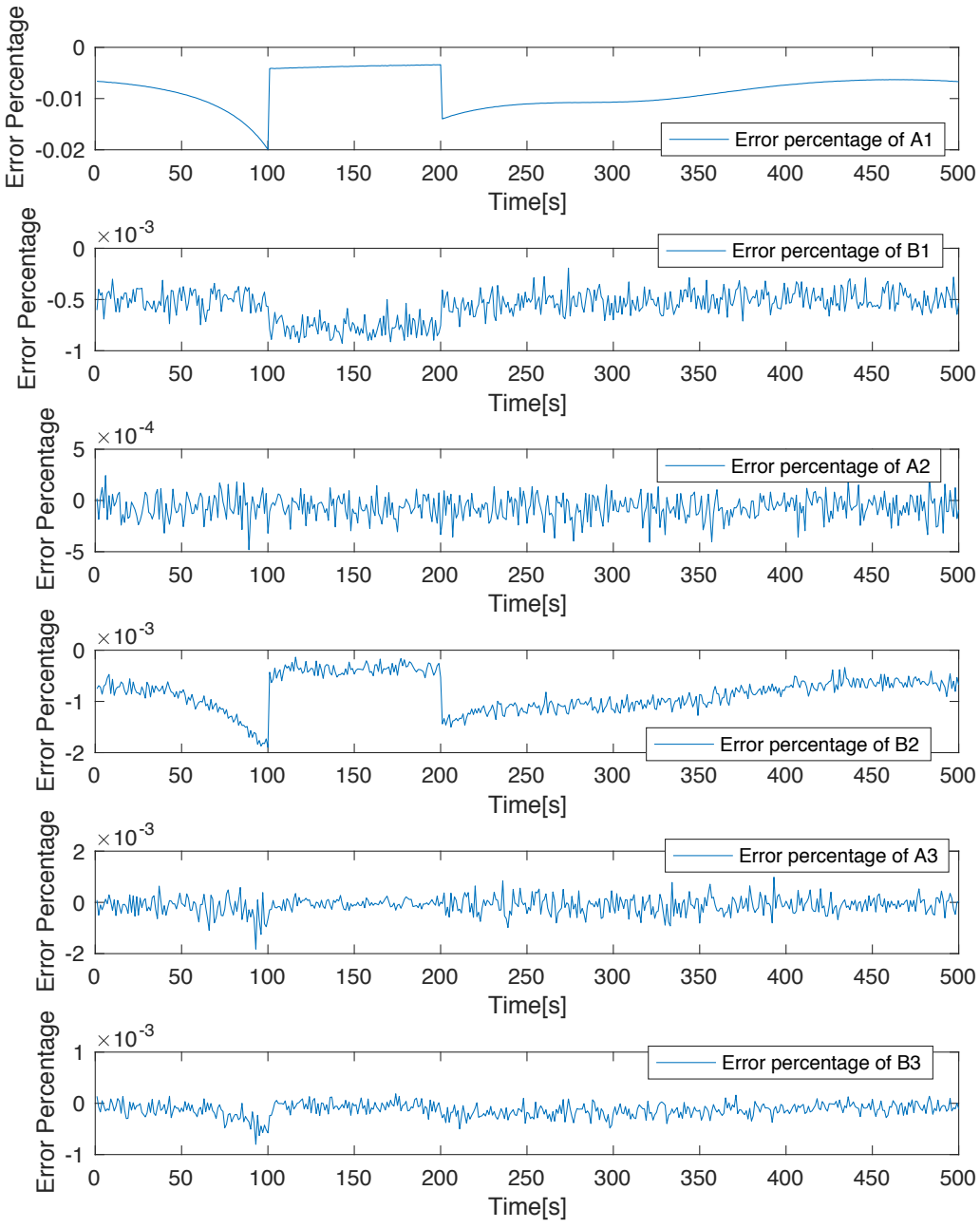

Figure 45 Magnitude error as a percentage

5.4 Experiment 3

Now we set the amplitudes of the fundamental frequency to in the case

$$V_{a1} = 110 \times (1.05 + 0.05\sin(2\pi t)),$$

$$V_{b1} = 110 \times \left(1.1 + 0.1\sin\left(2\pi t - \frac{2\pi}{3}\right)\right),$$

$$V_{c1} = \begin{cases} 110 \times \left(1.15 + 0.15\sin\left(2\pi t + \frac{2\pi}{3}\right)\right) & T_s < t < 100 \times T_s \\ 55 \times \left(1.15 + 0.15\sin\left(2\pi t + \frac{2\pi}{3}\right)\right) & \text{OW} \end{cases}$$

where $T_s = \frac{1}{500} s$.

At the same time, the 2nd harmonic and 3rd harmonic are defined to be 10%, and 5% of the fundamental frequency amplitudes. The amplitude waveforms of the fundamental frequency and harmonics are shown in Figure 46.

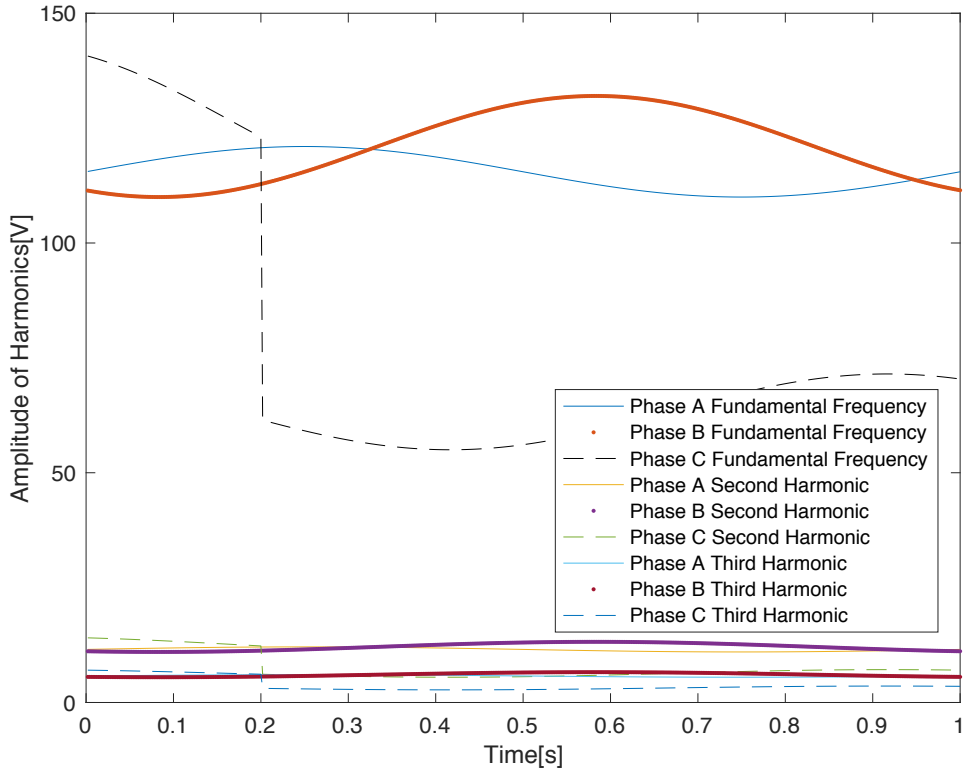

Figure 46 Amplitude of the fundamental frequency and harmonics

5.4.1 Linear frequency change results

In this experiment, the same input signal in Figure 1 is used here. The estimated state tracks the actual frequency change accurately as shown in figure 47. The amplitude errors are displayed in Figure 50. We can see that the maximum error is at sample 112, and the proportion of error and current frequency is $0.5904/55.2800 = 0.0107$. Furthermore, the RMSE over 500 independent runs for a linear variation in frequency is 0.1817.

$$RMSE = \sqrt{\frac{1}{500} \times \sum_{500}^{1} (f_{est} - f_{actual})^2} = 0.1817$$

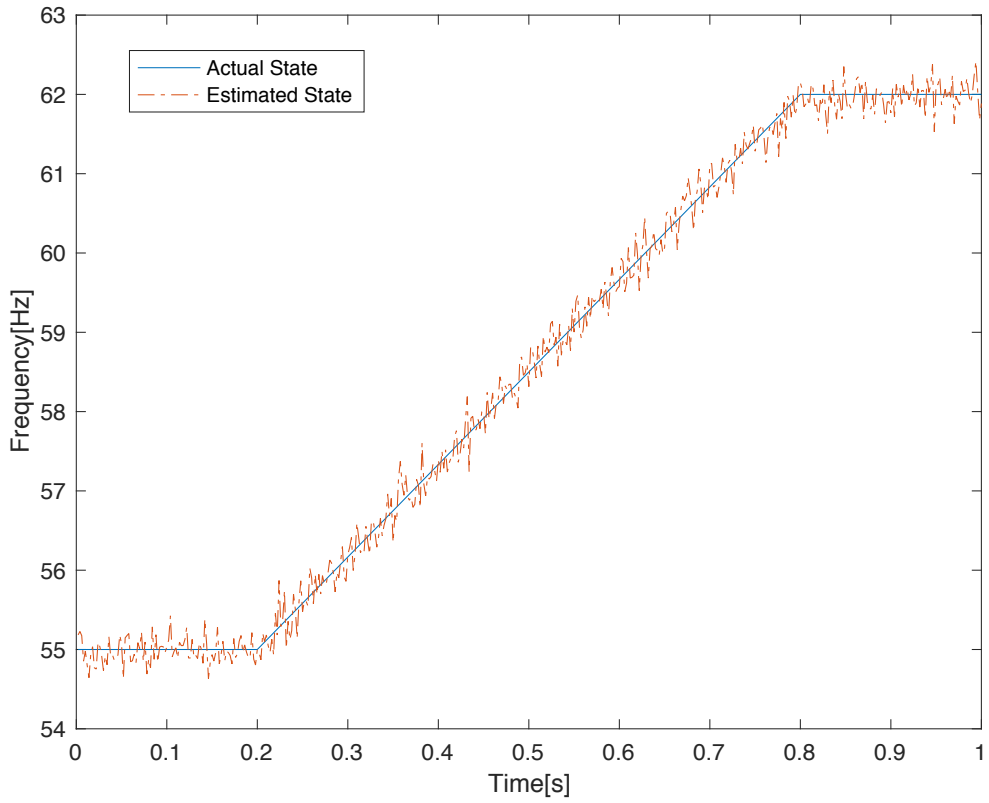

Figure 47 Linear frequency change

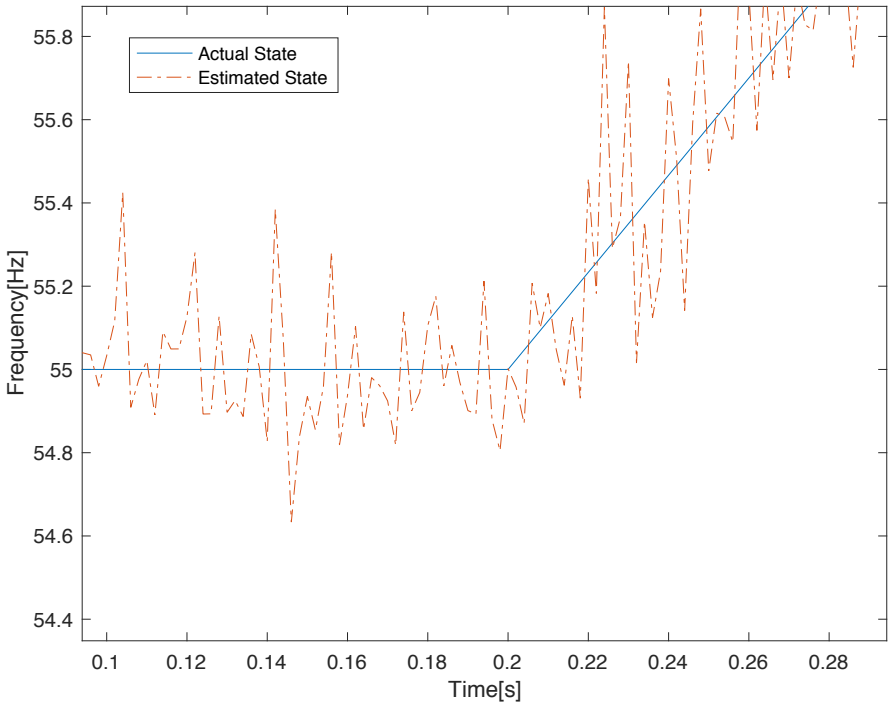

Figure 48 Linear frequency tracking around t = 0.2s

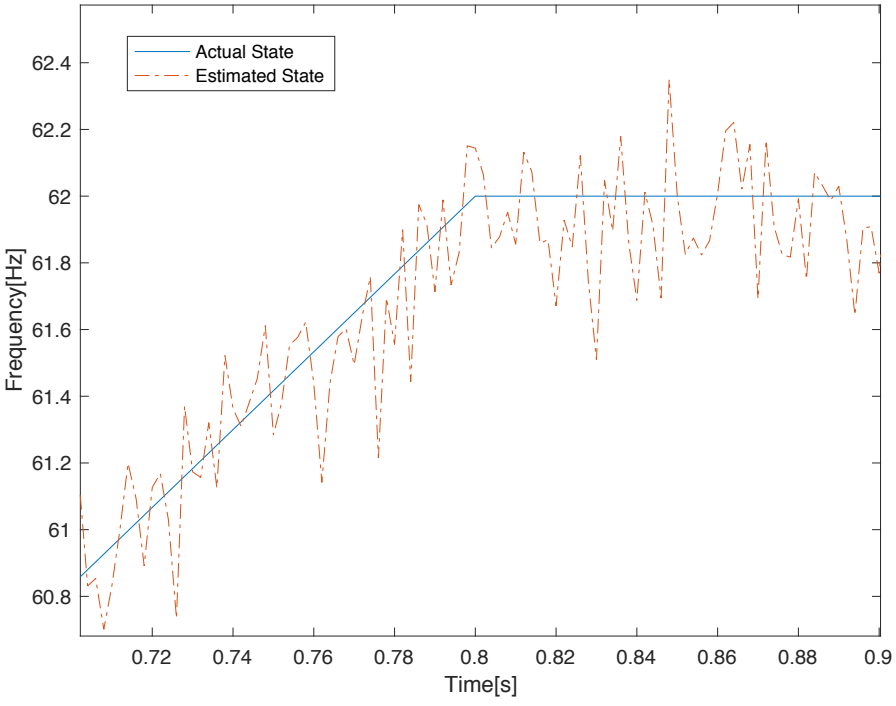

Figure 49 Linear frequency tracking around t = 0.8s

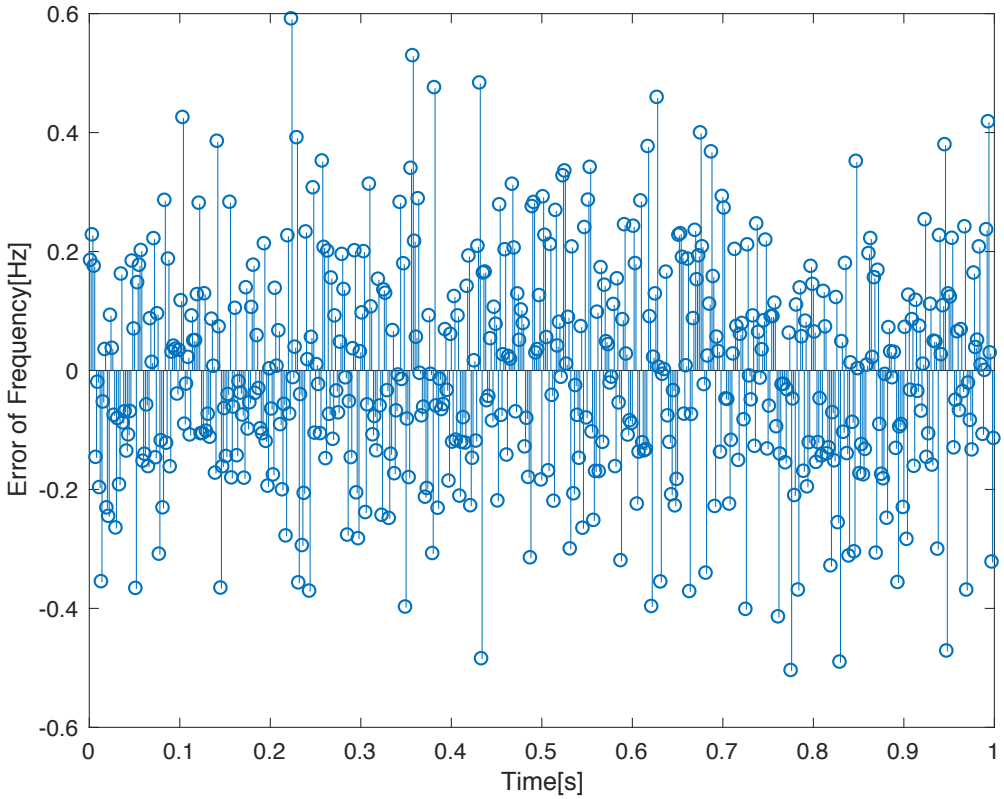

Figure 50 Errors between actual and estimated frequencies for linear change

In this situation, the actual and estimated amplitude are showed in figure 51 and 52.

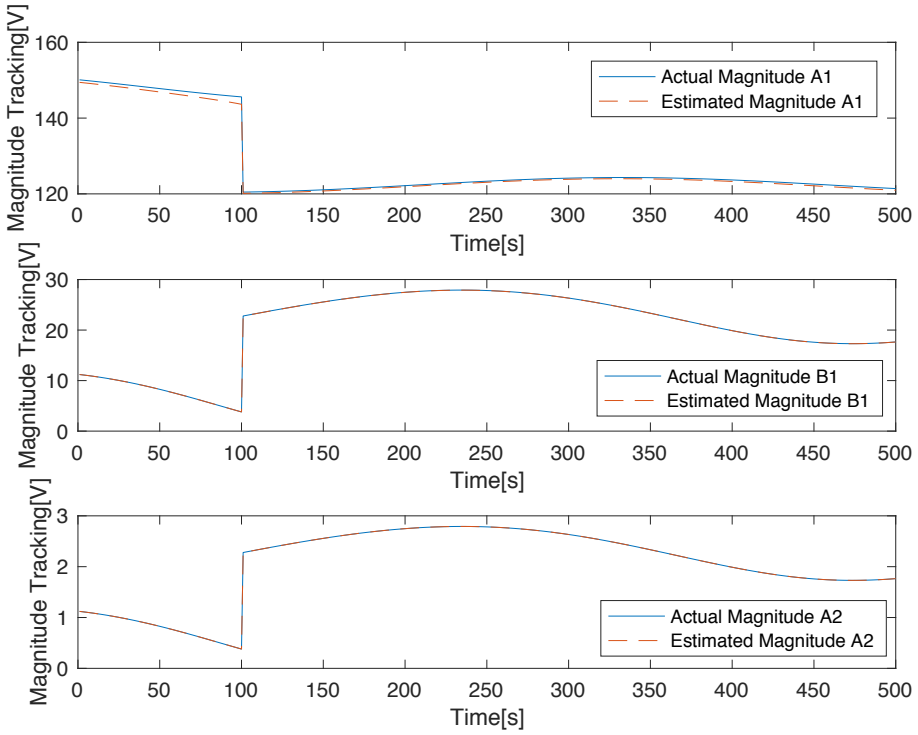

Figure 51 Errors between actual and estimated magnitude of A_1, B_1, A_2

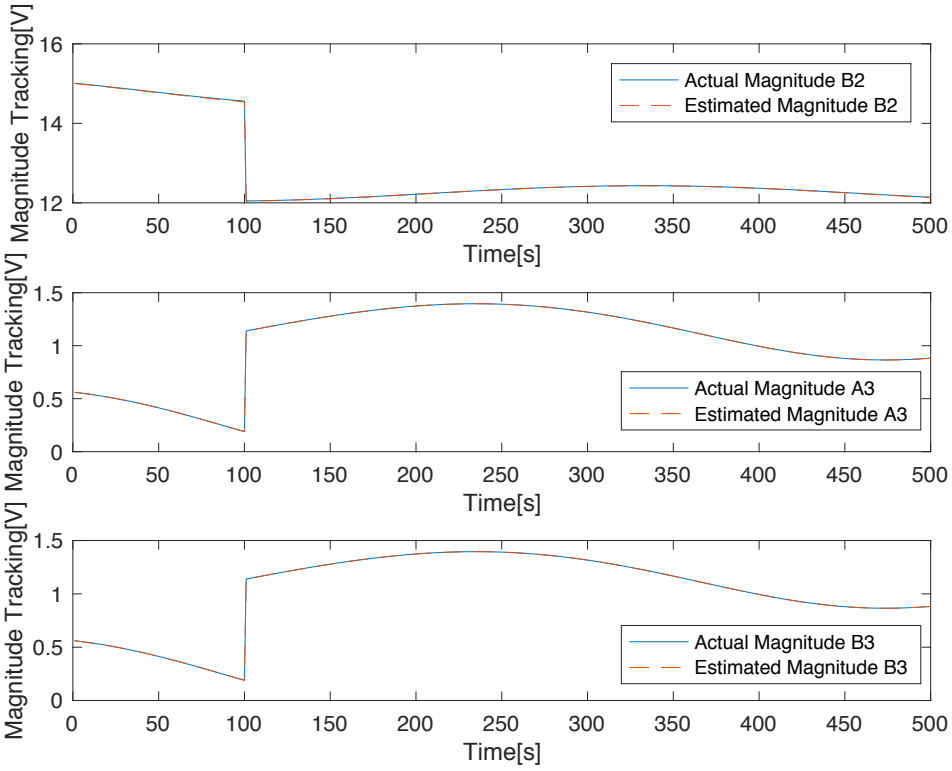

Figure 52 Errors between actual and estimated magnitude of B_2, A_3, B_3.

In order to show the amplitude error in every sampling instant, we plot them in figure 53.

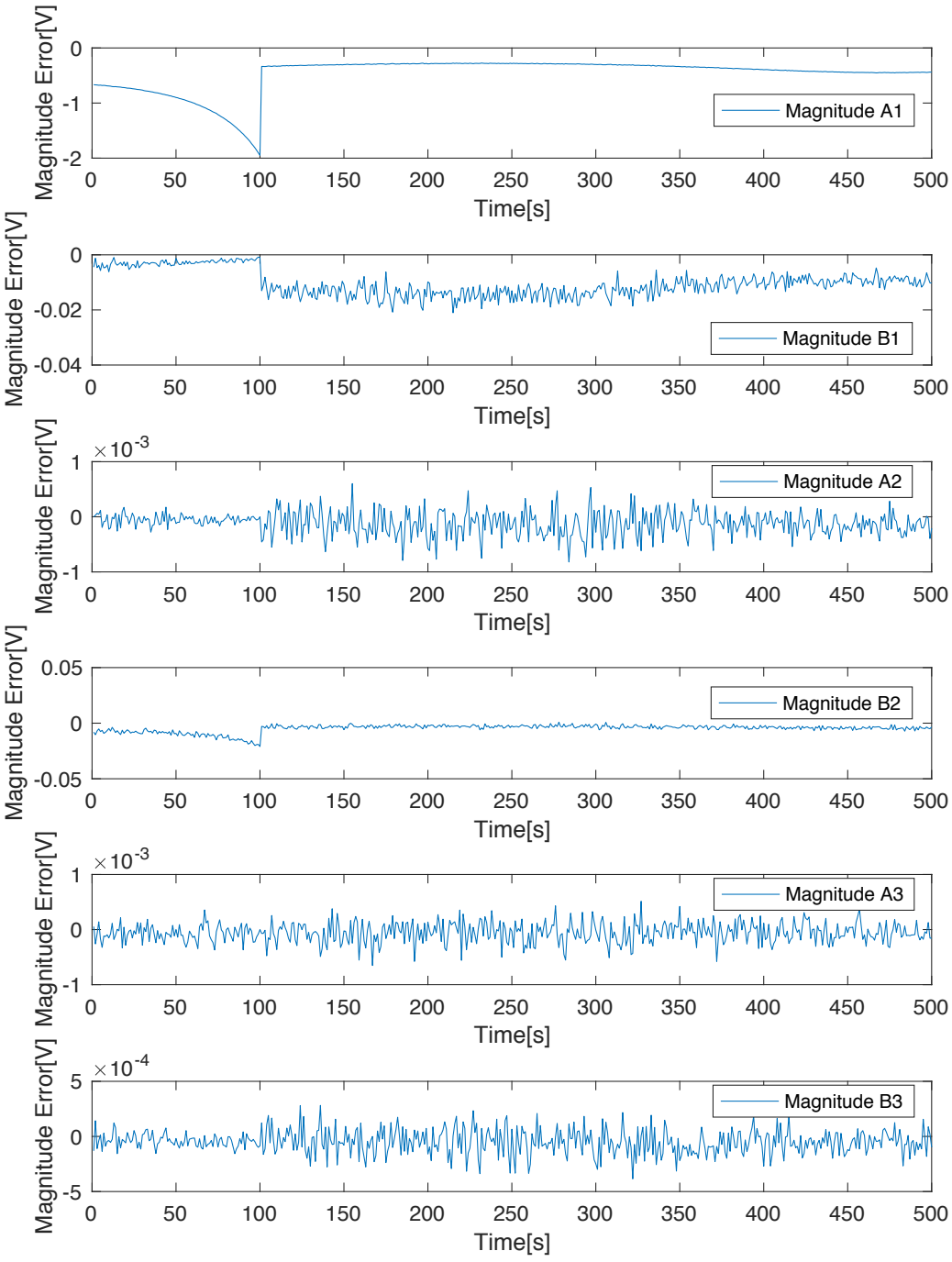

Figure 53 Error gaps of the coefficient magnitude

In figure 54, a direct view of the performances of the amplitude estimation is listed in percentage. We could easily observe the error coefficient magnitude.

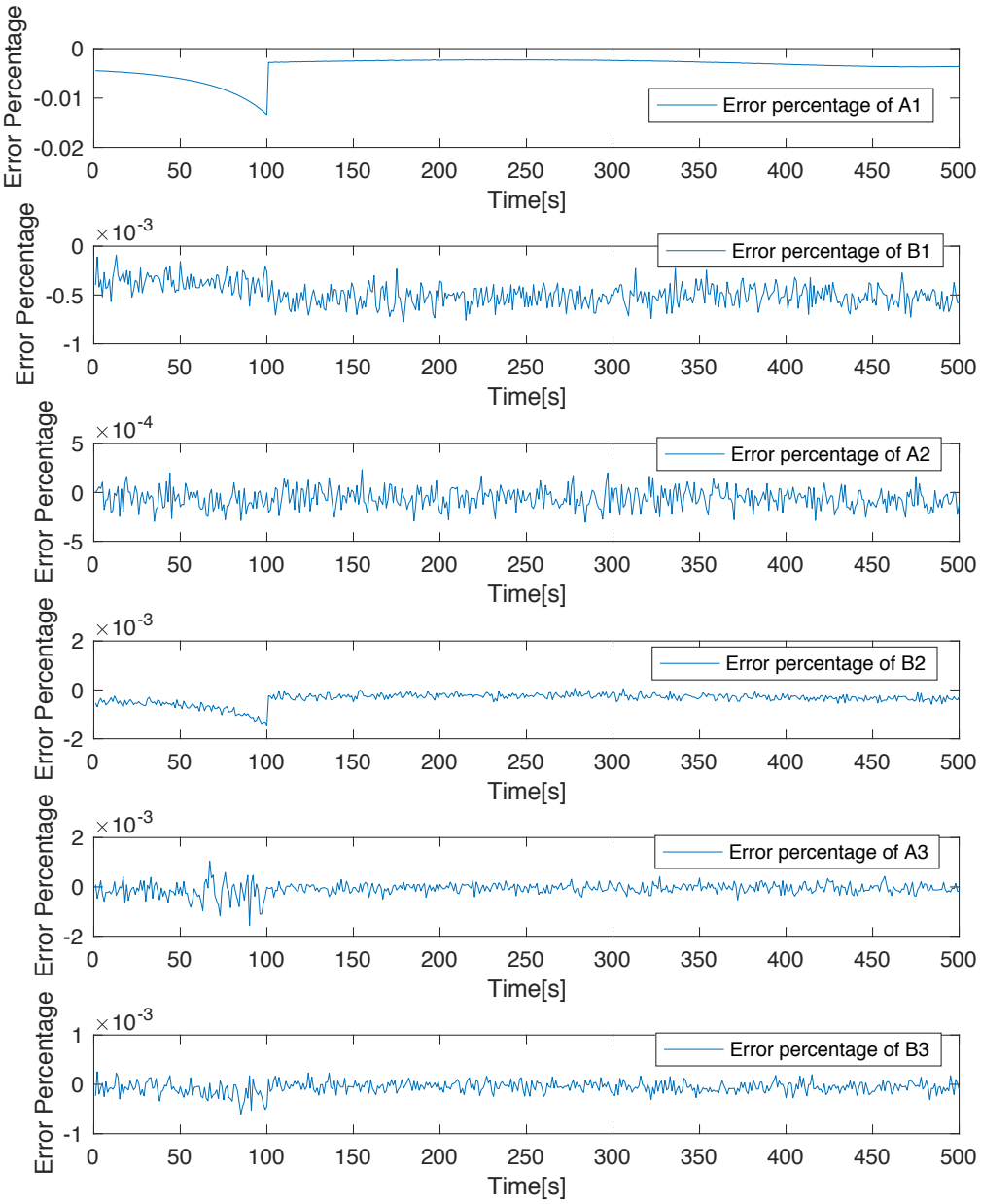

Figure 54 Magnitude error as a percentage

5.4.2 Step frequency change results

Under the step signal, we estimate the frequency and amplitude of the fundamental frequency, the 2nd harmonic and the 3rd harmonic. In figure 55, the frequency estimation is plotted and we can see in figure 56 that the convergence time is negligible. The maximum error is $0.5686/62 = 9.2\times10^{-3}$, which is presented at the 245th sampling instant in figure 49. Integrating the errors, we have the RMSE in this experiment is 0.1733.

$$RMSE = \sqrt{\frac{1}{500}\times\sum_{500}^{1}(f_{est}-f_{actual})^2} = 0.1733$$

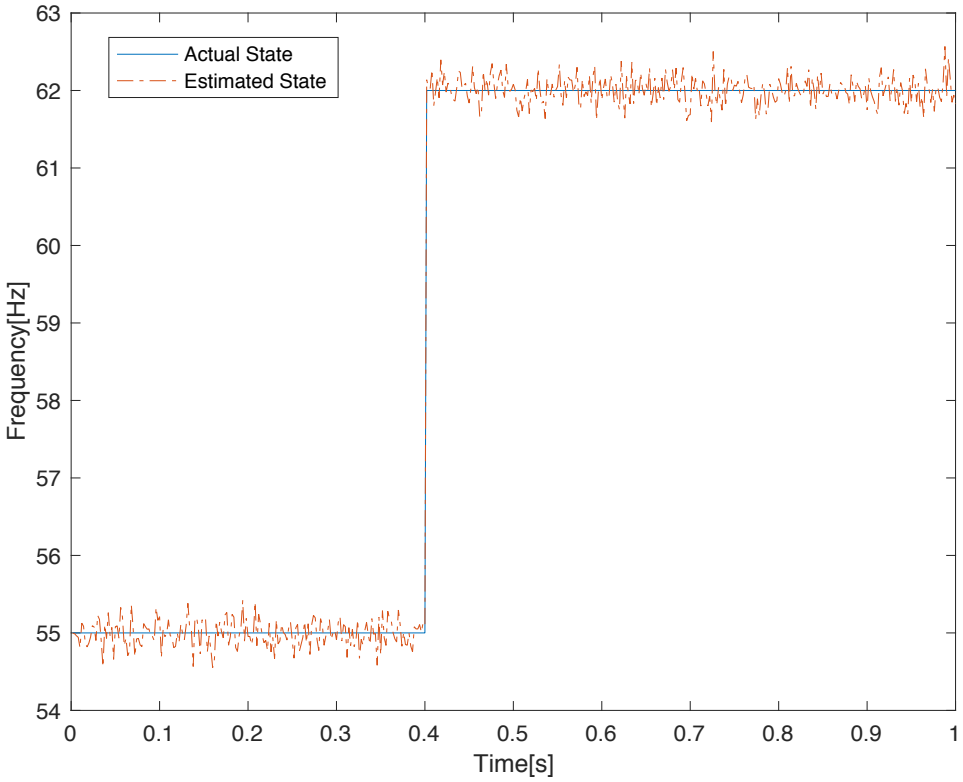

Figure 55 Step change of the fundamental frequency from 55Hz to 62Hz

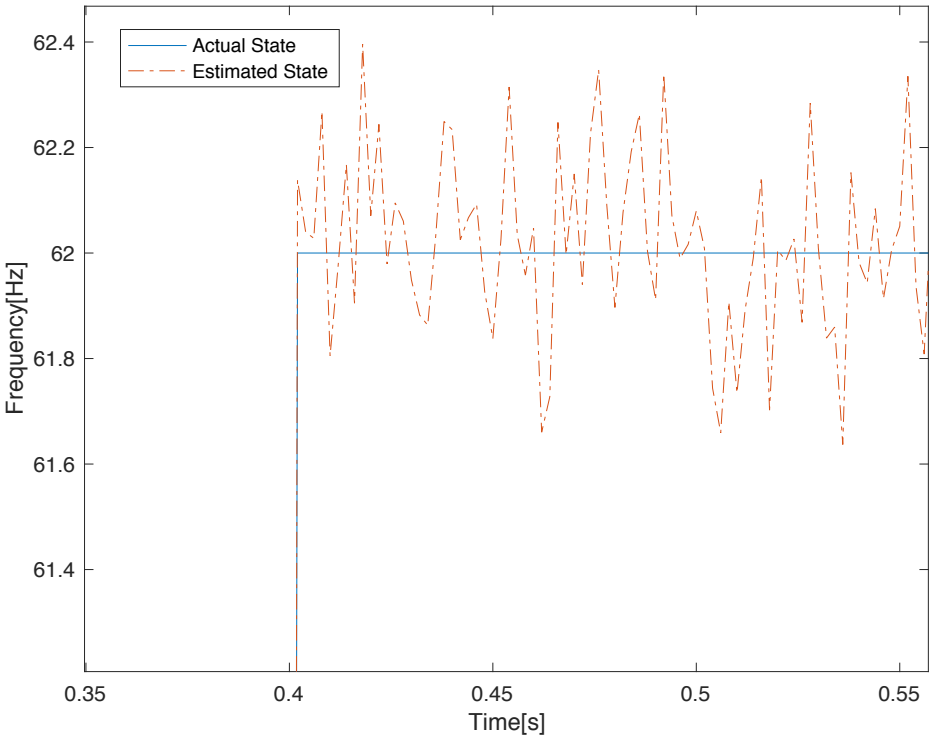

Figure 56 Top of step change

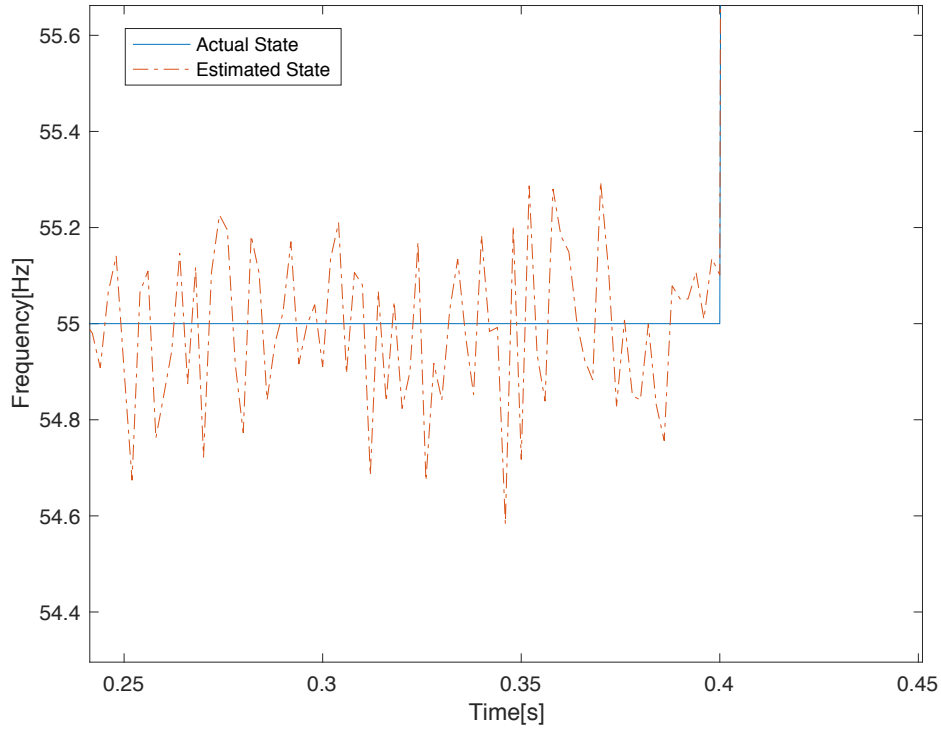

Figure 57 Bottom of step change

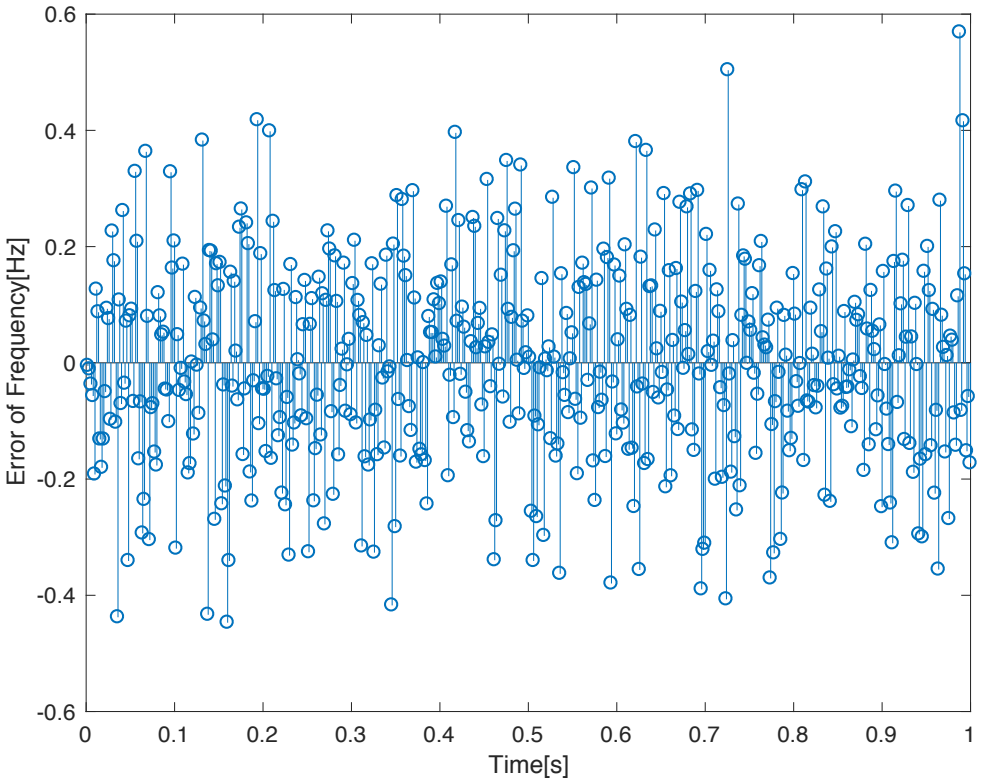

Figure 58 Errors between actual and estimated frequency for step change

In addition to the frequency estimation, we present the results of amplitude estimation under the same conditions. The estimation of complex coefficients is showed in figure 59.

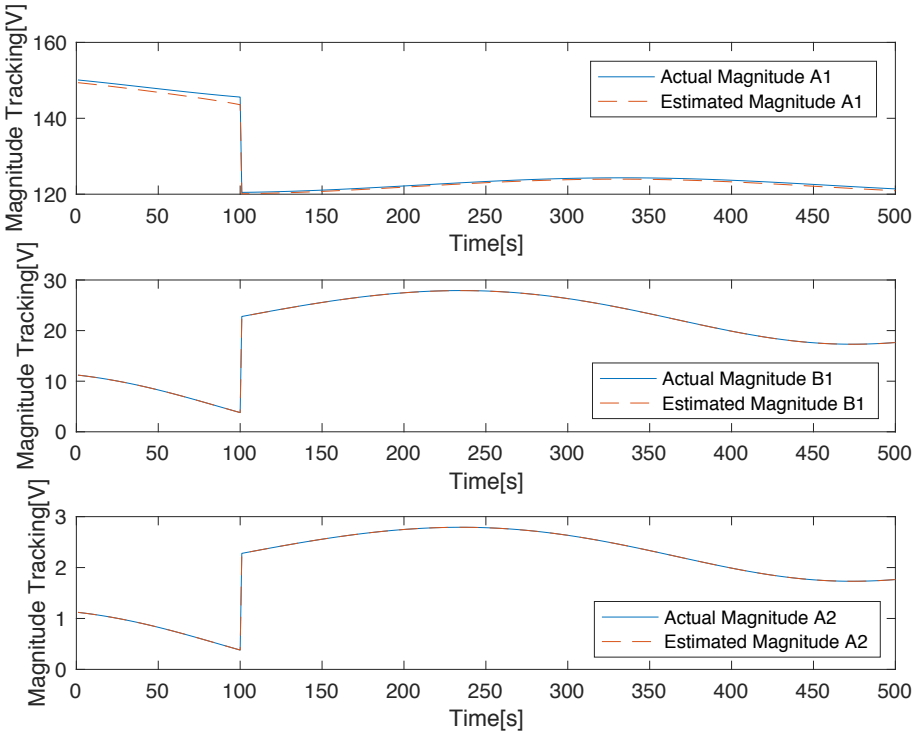

Figure 59 Errors between actual and estimated magnitude of A_1, B_1, A_2

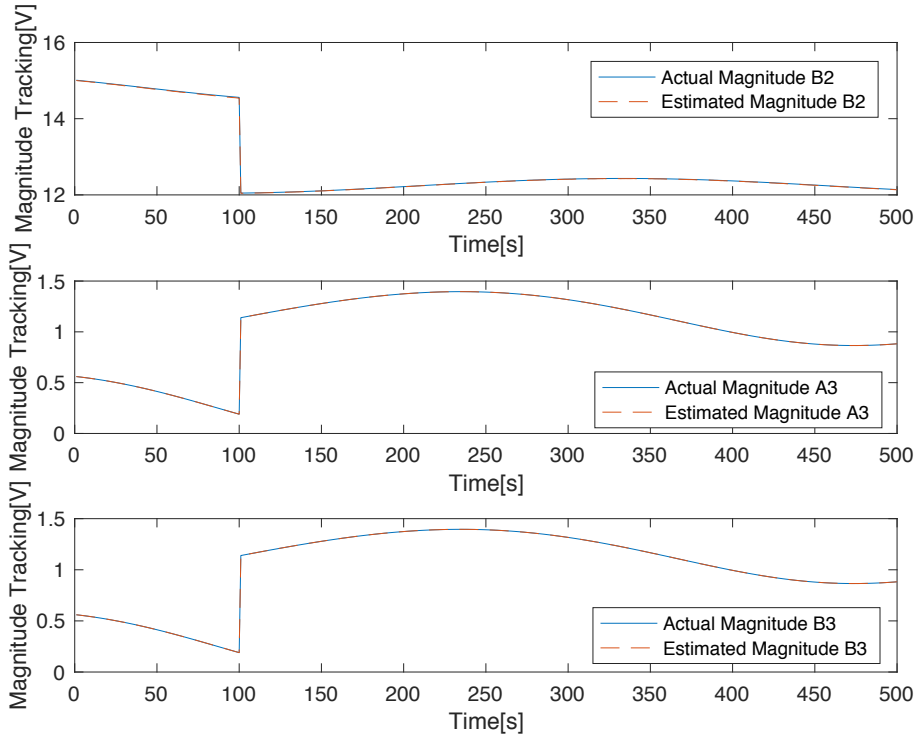

Figure 60 Errors between actual and estimated magnitude of B_2, A_3, B_3.

Meanwhile, the error gaps at each sampling instant are plotted in figure 61.

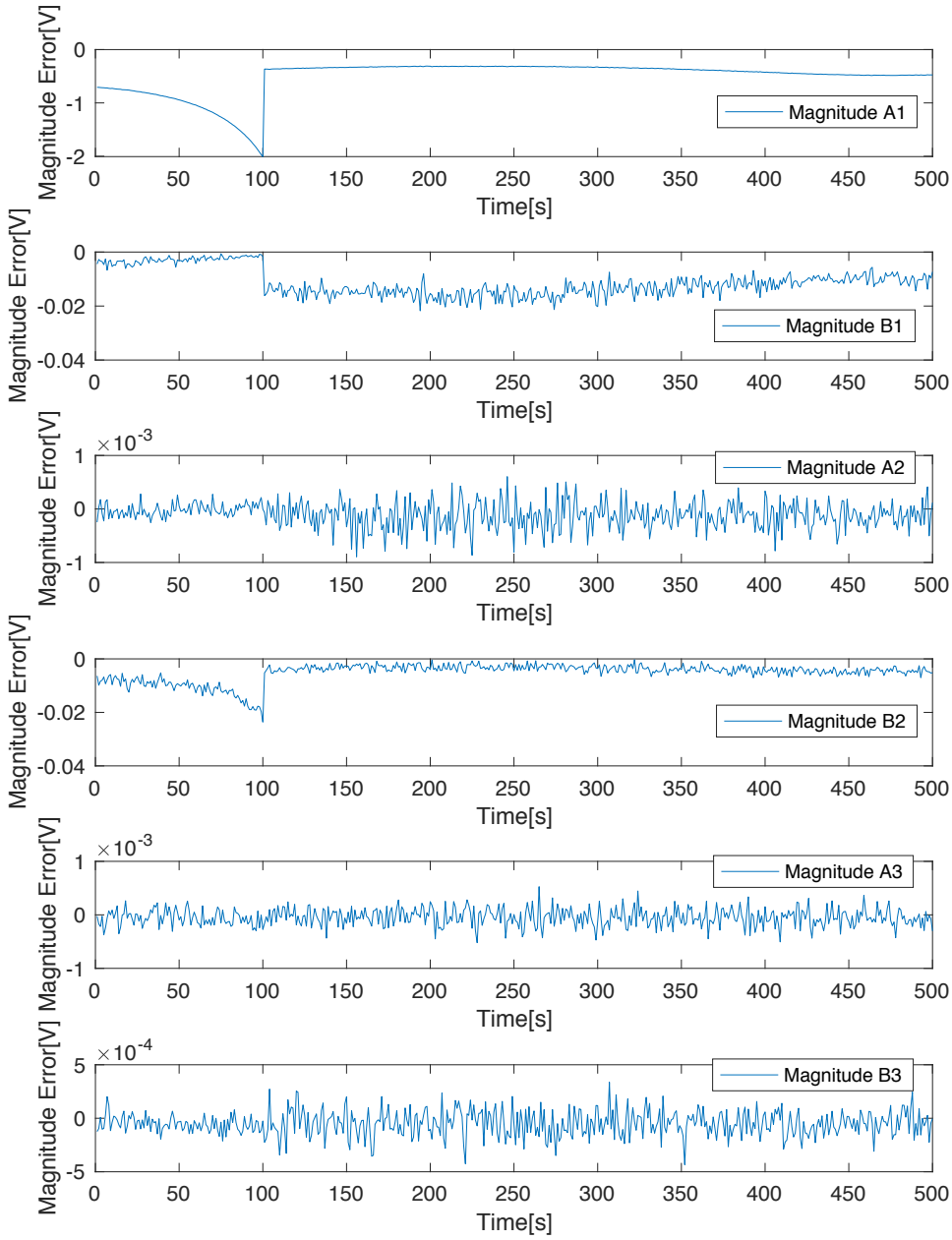

Figure 61 Error gap of the coefficient magnitude

Furthermore, we could get the direct views of the magnitude errors in percentage in figure 62. Then it is easy to compare the amplitude errors among A_1, B_1, A_2, B_2, A_3 and B_3.

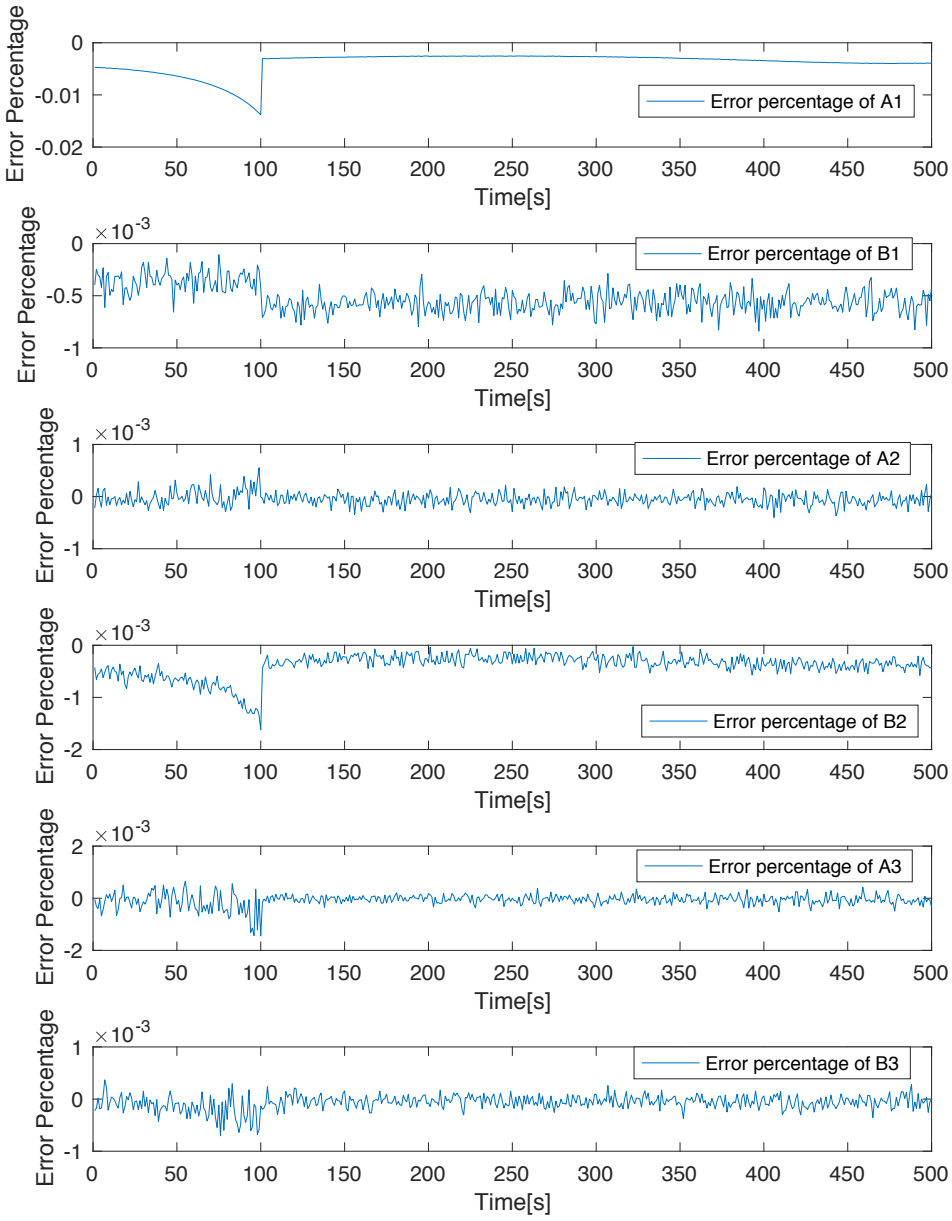

Figure 62 Magnitude error as a percentage

5.5 Experiment 4

In this experiment, we define the amplitudes of the fundamental frequency in more complex to

$$V_{a1} = 110 \times (1.05 + 0.05\sin(2\pi t)),$$

$$V_{b1} = \begin{cases} 165 \times \left(1.1 + 0.15\sin\left(2\pi t + \frac{2\pi}{3}\right)\right) & 31 \times T_s < t < 35 \times T_s \\ 110 \times \left(1.1 + 0.15\sin\left(2\pi t + \frac{2\pi}{3}\right)\right) & \text{OW} \end{cases}$$

$$V_{c1} = \begin{cases} 80 \times \left(1.15 + 0.15\sin\left(2\pi t + \frac{2\pi}{3}\right)\right) & 11 \times T_s < t < 25 \times T_s \\ 110 \times \left(1.15 + 0.15\sin\left(2\pi t + \frac{2\pi}{3}\right)\right) & \text{OW} \end{cases}$$

where $T_s = \frac{1}{500} s$. The 2nd harmonic and 3rd harmonic are set to be 10%, and 5% of the fundamental frequency amplitudes. The amplitude waveforms of the fundamental frequency and harmonics are shown in Figure 63.

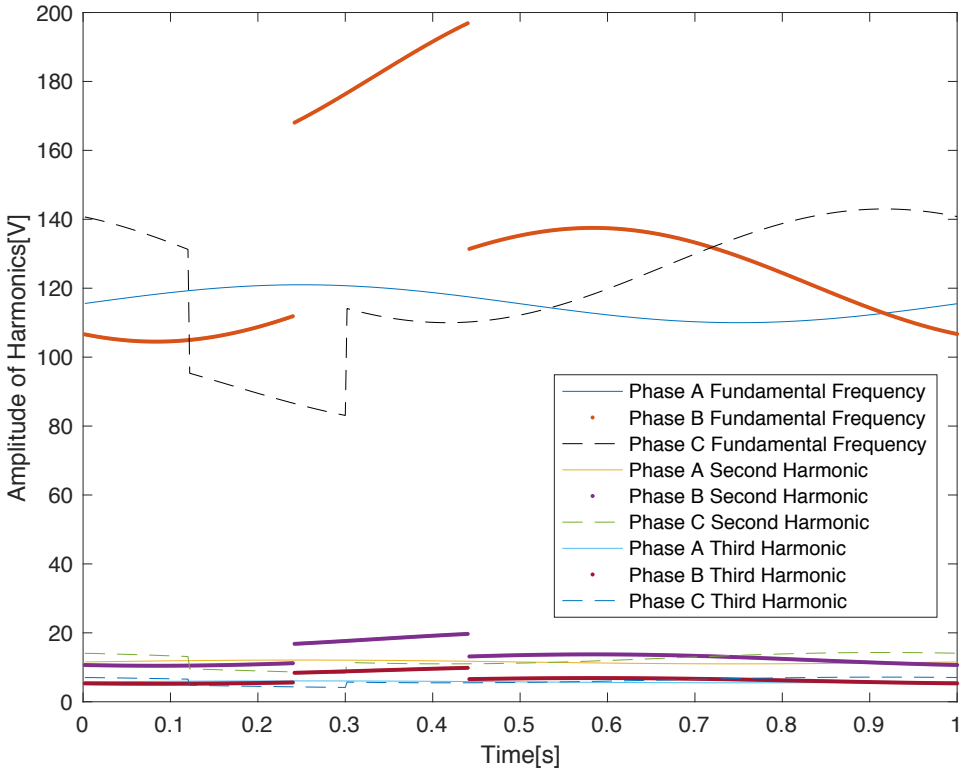

Figure 63 The amplitude of the fundamental frequency and harmonics

5.5.1 Linear frequency change results

In this experiment, we use the ramp signal as frequency change input. The actual and estimated state is shown in figure 64. The frequency errors on every run are plotted in figure 67. We can see that the maximum error is at sample 165, and the proportion of error and current frequency is $0.5291/56.5167 = 9.4\times10^{-3}$. Furthermore, the RMSE over 500 independent runs for a linear variation in frequency is 0.1817.

$$RMSE = \sqrt{\frac{1}{500}\times\sum_{500}^{1}(f_{est}-f_{actual})^2} = 0.1817$$

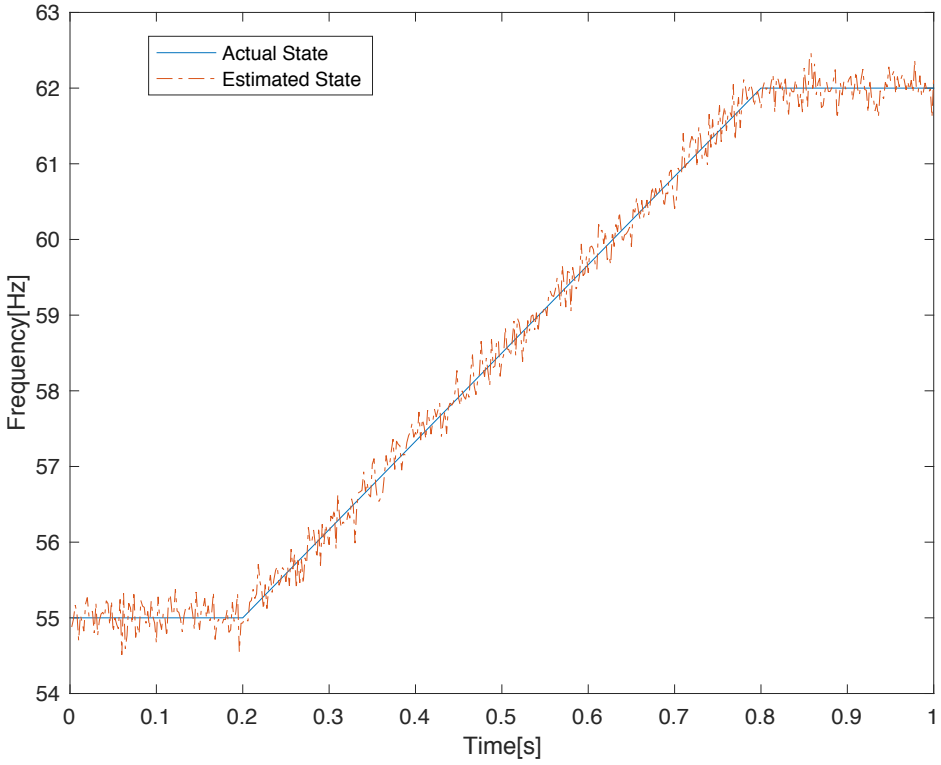

Figure 64 Linear frequency change

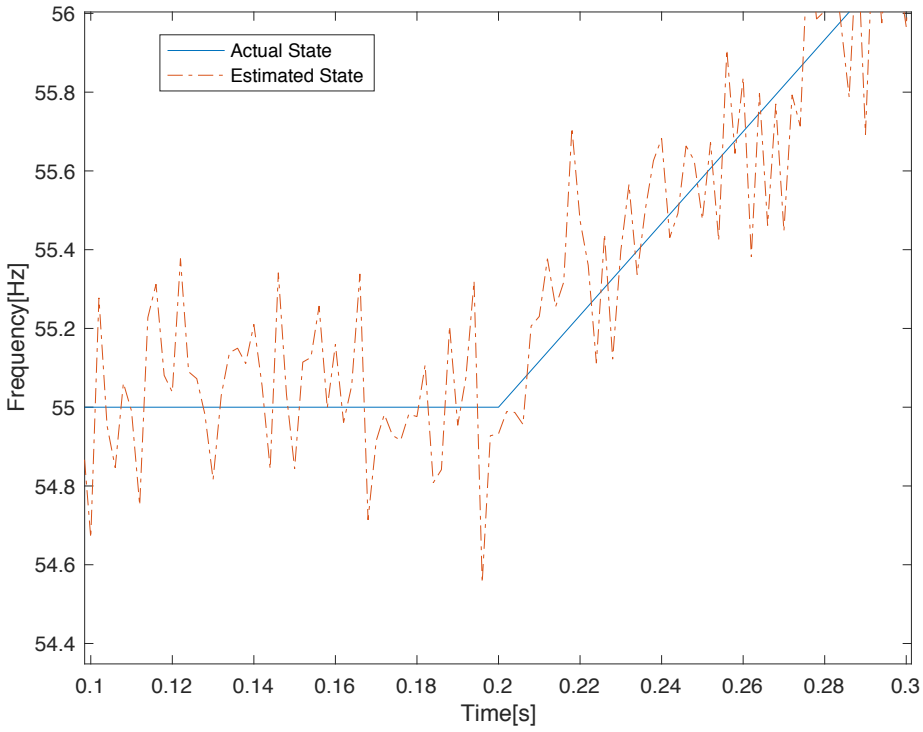

Figure 65 Linear frequency tracking around t = 0.2s

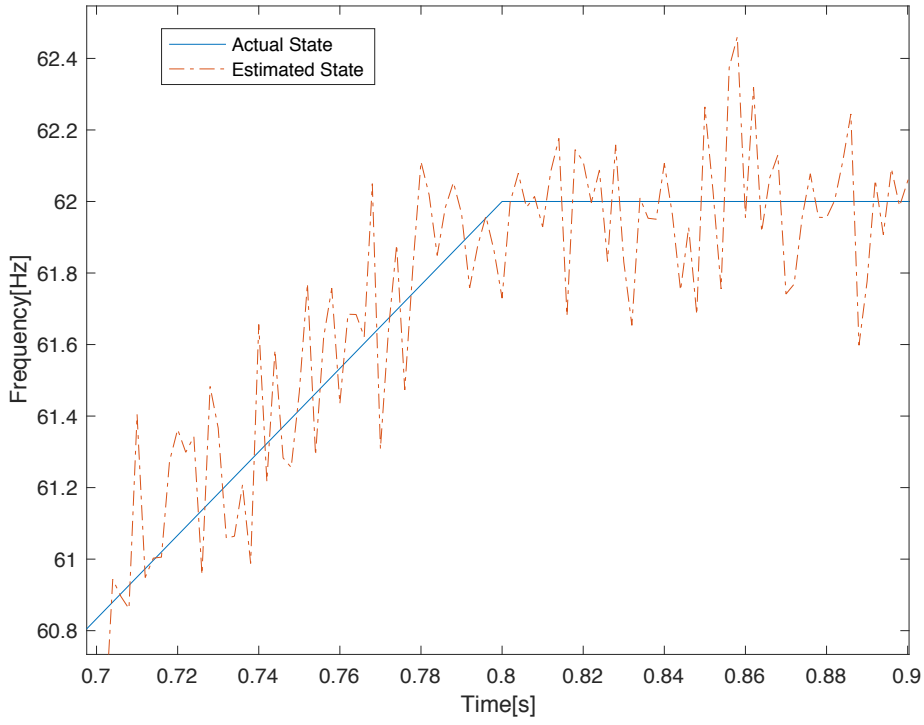

Figure 66 Linear frequency tacking around t = 0.8s

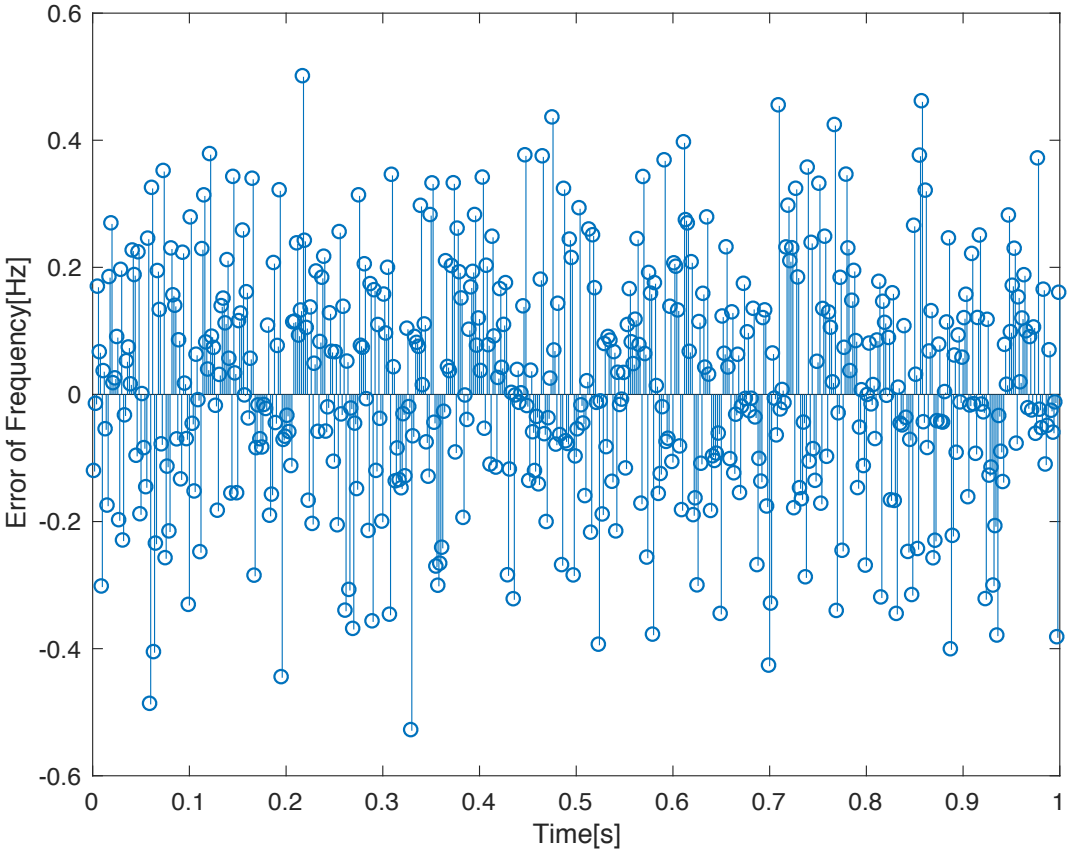

Figure 67 Errors between actual and estimated frequency for linear change

The estimated and actual coefficient magnitudes A_1, B_1, A_2, B_2, A_3 and B_3 are shown in figures 68 and 69.

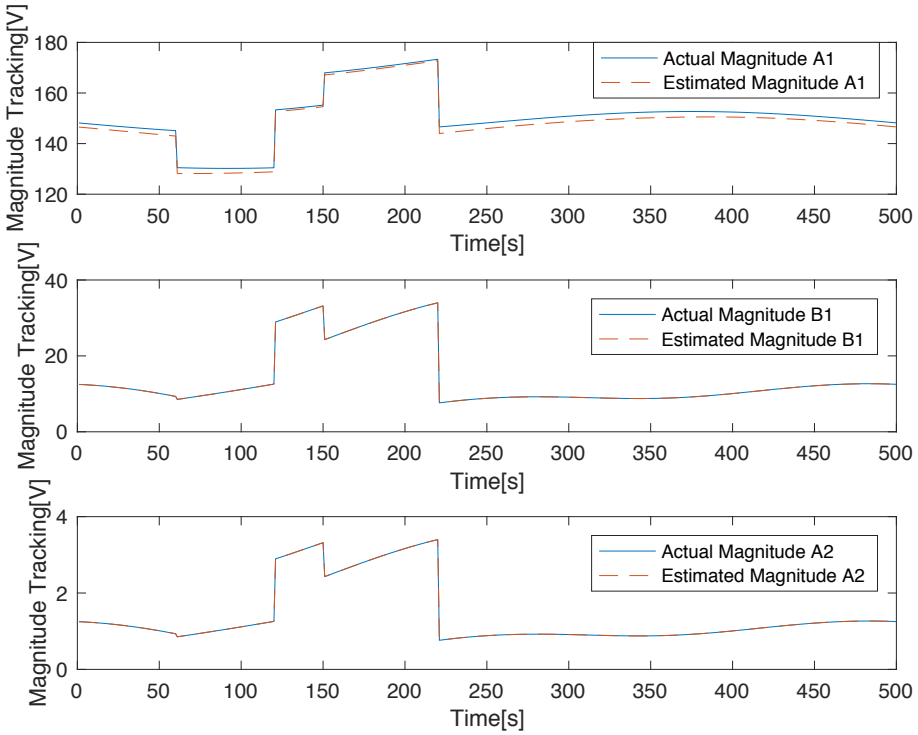

Figure 68 Errors between actual and estimated magnitude of A_1, B_1, A_2

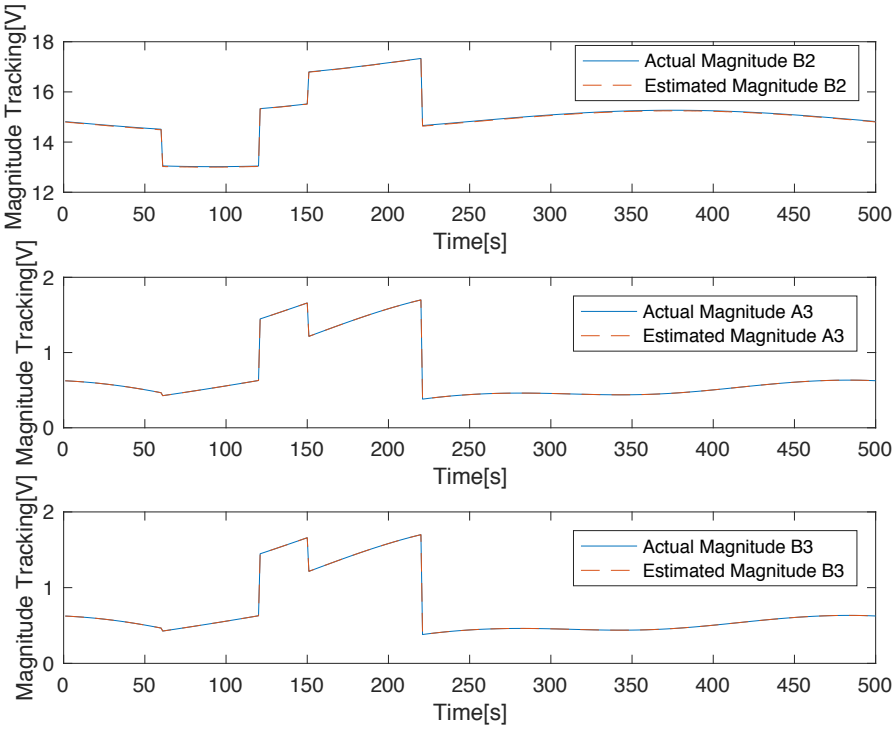

Figure 69 Errors between actual and estimated magnitude of B_2, A_3, B_3.

In figure 70, the blue line indicates the magnitude error at each sampling instant.

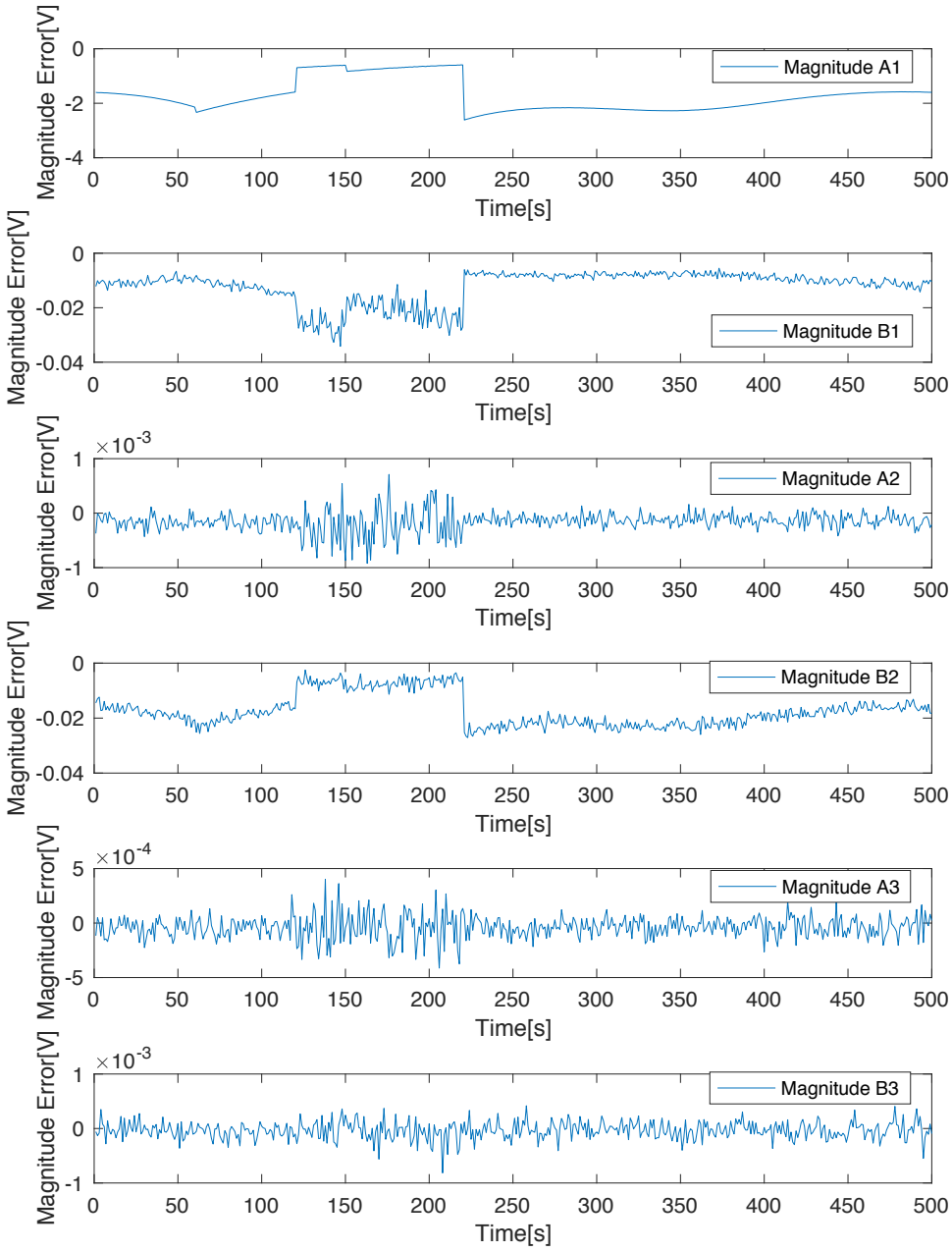

Figure 70 Error gaps of the coefficient magnitude

To compare the performances of different magnitude estimation, we express the absolute values of the magnitude errors as relative values in terms of a percentage. Figure 71 depicts the performances of the magnitude estimation.

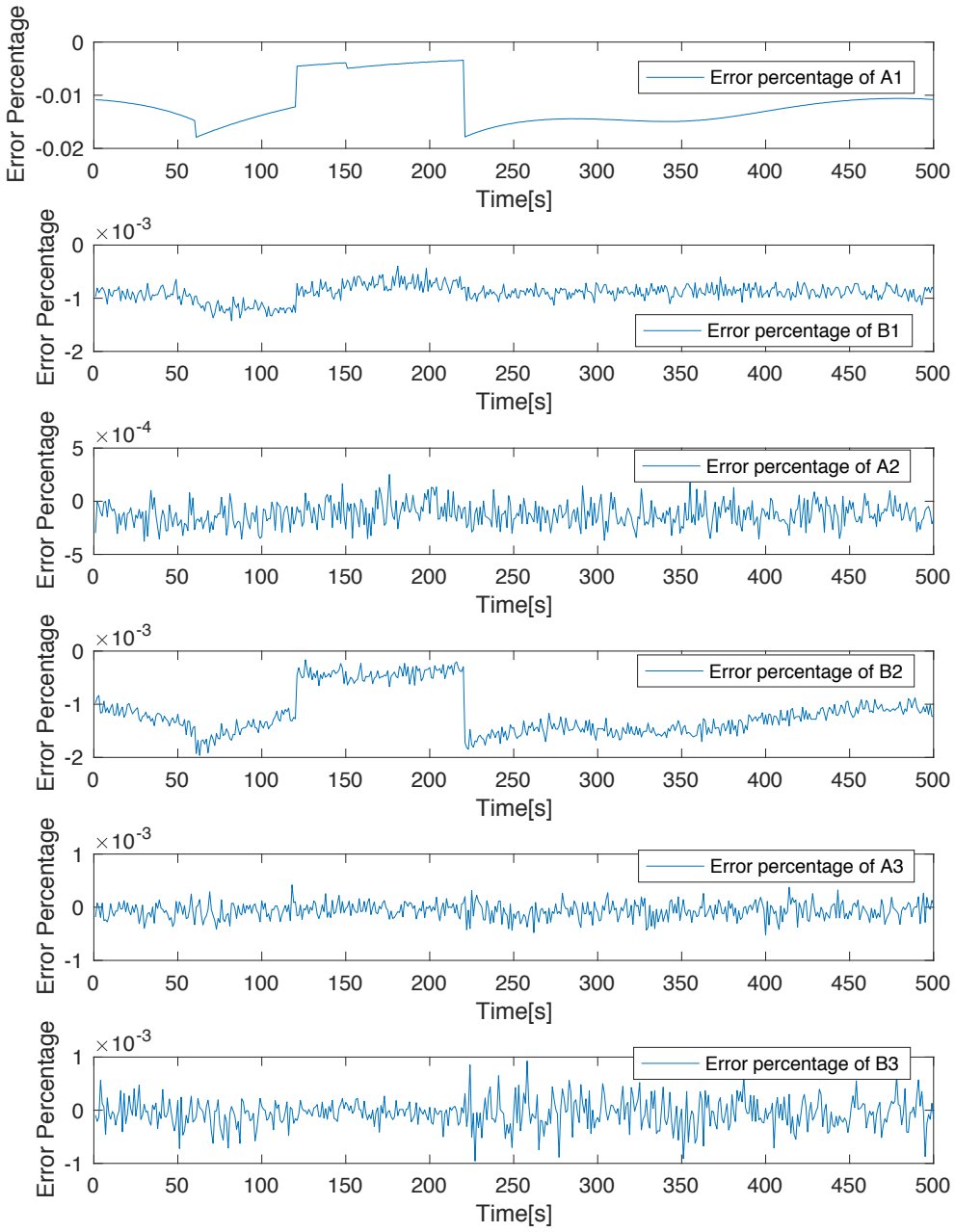

Figure 71 Magnitude error as a percentage

5.5.2 Step change frequency results

In the experiment, we estimated the frequency and magnitude of the fundamental frequency, the 2nd harmonic and the 3rd harmonic. The input signal is shown in figure 2. The results of frequency estimation are plotted in figure 72 and we can see in figure 73 that the convergence time. The maximum error is $0.7180/62 = 0.0116$, which is presented at the $430th$ sampling instant in figure 75. Integrating the errors, we have the RMSE in this experiment is 0.1712.

$$RMSE = \sqrt{\frac{1}{500} \times \sum_{500}^{1} (f_{est} - f_{actual})^2} = 0.1712$$

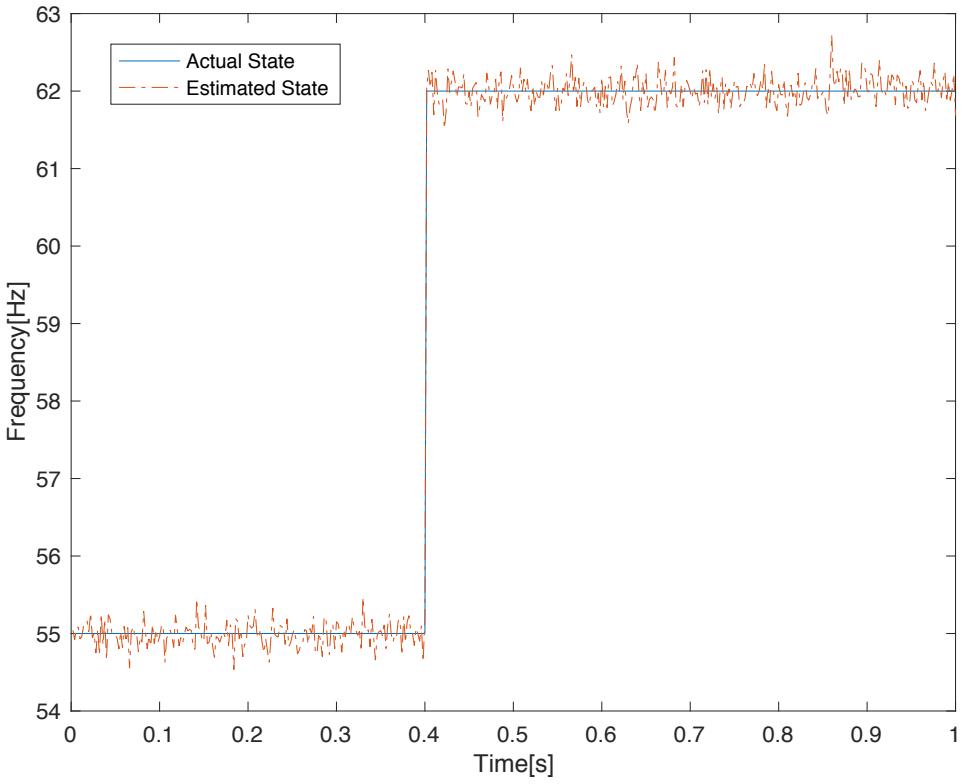

Figure 72 Step change of the fundamental frequency from 55Hz to 62Hz

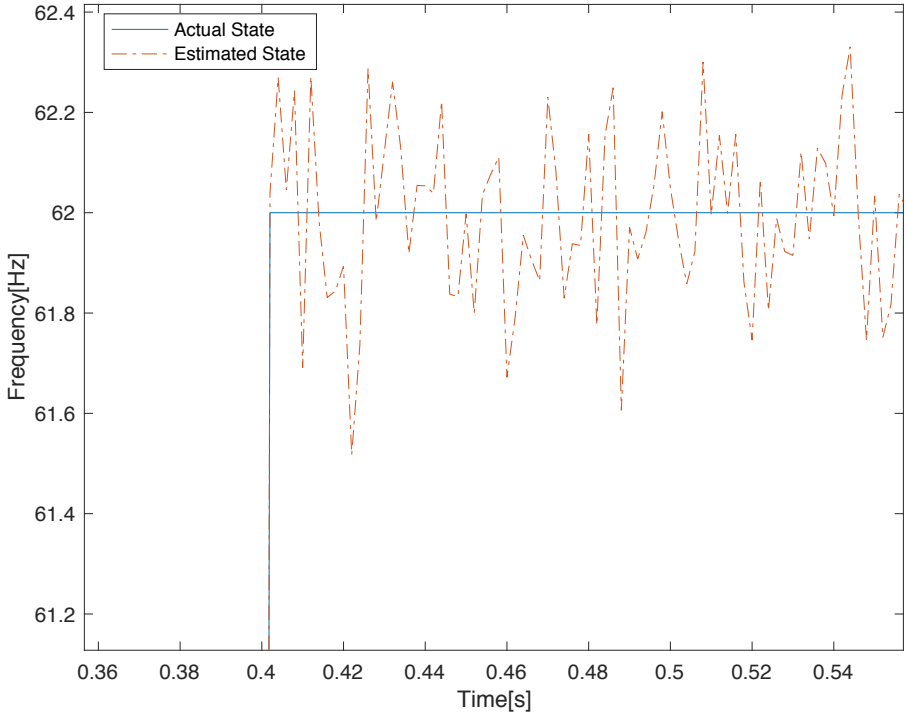

Figure 73 Upper part of step change

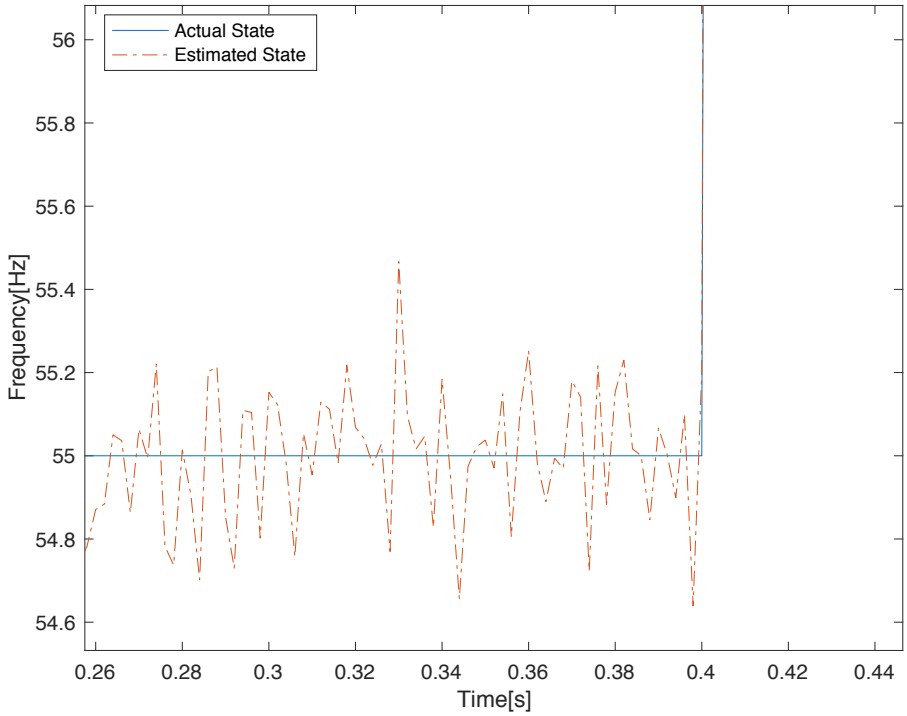

Figure 74 Lower part of step change

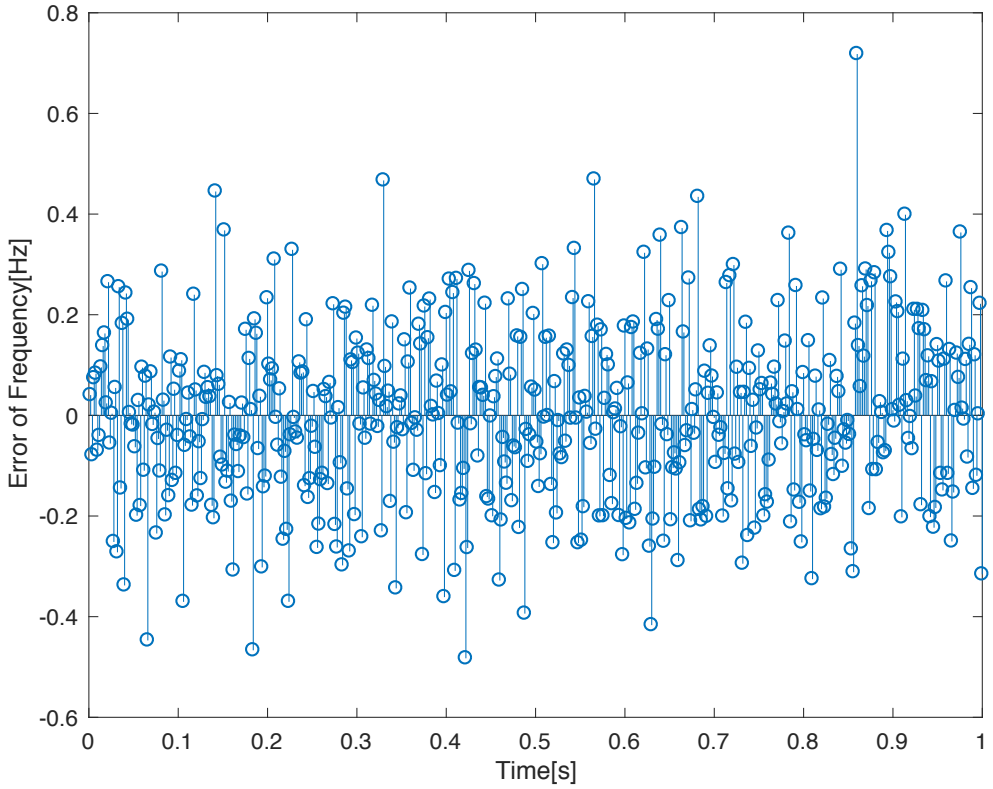

Figure 75 Errors between actual and estimated frequency for step change

Another purpose of this experiment is the magnitude estimation. We do the amplitude estimation under the same conditions as the previous frequency estimation. The estimation of complex coefficients $A_1, B_1, A_2, B_2,\ A_3$ and B_3 is shown in figure 76 and 77.

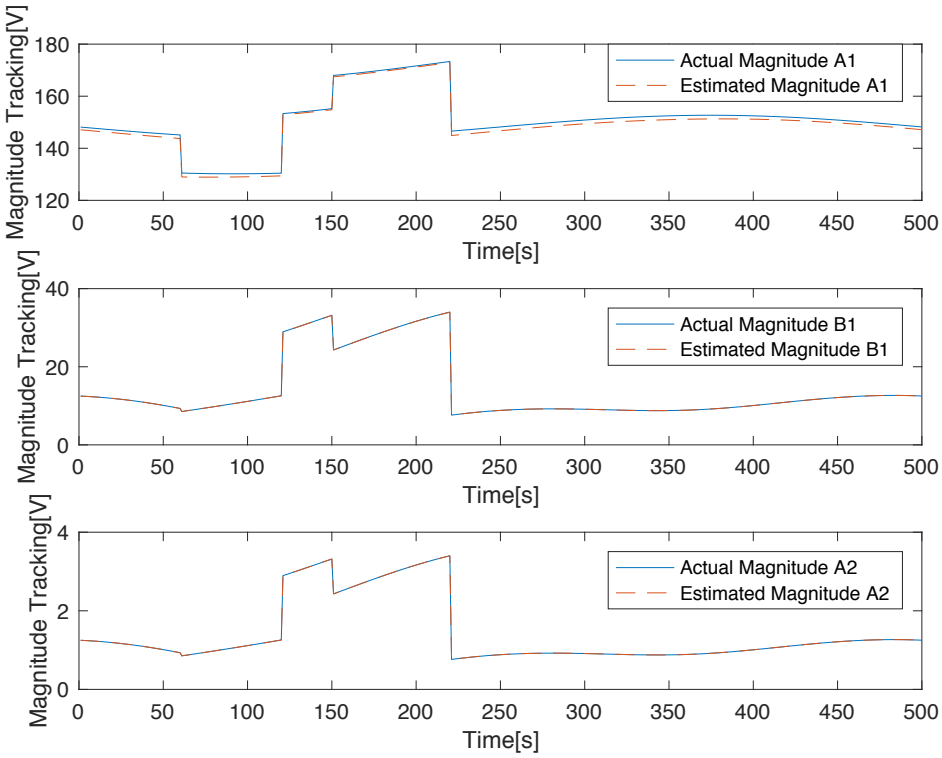

Figure 76 Errors between actual and estimated magnitude of A_1, B_1, A_2

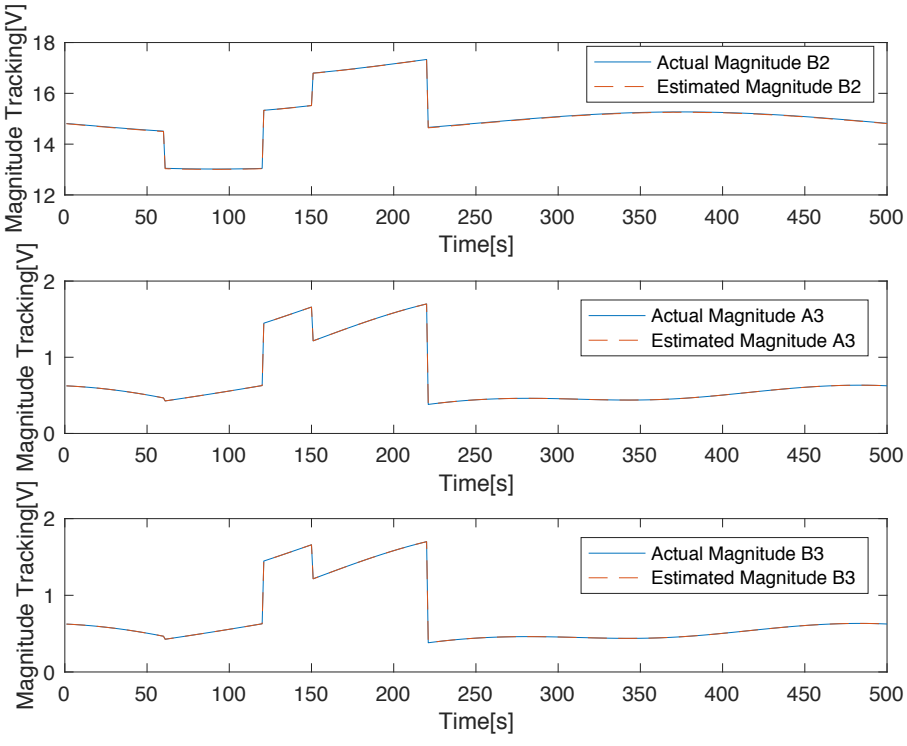

Figure 77 Errors between actual and estimated magnitude of B_2, A_3, B_3.

To view the specific errors at each sampling instant, the magnitude errors are plotted in figure 78.

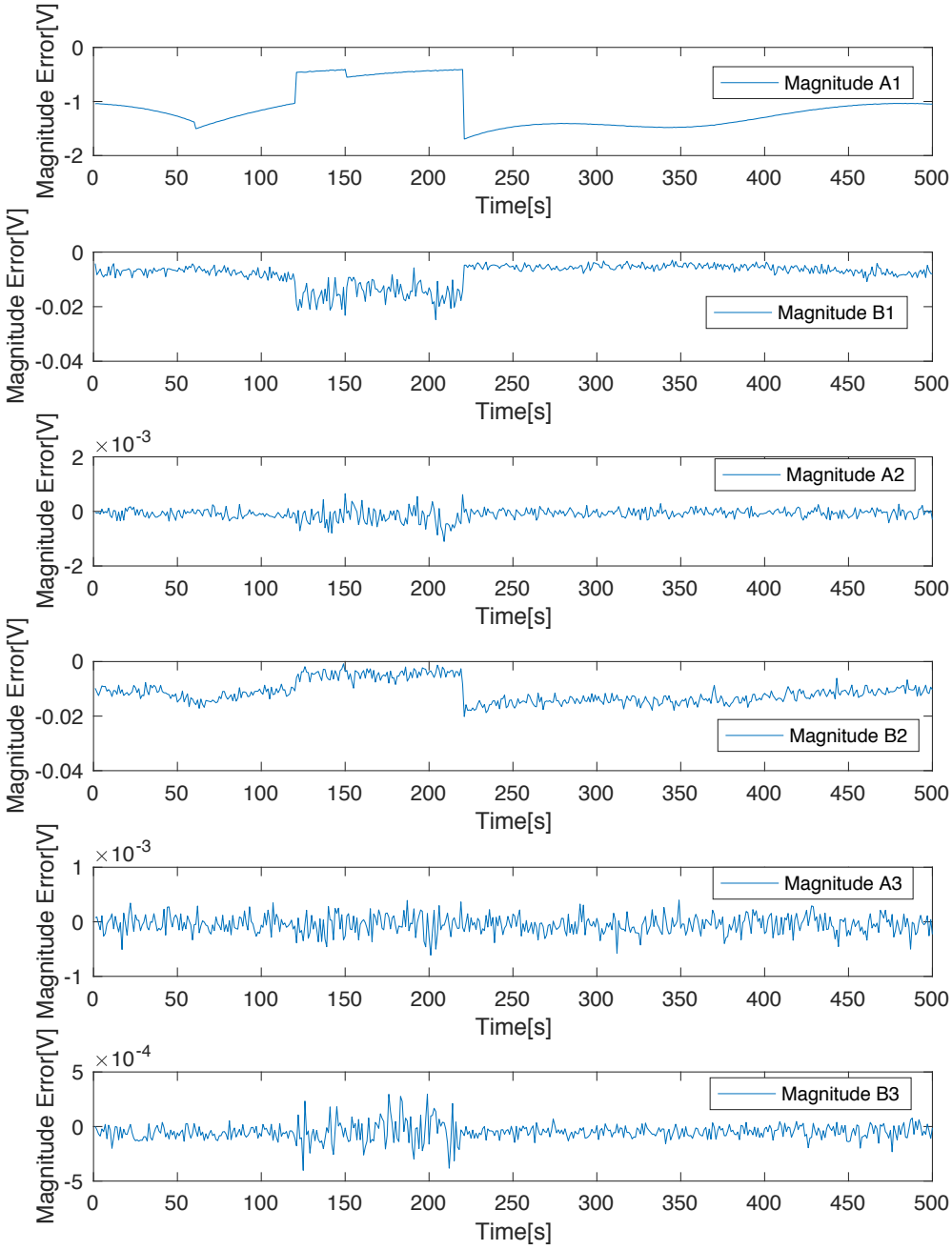

Figure 78 Error gaps of the coefficient magnitude

Not only the estimation errors are valuable, but we also have direct views of the magnitude errors in percentage in figure 79. Now we could compare the magnitude errors among A_1, B_1, A_2, B_2, A_3 and B_3.

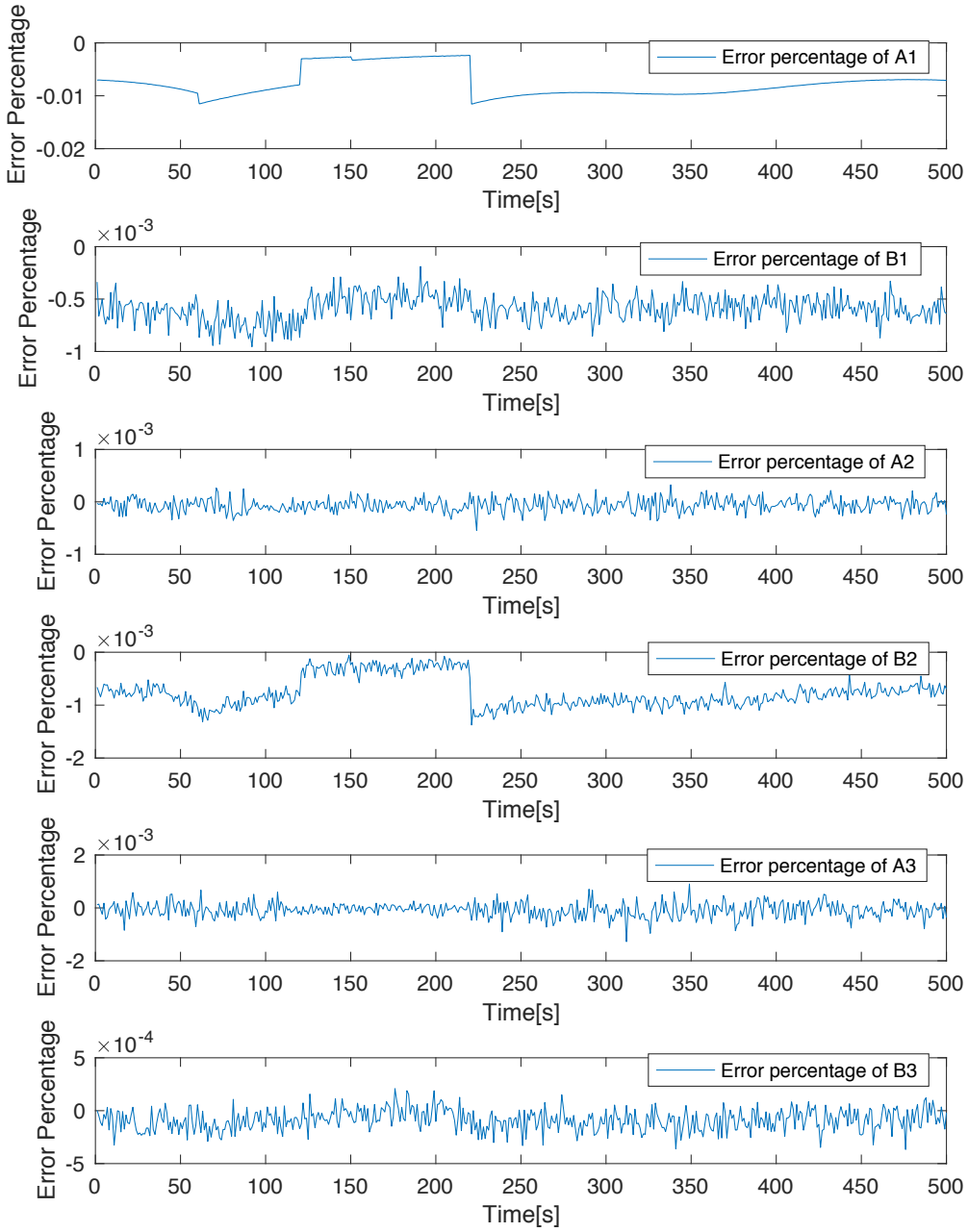

Figure 79 Magnitude error as a percentage

6 Conclusions

In this thesis the estimation technique based on the Unscented Kalman filter for frequency and amplitude tracking under balanced and unbalanced power system condition is presented. Various simulations are carried out to analyze the dynamic performance of the UKF, based on realistic data.

Generally, the speed of response and accuracy are two crucial factors when performing dynamic state estimation using the Kalman filter. In our work, we carried out the estimation for two frequency changes of the input signals under the same initial conditions for both balanced and unbalanced power systems. Moreover, we considered four other types of three phase amplitudes changes to estimate the magnitude in unbalanced power system.

In the balanced system case, we only estimate the frequency of three-phase voltages in complex domain. The simulation results confirmed that the Unscented Kalman filter (UKF) has good performance in terms of convergence time. Regardless of the change, (step or linear frequency change), the root mean square errors (RMSE) are around $0.12 \sim 0.13$. Furthermore, the maximum error of single run is not more than $0.4\ Hz$, which means the error percentage is under 0.727%. Therefore, the Unscented Kalman filter performed well in terms of tracking accuracy as well.

In unbalanced power system case, we presented four experiments for frequency and magnitude estimation. In every experiment, we assumed a type of amplitude change happened and track the magnitude. Meanwhile, we do frequency estimation for the two types of input frequency changes as shown in figure 1 and 2 under the amplitude changed environment. We found that no matter how the amplitude changed, the estimator showed good tracking accuracy of the original signal as well as the magnitude tracking simultaneously. The RMSE of frequency estimation under the sharp and linear change input signal are around $0.17 \sim 0.18$ and the error percentage is around 1%. Moreover, the error percentage of the magnitude estimation is below 2%.

In general, the UKF performs well in terms of response speed, convergence time and tracking accuracy in both balanced and unbalanced power systems. The RMSE and maximum error percentage of a single run, the performance in unbalanced system a bit worse than in the

balanced power system case. All in all, we achieved good frequency and magnitude estimation for both balanced and unbalanced systems. However, the performance of the Unscented Kalman filter (UKF) in unbalanced power system case is not as such good as when applied to a balanced power system.

Bibliography

[1] M. S. Sachdev and M. M. Giray, “A least error squares technique for determing power system frequency,” *IEEE Trans. Power App. Syst.,* vol. PAS-104, no. 4, pp. 1025-1038, Feb. 1983
[2] H. Novanda, P. Regulski, F. Gonzalez-Longatt, and V. Terzija, “Unscented kalman filter for frequency and amplitude estimation,” in IEEE Trondheim, PowerTech, 2011, pp. 1–6.
[3] Xia, Y., Blazic, Z., and Mandic, D. P. : ‘Complex-valued least squares frequency estimation for unbalanced power systems,’ IEEE Transactions on Instrumentation and Measurement, 2015, 64, (3), pp. 638-648.
[4] A. G. Phadke, J. S. Thorp, and M. G. Adamiak, “A new measurement technique for tracking voltage phasors, local system frequency, and rate of change of frequency,” IEEE Trans. Instrum. Meas., vol. 102, no. 5, pp. 1025-1038, May 1983.
[5] O. Vainio and S. J. Ovaska, “Digital filtering for robust 50/60 Hz zero crossing detectors”, IEEE Transaction Instrumentation and Measurement, Vol. 45, No. 2, pp. 426-430, Feb. 1996
[6] Xia, Yili, Zoran Blazic, and Danilo P. Mandic. "Complex-valued least squares frequency estimation for unbalanced power systems." IEEE Transactions on Instrumentation and Measurement 64.3 (2015): 638-648.
[7] Ren, J. and Kezunovic, M. : ‘A hybrid method for power system frequency estimation,’ IEEE Transactions on Power Delivery, 2012, 27, (3), pp. 1252-1259.
[8] Fan, L. and Qi, G. : ‘A new synthetic frequency estimation method of sinusoid based and interpolated FFT,’ 2015 Fifth Int. Conference on Instrumentation and Measurement, Computer, Communication and Control, pp. 1725-1729.
[9] A. Cataliotti, V. Cosentino, S. Nuccio, "A phase-locked loop for the synchronization of power quality instruments in the presence of stationary and transient disturbances", IEEE Trans. Instrum. Meas., vol. 56, no. 6, pp. 2232-2239, Dec. 2007.
[10] F. D. Freijedo, A. G. Yepes, O. Lopez, P. Fernandez-Comesana, J. Doval-Gandoy, "An optimized implementation of phase locked loops for grid applications", IEEE Trans. Instrum. Meas., vol. 60, no. 9, pp. 3110-3119, Sep. 2011.
[11] A. Nicastri, A. Nagliero, "Comparison and evaluation of the PLL techniques for the design of the grid-connected inverter systems", Proc. IEEE Int. Symp. Ind. Electron., pp. 3865-3870, 2010.
[12] R. M. Santos Filho, P. F. Seixas, P. C. Cortizo, L. A. Torres, A. F. Souza, "Comparison of three single-phase PLL algorithms for UPS applications", IEEE Trans. Ind. Electron., vol. 55, no. 8, pp. 2923-2932, Aug. 2008.
[13] M. Karimi-Ghartemani, H. Karimi, M. R. Iravani, "A magnitude/phase locked loop system based on estimation of frequency and in-phase/quadrature-phase amplitudes", IEEE Trans. Ind. Electron., vol. 51, no. 2, pp. 511-517, Apr. 2004.
[14] T. Thacker, D. Boroyevich, R. Burgos, F. Wang, "Phase-locked loops using state variable feedback for single-phase converter systems", Proc. 24th Annu. IEEE Appl. Power Electron. Conf., pp. 864-870, 2009.
[15] T. Thacker, R. Wang, D. Dong, R. Burgos, F. Wang, D. Boroyevich, "Phase-locked loop noise reduction via phase detector implementation for single-phase systems", IEEE Trans. Ind. Electron., vol. 58, no. 6, pp. 2482-2490, Jun. 2011.
[16] Pradhan, A. K., Routray, A., and Basak, A. : ‘Power system frequency estimation using least mean square technique,’ 2005, IEEE Transactions on Power Delivery, 20, (3), pp. 1812-1816.
[17] Chudamani, R., Vasudevan, K. and Ramalingam, C.S.: ‘Real-time estimation of power system frequency using nonlinear least squares,’ IEEE Trans. on Power Delivery, 2009, 24, (3), pp. 1021-1028.
[18] L. Sujbert, G. Péceli, G. Simon, "Resonator-based nonparametric identification of linear systems", IEEE Trans. Instrum. Meas., vol. 54, no. 1, pp. 386-390, Feb. 2005.
[19] Xia, Y. and Mandic, D. P. : ‘Widely linear adaptive frequency estimation of unbalanced three-phase power systems,’ IEEE Transactions on Instrumentation and Measurement, 2012, 61, (1), pp. 74-83.
[20] Wiltshire, R., Ledwich, G., and O’Shea, P.: ‘A Kalman filtering approach to rapidly detecting modal changes in power systems,’ IEEE Trans. Power Syst., 2007, 22, (4), pp. 1698–1706.
[21] S. J. Julier and J. K. Uhlmann, "A New Extension of the Kalman Filter to Nonlinear Systems", in Proc. of the 4th Conference on Signal Processing, Sensor Fusion and Target Recognition, vol. 3068, pp. 182-193, 1997.
[22] S. J. Julier and J. K. Uhlmann, "Unscented filtering and nonlinear estimation," in Proceedings of the IEEE, vol. 92, pp. 401-422, 2004.

[23] E.A. Wan and R. van der Merwe, ‘‘The unscented Kalman filter for nonlinear estimation, in Proceedings of Symposium 2000 on Adaptive Systems for Signal Processing, Communication and Control (AS-SPCC), IEEE, Lake Louise, Alberta, Canada, October 2000.
[24] M. Brown, M. Biswal, S. Brahma, S. J Ranade and H. Cao, “Characterizing and quantifying noise in PMU data,” Proc. IEEE PES General Meeting, July 2016, Boston, MA
[25] J. Muñoz, M. E. Magaña and E. Cotilla-Sánchez, “Adaptive Master-Slave Unscented Kalman Filter for Grid Voltage Frequency Estimation.” IET Signal Processing.